Electrochemical Oxide Growth on Polycrystalline Platinum

by

Yin Huang
B.Sc., Xiamen University, 1994

A Thesis Submitted in Partial Fulfillment of the
Requirements for the Degree of

MASTER OF SCIENCE

in the Department of Chemistry

We accept this thesis as conforming
to the required standard

[redacted]

Dr. David A. Harrington, Supervisor (Department of Chemistry)

[redacted]

Dr. Charles X.W. Qian, Departmental Member (Department of Chemistry)

[redacted]

Dr. Arthur Watton, Outside Member (Department of Physics)

[redacted]

Dr. Zuomin Dong, External Examiner (Department of Mechanical Engineering)

University of Victoria

Supervisor: Dr. David. A. Harrington

ABSTRACT

Sweep-hold voltammetry and solution exchange experiments have been used to study the electrochemical oxide growth on platinum. The effect of some anions on Pt electrochemistry was also investigated.

Sweep-hold methods were employed to study the kinetics of the oxide growth for different sweep rates and different hold potentials. Nonlinear regression results of the sweep-hold data indicated agreement with the direct logarithmic rate law. The relationship of the parameters used in fitting with the oxide charge density and electrode potential were explored in new empirical forms although the theoretical justification for them is unclear. The results imply that at least two different processes take place for platinum oxidation: one for the earlier stage and another for later oxide growth. Conway's model was compared to the data. The model could correctly predict the constancy of the OH adsorption charge density, but at higher potentials the estimated value of the charge was unreasonable, indicating a problem with this model.

Hydrogen was found to be a very good indicator for the oxide growth study. The number of bare platinum sites inferred from the hydrogen oxidation current was compared with the charge of oxide growth, and it was concluded that the oxide formed in the earlier stage must be a Pt(I) compound. Combined with the previous EQCM experimental results, the oxide was suggested to be Pt_2O. A corresponding mechanism for the oxide growth with this intermediate involved was then proposed.

The effect of some anions and small organic molecules was also studied by solution-exchange experiments. The adsorption of bisulfate was found to involve electron transfer. Chloride was found to dissolve the oxide already formed on the surface. Cl^-, SCN^- and thiol were found to adsorb oxidatively on platinum.

Keywords: Platinum electrode, cyclic voltammetry, anion adsorption, oxidation mechanism.

Examiners:

[redacted]

Dr. David A. Harrington, Supervisor (Department of Chemistry)

[redacted]

Dr. Charles X.W. Qian, Departmental Member (Department of Chemistry)

[redacted]

Dr. Arthur Watton, Outside Member (Department of Physics)

[redacted]

Dr. Zuomin Dong, External Examiner (Department of Mechanical Engineering)

Table of Contents

Acknowledgements

This project and work was carried out under the supervision of Dr. David. A. Harrington. First of all, I would like to pay my special thanks to him. His learned knowledge and skills in mathematics deeply impressed me. His ability to direct me in solving a real problem was really helpful. His ability to find profound information out of even a simple experimental result helped me in the way I do research. I was especially grateful for his patience in correcting my poor English in the writing of this thesis.

Laboratory mates Scott Furman and Miguel Labayen helped me with the instrumentation and this help is also much appreciated.

The group of Dr. Cornelia Bohne, especially Dr. Laura Okano, helped me with some fluorescence experiments not reported here. I also thank to Sean Adams in the Glass shop who helped me to design the electrochemical cells and seal the platinum wire in soft glass.

I thank all the professors in the Department of Chemistry. They drew me out of my shyness and helped me to become a qualified TA. The efforts of the secretaries in the general office facilitated my daily life in the department and are also much appreciated.

During my stay in Victoria, those Chinese fellows, especially those in this department have accompanied me everyday for a very nice lunch period.

Grateful acknowledgement is made to the Natural Sciences and Engineering Research Council of Canada (NSERC) and University of Victoria for financial support to this work.

At last, I owe a lot to my dear wife, Ms. Liu Chuping, and my parents far away in China. They have always encouraged me in my study an this university.

List of Symbols

σ: charge density
θ: coverage of adsorbate
η: overpotential
Γ: surface concentration
σ_0: overall oxide charge density
θ_{equ}: adsorption coverage in equilibrium
θ_{OH}: OH adsorption coverage
σ_{OH}: oxide charge density of OH adsorption
σ_{ox}: oxide charge density due to further oxidation
a, b, c, a_0: parameters used for simulation in sweep-hold experiments
ac: alternating current
ads: adsorbed state
aq: aqueous solution state
C: filtering capacitor
CE: counter electrode
CV: cyclic voltammogram
dc: direct current
E: potential
E_h: held potential
eq: (value) at equilibrium
F: Faraday's constant
FTIR: Fourier Transform Infrared (Spectroscopy)
GPIB: General Purpose Interface Bus
i: current
j: current density
j_0: current density at held time t_0 in a sweep-hold experiment
P_1, P_2, P_3: parameters used for simulation in sweep-hold experiments
q: charge
R: gas constant
R: sampling resistor
RE: reference electrode
RHE: reversible hydrogen electrode
T: temperature
t: time
t_0: held time (experimental parameter)
v: sweep rate
WE: working electrode

1 Introduction & Background

1.1 Overview and the Objectives of this Work

The electrochemistry of platinum has been an active topic of research in the last two decades. As the mercury electrode served as a model surface to study the structure and properties of the electrochemical double-layer and some kinetics of weakly adsorbed species, so the platinum electrode has been widely used to study the phenomena of electrocatalysis of small organic molecules and also hydrogen and oxygen chemisorption in electrochemical surface science. This field has also been stimulated by the development of fuel cells in which platinum is used in dispersed form as the catalyst for the oxidation of hydrogen, the oxidation of small organic molecules and hydrocarbons and also for the reduction of oxygen. It was also found that the initial stage of platinum oxide growth involves an oxygen-containing species, that may be involved in the heterogeneous anodic oxidation of small organic molecules e.g., methanol, formic acid and other alcohols. Research on the thin oxide film formed on platinum can also be the bridge to study the surface oxide structure transition from a purely 2-dimensional surface process to quasi 3-dimensional and 3-dimensional growth of bulk oxide films or phases [1-3].

Despite lots of studies already, the mechanism of the growth process and the oxide components of the thin film formed at potential less than 2 V vs. RHE are still unclear. The kinetic explanation with model of the oxide growth process needs more exploring. This research uses cyclic voltammetry to study the oxide growth of polycrystalline platinum electrode in strong acid solution. With some variation, i.e., potential hold during

scanning, cyclic voltammetry is a very convenient and versatile technique to study the mechanism of oxide growth. The sweep-hold experimental technique used in this research proved to be able to simplify the data fitting and modeling. We argue that the parameters used before to describe the direct logarithmic rate law are not constant or exponential with the potential as stated by the literature. A revised form of the rate law is then derived. We also suggest that there exist two processes by studying the relationship of the parameters with potential.

Some chemical methods are explored to study the platinum surface. In hydrogen saturation experiments the electrolyte is saturated with hydrogen. The plot of the hydrogen oxidation current vs. the oxide charge calculated from cyclic voltammograms shows that the earliest stage oxide formed is a Pt (I) species. We propose that this species is Pt_2O, instead of the PtOH suggested in the literature, and show how the observed direct logarithmic rate law is consistent with this assignment.

Some solution-exchange experiments are also performed to study the nature of the oxide growth and the effects of anion adsorption. An injection procedure is used to facilitate the mixing of extra anions with the bulk solution as required. We conclude that the adsorption of bisulfate occurs with charge transfer. Other anions are found to have large effects on further oxide growth and on pre-existing oxide.

Some background knowledge for electrochemistry is presented before the literature survey.

1.2 Theoretical Basis of Electrochemical Methods

1.2.1 Double-Layer Structure:

Electrochemistry mainly studies the interface between the electrode and the electrolyte solution. This interface is made up of electrons, solvent molecules and ions. Interfacial charge transfer is the essential step giving rise to the field of electrochemistry. The common name for the interfacial region is the "double-layer", which arises from the first theory to describe this charged interphase by Helmholtz in the 19th century. As a simple picture, it was imagined that the excess charges on the metal side are balanced by an equal number of excess charges, also arranged to be all in one plane, on the solution side. The double-layer behaves as a simple parallel-plate capacitor. A picture of the double-layer region is shown in Fig. 1.1.

In this model, the solution side of the double-layer is made up of several "layers". The layer closest to the electrode is the inner layer, containing solvent molecules and sometimes other species (ions or molecules) that are called specifically adsorbed species. This inner layer is also called the compact layer. The locus of the electrical centers of these specifically adsorbed species is called the inner Helmholtz plane (IHP). The solvated ions can only approach to the outer Helmholtz plane (OHP). The interaction of the solvated ions with the electrode involves only long-range electrostatic forces, independent of the chemical properties of the ions and electrode. These ions are said to be nonspecifically adsorbed. Due to the thermal agitation in the solution, the nonspecifically adsorbed ions are distributed in a 3-dimensional region, called the diffuse layer, extending from the OHP into the bulk of the solution. The thickness of the diffuse layer

depends on the total ionic concentration of the electrolyte solution. For the above model, the equivalent circuit of the double-layer can be considered to be two capacitors in series:

$$\frac{1}{C_{dl}} = \frac{1}{C_{compact}} + \frac{1}{C_{diffuse}} \qquad (1.1)$$

where $C_{compact}$ is the capacitance of the inner layer and $C_{diffuse}$ is the capacitance of the diffuse layer.

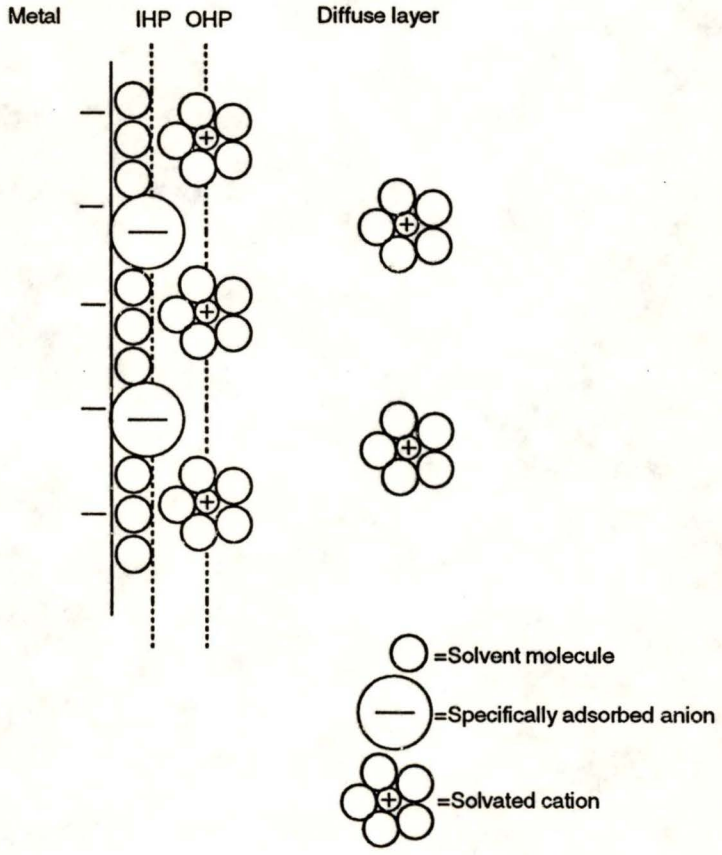

Fig. 1.1 A diagram of modern double-layer structure [4].

1.2.2 Electrode Processes

Two kinds of processes may occur at electrodes: Faradaic and non-Faradaic. The Faradaic process involves electron transfer across the double-layer region, causing oxidation or reduction reactions. From the double-layer diagram shown in Fig. 1.1, it is seen that the double-layer behaves like a capacitor which implies that another kind of process can take place. In this non-Faradaic process, there is no electron transfer across the interface, but the double-layer structure or properties changes. For example, an adsorption or desorption process without electron transfer can change the charge distribution at the electrode and also in the electrolyte. Under these conditions, an external transient current can flow.

1.2.3 Kinetics in Electrochemistry

1.2.3.1 General Electrochemical Reaction Kinetics:

For the simple single-step (no adsorption) reaction:

$$A + e^- \underset{k_{-1}}{\overset{k_1}{\rightleftharpoons}} A^- \tag{1.2}$$

The reaction rate can be expressed as

$$v = k_1^{eq} C_{A,S} e^{-\beta F\eta/RT} - k_{-1}^{eq} C_{A^-,S} e^{(1-\beta)F\eta/RT} \tag{1.3}$$

where β is the symmetry factor which measures the influence of the change of potential on the activation energy of both the forward and backward reactions, η is the over-potential which is the potential difference between the applied electrode potential and the equilibrium state electrode potential (η=E-E_{eq}). $C_{A,S}$ and $C_{A^-,S}$ are the concentrations of the species at the electrode surface. k_1^{eq} and k_{-1}^{eq} are the rate constants at equilibrium of

the forward and backward reactions respectively. The first term is the forward reaction rate, and the second term is the backward reaction rate. Indeed this equation becomes the Bulter-Volmer equation for a single-electron transfer reaction when multiplied by *F*. When the reaction is at equilibrium, then we find:

$$\frac{C_{A^-,S}}{C_{A,S}} = K\exp(-\frac{\eta F}{RT}) \tag{1.4}$$

In electrochemistry, the current is proportional to the reaction rate:

$$i = -nFAv \tag{1.5}$$

Here n is the number of electrons in the reaction, F is Faraday's constant, and A is the electrode area. The current density, j, can be expressed as

$$j = i/A = -nFv \tag{1.6}$$

Thus, for the simple one-electron transfer reaction above, the relationship between the current density and the electrode potential is:

$$j = -F(k_1^{eq}C_{A,S}e^{-\beta F(E-E_{eq})/RT} - k_{-1}^{eq}C_{A^-,S}e^{(1-\beta)F(E-E_{eq})/RT} \tag{1.7}$$

1.2.3.2 Adsorption reactions:

(i) Adsorption isotherm

For an adsorbed species, the surface concentration is related to the coverage on the electrode surface. We use Γ to represent the surface concentration (mol m^{-2}) and θ for adsorption coverage. The relationship between Γ and θ is

$$\Gamma = \Gamma_m\theta \tag{1.8}$$

where Γ_m is the maximum surface concentration of that species. The relationship between coverage, θ, and electrode potential is called the adsorption isotherm. The

simplest adsorption isotherm is the Langmuir isotherm that assumes no interaction between adsorbed species. For the simple reaction of

$$M(site) + A + e^- \underset{k_{-1}}{\overset{k_1}{\rightleftharpoons}} MA^-(ads) \tag{1.9}$$

(M is the electrode metal), the Langmuir isotherm can be expressed as

$$\frac{\theta}{1-\theta} = Ke^{-FE/RT} \tag{1.10}$$

Here $K = k_1 / k_{-1}$. Another popular isotherm is the Frumkin isotherm. For this reaction, the Frumkin isotherm can be written as:

$$\frac{\theta}{1-\theta} = Ke^{-g\theta}e^{-FE/RT} \tag{1.11}$$

where g is an interaction parameter.

(ii) Reaction rate:

For reaction (1.9), the reaction rate is:

$$\begin{aligned} v &= \frac{d\Gamma}{dt} = \Gamma_m \frac{d\theta}{dt} \\ &= k_1^0(1-\theta)C_A e^{-g\theta/2}e^{-\beta F(E-E^0)/RT} - k_1^0\theta e^{g\theta/2}e^{(1-\beta)F(E-E^0)/RT} \end{aligned} \tag{1.12}$$

if using the Frumkin isotherm. For the Langmuir isotherm the reaction rate is:

$$v = \frac{d\Gamma}{dt} = \Gamma_m \frac{d\theta}{dt} = k_1^0(1-\theta)C_A e^{-\beta F(E-E^0)/RT} - k_1^0\theta e^{(1-\beta)F(E-E^0)/RT} \tag{1.13}$$

1.2.4 Cyclic Voltammetry

Cyclic voltammetry is a technique in which the potential is swept forward and backward at linear rate and the current response to the potential sweep is monitored. The

curve from cyclic voltammetry is called a cyclic voltammogram. Sometimes it is also called electrochemical spectroscopy.

When no reaction occurs on the surface, the only process is the double-layer charging. If no adsorption takes place, the double-layer capacitance does not change significantly. The current response to the sweeping potential is a horizontal line because

$$j = C_{dl}\frac{dE}{dt} = C_{dl}v \tag{1.14}$$

For the simple reaction: $R \rightarrow O + ne^-$ where both O and R are soluble in the solution and there is no adsorption, then at a certain sweep rate, a peak can be observed on the cyclic voltammogram. When the potential is not positive enough, R cannot be oxidized. When the potential becomes more positive, the current rises with the potential because the oxidation rate varies exponentially with the overpotential. When the potential is high enough, the diffusion of R from the bulk solution to surface cannot keep up with the rate of oxidation, diffusion becomes rate-determining step and the current drops. Similar phenomena happen for the reverse scan. The peak height, width and also the potential difference between the two peaks are used to determine whether this reaction is reversible, quasi-reversible or irreversible.

1.3 Literature Survey on Electrochemical Oxide Growth on Pt

The oxide growth on platinum has been studied by many researchers using various methods including cyclic voltammetry, chronoamperometry, chronopotentiometry, ac voltammetry, ac impedance, optical methods, XPS (X-ray Photoelectron Spectroscopy), AES (Auger Electron Spectroscopy), LEED (Low Energy Electron Diffraction), EQCM (Electrochemical Quartz Crystal Microbalance), photoelectrochemical methods and also

STM (Scanning Tunneling Microscopy). These researches have been reviewed recently by Conway [1, 2], and earlier by others, e.g., Gilman [5]. Two types of anodically-formed platinum oxide are distinguished in the literature, referred as the α-oxide (thin oxide film formed before oxygen evolution) and the β-oxide (thicker oxide film formed under strong anodic conditions, e.g., > 2 V). They are discussed separately.

1.3.1 α-Oxide

1.3.1.1 Chronoamperometry and Chronopotentiometry

In the two important papers by Vetter and Schultze [6, 7], potentiostatic and galvanostatic pulse measurements were employed to investigate the anodic formation of platinum oxide layers according to this reaction

$$Pt + H_2O \rightleftharpoons Pt\text{-}O + 2H^+ + 2e^- \qquad (1.15)$$

They concluded that the properties of the oxide layer were dependent on the formation conditions of the layer, i.e., the formation rate, the aging of the layer, and the method of the setting of the coverage (initial state). The kinetics of the layer formation was explained by this model: oxygen ions are chemisorbed from the electrolyte solution in an equilibrium reaction, $H_2O \longleftrightarrow O^{2-} + 2H^+(aq)$. But the oxygen coverage cannot exceed a few percent and then the adsorbed oxygen ions are exchanged for platinum ions from the first atomic layers (place-exchange). The place-exchange step was considered to be rate-determining and dependent on the field strength. Thicker oxide layers are formed in a similar place exchange reaction at the metal/oxide and oxide/electrolyte interfaces, followed by a migration of platinum and oxygen ions over vacancies or interstitial

positions in a high electric field. They also discussed the double-layer capacity which decreased with oxide formation according to this equation:

$$\frac{1}{C_{dl}} = \frac{1}{C_i}(1+1.2\theta) \qquad (1.16)$$

where C_i is the double-layer capacity without the oxygen layer.

In their potentiostatic study, the direct logarithmic law was found[7], which corresponded to an anodic growth current inversely proportional to time. The constants in the rate law are dependent on the potential. At constant coverage the relation between the current and the potential could be described approximately by the Tafel equation.

It should be noted here that although they wrote the reaction of oxidation as $Pt + H_2O \rightleftharpoons Pt\text{-}O + 2H^+ + 2e^-$, they assumed this process involves the water dissociation step $H_2O \rightleftharpoons O^{2-} + 2H^+(aq)$. This assumes that the oxide PtO is ionic, not covalent. Because they started their experiments at 1.0 V, the initial stage of the oxide growth was missed.

1.3.1.2 Cyclic Voltammetry (Linear Sweep Voltammetry)

Cyclic voltammetry, or linear sweep voltammetry is the most used method in this field due to its convenience. In the most well-known paper using cyclic voltammetry by Kozlowska and Conway and Sharp [8], three peaks were resolved in the initial stages of Pt surface oxidation below a monolayer coverage (1 electron per Pt atom) in pure dilute solutions of perchloric acid and sulfuric acid in pyrodistilled water, as can also be observed at single crystal Pt. In this paper, these authors introduced the concepts of surface chemistry to understand the three distinguishable but overlapping peaks (noted as OA1-3). They were suggested to correspond to successive stages of 2-dimensional

occupancy of the Pt surface lattice by OH or O overlay arrays which could be written as Pt_4/OH, Pt_2/OH and Pt/OH for a Pt (100) surface. They admitted that the designations of Pt_4/OH, Pt_2/OH and Pt/OH did not represent stoichiometric compounds but rather the lattice occupancy ratio by OH and Pt. In their work, the mechanism of OH adsorption was proposed as:

$$Pt + H_2O \longrightarrow \text{"PtOH"} + H^+ + e^- \qquad (1.17)$$

$$\text{"PtOH"} \longrightarrow \text{"PtO"} + H^+ + e^- \qquad (1.18)$$

and the three peaks corresponded to these reactions:

$$Pt + H_2O \longrightarrow Pt_4OH + H^+ + e^- \ (55\ \mu C\ cm^{-2}) \qquad (1.19)$$

$$Pt_4OH + H_2O \longrightarrow Pt_2OH + H^+ + e^- \ (55\ \mu C\ cm^{-2}) \qquad (1.20)$$

$$Pt_2OH + H_2O \longrightarrow PtOH + H^+ + e^- \ (110\ \mu C\ cm^{-2}) \qquad (1.21)$$

They also studied the reversibility of various stages of the oxide growth. They observed that when the potential was less than 1.2-1.4 V, the cyclic voltammogram showed the typical hyseresis, e.g., the potential range of the reduction and the shape of the reduction peak are different from those for oxidation. Potential sweeps taken to progressively less positive potentials showed that the electrosorption of oxide material became less irreversible. For example, the anodic-going sweeps taken up to the potential of 0.85 V in the OA1 region gave, upon reversal, an immediate fall of the current and a corresponding cathodic peak at almost the same potential in the reverse direction of sweep, characteristic of almost reversible oxidation. When the anodic sweeps went to higher potential values (>1.2 V), the cathodic peak potential did not change further, indicating greater irreversibility. From the investigation of time effects in the irreversibility they suggested that when the potential was held some rearranged oxide was

formed, even at low coverages, that required a more cathodic potential for its reduction. They suggested that the rearrangement could not involve surface diffusion to form islands or patches since on the slow sweep (1 mV s^{-1}), or after holding, the same CV profile for the remaining oxidation of the surface was observed. They concluded that two types of processes are involved in the growth of the surface oxide layer. The place-exchange mechanism converted the increasing quantity of the initially-electrosorbed species into a more stable species characterized by a less positive reduction potential. The three anodic distinguishable peaks below a monolayer of OH were considered to be of the reversible kind, since their peak potentials are independent of sweep rate. Their model of the oxide growth is shown in Fig. 1.2.

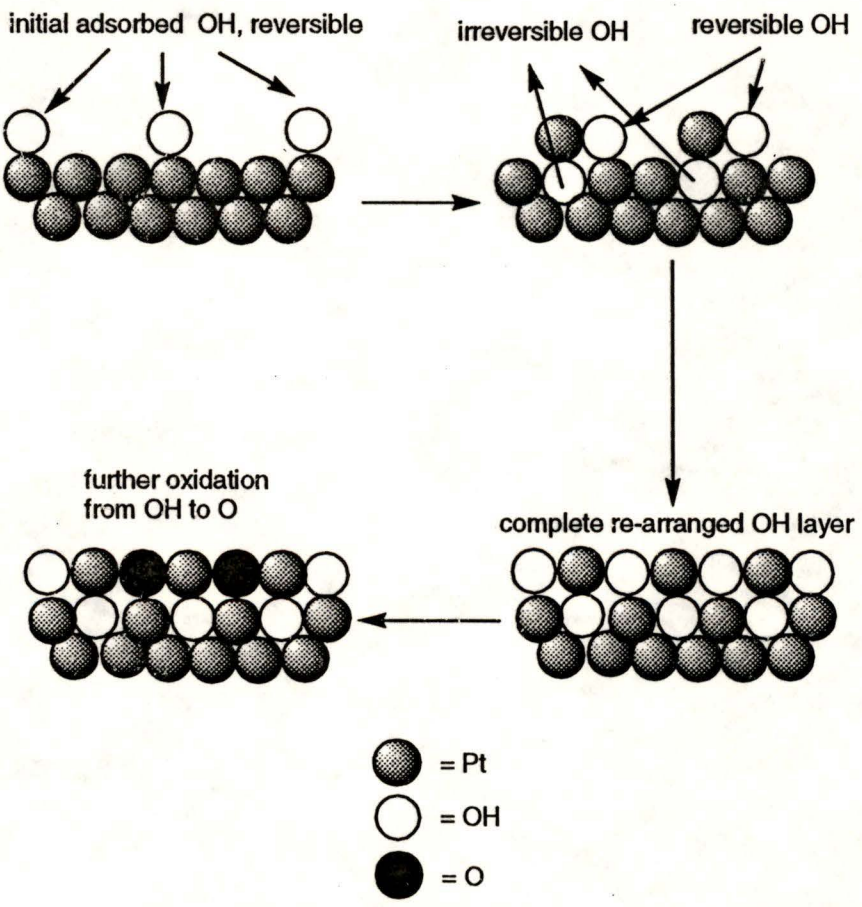

Fig. 1.2 Cartoon of Conway's model of OH adsorption and place exchange. [1]

In their following work, they explored the 880 μC cm^{-2} limit of α-oxide growth, equivalent to two monolayers of "PtO", corresponding only to the development of a quasi-two-dimensional film (in the +II oxidation state of Pt) [9]. Based on ellipsometry measurements by Parsons and Visscher [10], this limit of oxide film formation is assigned to "Pt-O-Pt-O".

1.3.1.3 AC Techniques

AC voltammetry experiments on oxide growth were first carried out by Breiter [11] who explained the results principally in terms of double-layer charging. He suggested that an electrochemical reaction contributed to the frequency dispersion of capacitance at frequencies smaller than 1 kHz. He also found that the adsorption of sulfate anions caused a decrease of the double-layer capacity with increasing concentration in the double-layer region.

In Conway and Gottesfeld's paper [12], they interpreted the increase of capacitance in the earlier stage of oxide growth as mainly due to the increase of pseudocapacitance resulting from the OH adsorption process rather than from a change in the double layer.

The frequency dispersion of the double-layer was studied in detail by van der Geest, Dangerfield and Harrington [13]. The theoretical basis of ac voltammetry was discussed by Harrington [14]. The shape of the AC voltammogram did not change much with frequency, which suggested a single time constant for oxide growth. No features were seen in the early stages of growth that could be assigned to fast OH electrosorption because fast adsorption of OH before a slow rate-determining step would necessarily lead to high-frequency features in the ac impedance spectrum, contrary to their observations.

They interpreted the frequency dispersion by the concepts of reconstruction of the surface and surface diffusion of the oxidized species. They believed that only the slow process depends on the surface structure, e.g., the removal of the Pt atom from its lattice requiring bond breaking which was expected to be site and surface dependent. A one-step oxidation process was proposed:

$$Pt(\text{site 1}) + H_2O \rightleftharpoons PtO(\text{site 2}) + 2H^+ + 2e^- \quad (1.22)$$

$$PtO(\text{site 2}) \rightleftharpoons PtO(\text{site 3}) \quad (\text{surface diffusion}) \quad (1.23)$$

1.3.1.4 UHV (Ultra High Vacuum) Techniques:

XPS (X-ray Photoelectron Spectroscopy) was mainly used to identify the oxide components. An early work using XPS measurements by Parsons et al [15] postulated the α-oxide limited by 880 μC cm^{-2} be $Pt(OH)_2$ or $PtO{\bullet}H_2O$ with a greater degree of covalency in the Pt-O bond, which was inferred from the small Pt $4f_{7/2}$ peak shift relative to that for the pure metal (1.3 eV). Later work by Dickinson et al [16] concluded that PtO was the dominant component of the α-oxide. Hammond and Winograd agreed that the α-oxide has a Pt (II) oxidation state, but the oxide had a binding energy (73.6 eV) characteristic of neither PtO, $Pt(OH)_2$ or PtO_2 [17]. Later XPS was also used by some other groups to investigate the oxide components [18, 19], but there is still no agreement about whether the oxide is hydrous or anhydrous.

Other UHV techniques including LEED and AES were also employed to study the oxide growth on single-crystal platinum [20, 21].

1.3.1.5 Optical Methods

Optical methods, such as infrared (IR) absorption and reflectivity techniques involving direct and modulated reflectance, ellipsometry or second-harmonic reflectance can characterize the oxide films and also adsorbed species *in situ*. Conway [22] and Gottesfeld [23] showed that the differential reflectance (reflectance over the potential modulation) was sensitive to the reversibly reducible oxide but was insensitive to other components which are irreversibly reduced. By comparing with the oxidation of Ir, they concluded that a difference between the cases of Pt and Ir must be dued to a change of mechanism of Pt oxidation as the potential increased beyond 0.9 V. It was also found that in the plot of direct reflectance with the oxide charge, the slope changed at around 1.1 V, indicating that a different oxide layer started to form at 1.1 V.

An IR spectroscopy study by Benziger et al [24] suggested that OH adsorbed on the surface at potentials greater than 0.5 V since a broad OH stretching peak was observed in the spectra.

1.3.1.6 Other Methods

EQCM – *in situ* mass measurement of the adsorbate on electrode surface is available using the extraordinarily sensitive quartz crystal microbalance. A constant 8±0.5 g mass change per mole of electrons was observed by Birss et al [25]. We know from the reactions:

$$Pt + H_2O \rightarrow PtO + 2H^+ + 2e^- \qquad (1.24)$$

$$Pt + 2H_2O \rightarrow PtO_2 + 4H^+ + 4e^- \qquad (1.25)$$

that if the oxide is anhydrous, then the expected mass change per mol electrons will be 8 g mol^{-1}. For hydrous oxide products, the expected mass change per mole of electrons will be 17 g mol^{-1}. Therefore the main conclusion from mass measurement experiments is that the oxide is anhydrous. Unfortunately, this kind of mass experiment cannot distinguish the Pt (II) and Pt (IV) forms of the α-oxide.

STM: Direct in situ images of reconstructed single-crystal platinum surfaces were obtained by STM by Itaya et al [26, 27]. Their results indicated that after a single oxidation-reduction cycle, the surface had isolated Pt adatoms on the terraces. After multiple cycles the surface showed an unusual "rolling hills" reconstruction. The hills in this reconstruction are about 5 nm apart, have diameters of 2 to 3 nm and are 2 to 3 atoms high.

Photoelectrochemical techniques: Photocurrent responses at polycrystalline platinum electrodes oxidized to different extents were reported by Peter et al [28].

1.3.1.7 Kinetic of the Oxide Film Growth Process

As was mentioned above, for the α-oxide growth, under constant potential conditions, the process follows an empirical equation called the direct logarithmic rate law. A general form of the rate law is

$$j = \frac{d\sigma}{dt} = a\exp(-b\sigma) \tag{1.26}$$

where j is the current density, σ is the charge density, t is time, and a and b are parameters. Integration gives a linear relationship between σ and $\log(t)$. The kinetics of this α-oxide growth has been dealt with in some ways in various publications [29, 30].

Conway's basis for this rate law is that the rate-determining step is the place-exchange process, with the electric field across the developing oxide film as the driving force to flip the PtOH dipoles into OHPt ones. He showed theoretically that the b in the rate law is a potential-independent parameter with an experimental value of about ln(10)/40 = 0.058 $\mu C\ cm^{-2}$. He also predicted that a should depend exponentially on the applied potential.

The parameter a was further explored by Harrington et al [31]. They suggested a had the potential dependence:

$$a = a_0 \exp(cE) \tag{1.27}$$

Therefore, by using this rate law: $j = \frac{d\sigma_{ox}}{dt} = a_0 \exp(cE)\exp(-b\sigma_{ox})$, they explained the observed form of the oxide place-exchange current in constant potential experiments and also in cyclic voltammetry. A plateau could be predicted by this law in cyclic voltammetry, with the plateau current proportional to sweep rate. The parameter values were as follows: $-\log(a_0) \approx 8\text{-}13$, $b \approx 0.04\text{-}0.06\ cm^2\ \mu C^{-1}$ and $c \approx 20\text{-}35\ V^{-1}$. This rate law was also used to correctly predict the sweep-hold-sweep phenomena: the current on resuming the sweep after the hold period approaches that for an uninterrupted sweep, and the amounts of oxide formed are nearly independent of the hold time.

1.3.1.8 Mechanism of the Oxide Growth

Two main kinds of mechanism can be distinguished from the above literature survey. One is the two-step process involving fast OH or other O species adsorption, corresponding to this scheme:

$$Pt + H_2O \rightarrow "PtOH" + H^+ + e^- \qquad \text{(OH adsorption)} \tag{1.28}$$

$$"PtOH" \rightarrow "OHPt" \qquad \text{(place exchange, rate determining)} \tag{1.29}$$

$$\text{"OHPt"} \rightarrow \text{"PtO"} + H^+ + e^- \qquad \text{(further oxidation)} \qquad (1.30)$$

The place exchange process is the rate-determining step. Conway [29] has proposed a microscopic theory of this mechanism to explain the observed growth law, valid for submonolayer and multilayer oxide growth. He adopted the high electric field across the oxide as the driving force to flip the oxide dipoles. The electric field was considered to depend on the oxide amount and the flipped dipoles also influence the surface potential. In this theory, the parameters a and b of the growth law were shown to depend on microscopic quantities as shown in these equations:

$$a = Fk\exp(-2\beta(\Delta\phi - \chi_0)/dRT \qquad (1.31)$$

$$b = 8\pi N_A \beta\mu^2 / dFRT \qquad (1.32)$$

where μ is the dipole moment, d the thickness of the oxide film and β a barrier symmetry factor). The evidence for this kind of mechanism is mainly from the reversibility studies.

Recently another microscopic model of the growth of thin oxide film on Pt was reported by Harrington [32]. This newly proposed model included these two main elements: (a) the rate-determining step is two-electron oxidation of a Pt atom, with concomitant migration of the atom out of its metal lattice site; (b) the oxidized species surface diffuses until it sticks to a growing oxide island (or is reduced back to Pt metal). This corresponds to the following reaction scheme:

$$\text{Pt(site 1)} + H_2O \rightleftharpoons \text{PtO(site 2)} + 2H^+ + 2e^- \qquad (1.33)$$

$$\text{PtO(site 2)} \rightleftharpoons \text{PtO(site 3)} \quad \text{(surface diffusion)} \qquad (1.34)$$

Using this model, Harrington predicted the observed direct logarithmic growth law for potential step transients by a Monte Carlo simulation, although the slope was not in exact agreement with experiment. Surface diffusion was used to explain the origin of the

reversible components in CV as follows: with surface diffusion, the oxide species can move away from the site of its production and expose new active sites that allows continued oxide growth. After more extensive oxidation, the surface is rough and reduction will occur after only limited surface diffusion, leading to a more reconstructed final surface.

1.3.2 β-Oxide

As well as hundreds of publications on the α-oxide, the thicker oxide formation at strong anodic conditions was also studied extensively [1]. Nearly all the methods used in the study of the α-oxide were also applied to study the β-oxide. Compared to much disagreement remaining in the study of α-oxide, the β-oxide is well understood [1, 9]. There is no growth limit; the oxide thickness can be up to more than 50 monolayers. XPS data showed the β-oxide to be PtO_2 [16-19, 33-37]. Because this project is a study of the α-oxide, a detailed review will not presented here.

1.3.3 Adsorption of Anions and Small Molecules

The surface oxidation of Pt is very sensitive to the concentration and type of anions in the electrolyte. Anion effects were summarized by Kozlowska et al [38]: (1) adsorption of anions competes with OH/O deposition and blocks the initial stage of oxidation; (2) adsorption of anion also changes the inner-layer field and influences the place-exchange process and (3) lateral repulsion with metal oxygen dipoles by the adsorbed anions facilitates place-exchange.

1.3.3.1 Bisulfate/Sulfate Adsorption

Bisulfate/sulfate adsorption is very important in the previous work since most of the experiments about platinum in acid solution were carried out in sulfuric acid. This is due to the difficulty in getting pure perchloric acid, which is expected to have less adsorption effect on platinum oxide growth. Many methods have been applied to this study. Here are some literature results:

Normal Electrochemical Studies:

Cyclic voltammograms of single-crystal platinum (111) or (100) or (110) show a sharp peak just after the potential of UPD hydrogen desorption due to bisulfate/sulfate adsorption. At low concentration of sulfuric acid electrolyte (<5 mM), the hydrogen adsorption range does not overlap the bisulfate adsorption range at all, while at higher concentrations the two regions overlap to a small degree. The peak charge due to anion adsorption is about 1/3 monolayer [39].

Radiotracer Measurements:

Radiotracer measurements on the adsorption of sulfate species on polycrystalline platinum electrodes have been reported by Balashova [40] and later by Horanyi [41] et al. Recently, Krauskopf *et al [42]*, and Wieckowski *et al* [43] used this method to study the adsorption of bisulfate/sulfate on single-crystal Pt ((111) mostly). In such experiments sulfuric acid labeled with ^{35}S was used to prepare the electrolyte. No adsorption of sulfate species was observed at 0 mV vs. RHE. The adsorption became detectable above the potential of zero charge (pzc), at about 150 mV and reached a maximum at potentials between 600 mV to 700 mV. Then the signal decreased to very low values in the platinum oxide region and increased again, markedly, at potentials above 1.6 V. The

maximum adsorption coverage or surface concentration is about 1.3×10^{14} ions cm^{-2} for an ordered Pt(111) electrode in 0.1 M $HClO_4$ + 0.4 mM H_2SO_4 solution, which corresponds to 0.08 ions per Pt. Assuming that the adsorption structure has three-fold coordination, the maximum coverage of sulfate species on ordered Pt(111) is about 0.25 in this dilute solution. For disordered Pt (111) this number is slightly lower, about 0.20 times the maximum coverage. On platinized Pt, the shape of the adsorption coverage vs. potential relationship is similar to that on a single crystal. There was also a maximum coverage at about 700 mV vs. RHE. In 0.5 M sulfuric acid the maximum coverage is about 1.1×10^{-10} mol cm^{-2}, about 0.04 ions per platinum. For smooth polycrystalline platinum, this value would be lower. The shortcoming of a radiotracer measurement is that it cannot distinguish bisulfate from sulfate. The measured adsorbate coverage includes both of these.

Vibrational Spectroscopy Research:

FTIR or SNIFTIR is generally used for *in situ* measurements of adsorbates on electrodes because of their high sensitivity. The spectroscopy was obtained using the variation of vibrational spectrum of S-O bonds with potential based on the idea that the interaction of the substrate Pt with bisulfate/sulfate would shift the vibrational spectrum peak [35, 44, 45]. So indeed all these spectra are potential modulated. Data showed that on a Pt(111) electrode sulfate species are adsorbed in the form of SO_4^{2-} ions in the pH range of 0.23-2.8. One band located at 1220-1280 cm^{-1} was found to be dependent on potential. Adsorbed sulfate is three-fold coordinated with a C_{3v} symmetry but is randomly distributed on the surface. At increasing coverage the sulfate adlayer becomes more organized as deduced from the observed bandwidth narrowing. The maximum coverage

was found at 0.8 V vs. Pd/H_2. Asymmetric band shapes (in reflectance spectra) showed that the adsorbed ions could not move freely. The interaction/coupling between the adsorbed anions was deduced to be small from the small band shift with the coverage. It was also found that while the sulfate species adsorbed exhibits three-fold coordination at Pt(111) , it has twofold coordination at Pt(100) and Pt(110). At polycrystalline platinum electrodes and in mildly acid sulfate solution the main adsorbed species is SO_4^{2-} and a split in one of the bands indicates C_{2v} symmetry. This means SO_4^{2-} is coordinated to the metal through two oxygen atoms. The coverage reached a maximum at 600-650 mV, nearly the same as in the radiotracer experiments. Also no lateral interaction between the adsorbates was found. In the Pt oxide region it was suggested that SO_4^{2-} ions are included in the oxide layer to form a Pt (II) sulfate compound.

Ultrahigh Vacuum Technique measurements:

LEED (Low Energy Electron Diffraction), AES (Auger Electron Spectroscopy) and CEELS (Core-level Electron Energy Loss Spectroscopy) [46] were used to investigate the single-crystal platinum surface with and without sulfate species adsorption. The maximum coverage of bisulfate/sulfate adsorption is about 0.34 ± 0.02 ML (ca. 1/3 monolayer) and that coverage corresponds to a highly ordered Pt(111) $(\sqrt{3}\times\sqrt{3})$ R30° surface structure. The adsorbed bisulfate/sulfate exhibits three-fold coordination at Pt(111). S2p core-level loss spectra and LMM AES data indicate that the chemical state of bisulfate sulfur is +6, the same as in the sulfate anion in a sulfate salt matrix. However, the electron density on the adlattice sulfur (adsorption sulfur) is a little higher than in the salt, obviously due to the back-donation of electrons from the substrate platinum to the

adsorbate anions. It was then suggested that the back-donation electrons from platinum to bisulfate/sulfate plays an important role in the binding of anions to the surface.

***In Situ* Mass Measurements [43]:**

The quartz crystal microbalance/nanobalance is very useful to examine adsorption on electrodes. Experiments on polycrystalline platinum showed that no clear mass increase can be attributed to the adsorbed sulfate species because compared with the oxide or water, sulfate/bisulfate is much heavier than them, 96 g mol^{-1}. But by contrast the results of mass vs. potential plots in different solutions such as $HClO_4$, H_2SO_4 and NaOH showed that the mass increase before the oxide formation in sulfuric acid solution is somewhat higher than it is in $HClO_4$ and NaOH solution, which suggests a small amount of sulfate or bisulfate adsorption. The mass increase in the region of hydrogen desorption also suggests anion adsorption.

Based upon the above results, some conclusions can be made: There exists sulfate species adsorption on both single-crystal platinum and polycrystalline platinum in the double-layer potential region. The adsorption process is non-Faradaic, i.e., no electrons are transferred. The sulfur in adsorbed sulfate species is still in the +6 oxidation state. The adsorption is covalent.

The adsorption coverage of sulfate species is a little higher on single crystal than polycrystalline platinum. The sulfate adsorption coordination on single crystal platinum (111) is three, but on Pt(100) and Pt(110) it can only be two. On the polycrystalline platinum it was suggested to be one or two. The maximum coverage of sulfate/bisulfate on Pt(111) can reach one third ML considering the three-fold coordination, it can only be 0.1-0.2 ML on polycrystalline platinum or even less. At the potential just before the oxide

formation (0.85V), most of the adsorbed anions have desorbed. The coverage on Pt(111) is then about 0.15 ML. The coverage at polycrystalline platinum is estimated to be less than 0.08ML which is rather small.

1.3.3.2 Other Anions and Small Molecules e.g., Halides, CO

The onset potential of oxide growth is very sensitive to the concentration and type of anions in the electrolyte. Halide effects were found first and then studied in much detail [39, 47-49]. As suggested from the detailed study of adsorption on mercury electrodes, the potential of zero charge would shift with the desorption. But only some experimental phenomena are presented here to describe the effect of such anions.

The specificity of anion adsorption on platinum is clearly discernible from the effects anions have on: 1) the onset potential of oxide growth in sweep experiments; 2) the CV shape both in the oxidation part and also the reduction part; 3) the charge due to oxide growth due to surface sites blocked by the adsorbed anions. 4) the blocking effect on hydrogen adsorption.

Adsorbate experiments have been carried out firstly by Conway [39] with some organic compounds including thiourea, dimethyl sulfide, benzene, cyclohexane, acetonitrile and benzontrile, and later by Clavilier [47] with CO as a probe. Their experiments were based on the fact that addition of these compounds to a solution in which a Pt electrode is held potentiostatically at a potential in the hydrogen-adsorption region produces an anodic current transient. In Conway's work, it was concluded that the anodic transients observed with various compounds must arise from displacement of chemisorbed hydrogen atoms, that were already present on the surface at that potential, in an anodic process which can be formally written as:

$$R + Pt - H(ads) \rightarrow Pt - R(ads) + H^+ + e^- \quad (1.35)$$

A similar case applies to the adsorption of CO to displace the UPD hydrogen in Clavilier's experiments, which can be described as:

$$CO + Pt - H(ads) \rightarrow Pt - CO(ads) + H^+ + e^- \quad (1.36)$$

It was also demonstrated in his experiment that a cathodic process would take place corresponding to the displacement of adsorbed anions, e.g., chloride, bisulfate, bioxalate, acetate, or bromide by adsorbed CO following:

$$Pt - A + CO + e^- \rightarrow Pt - CO + A^- \quad (1.37)$$

This makes it possible to do solution exchange experiments using different adsorbates to probe the electrode surface and the adsorption behavior.

2 Experimental

2.1 Chemical Reagents

Seastar and Analar sulfuric acid were used to prepare the 0.5 M sulfuric acid electrolyte.

1-Butanethiol: 99 + %, Aldrich chemical.

Other chemicals including acetonitrile, KI, KIO_3, KCl, were analytical purity grade.

All solutions were prepared with 10 MΩ•m Millipore milli-Q deionized water.

2.2 Electrodes and Cell

Platinum wire from Johnson-Matthey (99.9998%) was sealed in soft glass to make all working, counter and reference electrodes. Reversible hydrogen electrode (RHE) in the same solution was used for all potential measurements, in which a platinum electrode is used in another separate compartment. A glass cell of conventional design was used, shown in Fig. 2.1. Before the cell and electrodes were used, they were cleaned in hot chromic acid (>60 °C) or concentrated sulfuric acid (95%-98%) and then thoroughly rinsed with Millipore water several times. The electrodes and cell were also always left in the Millipore water for some time (>30 minutes) to ensure a clean system. Pure argon (>99%) was bubbled through the solution more than 30 minutes before all experiments and kept flowing through the cell during measurements. Several cycles of cyclic voltammograms were run to achieve a reproducible curve before the data collection.

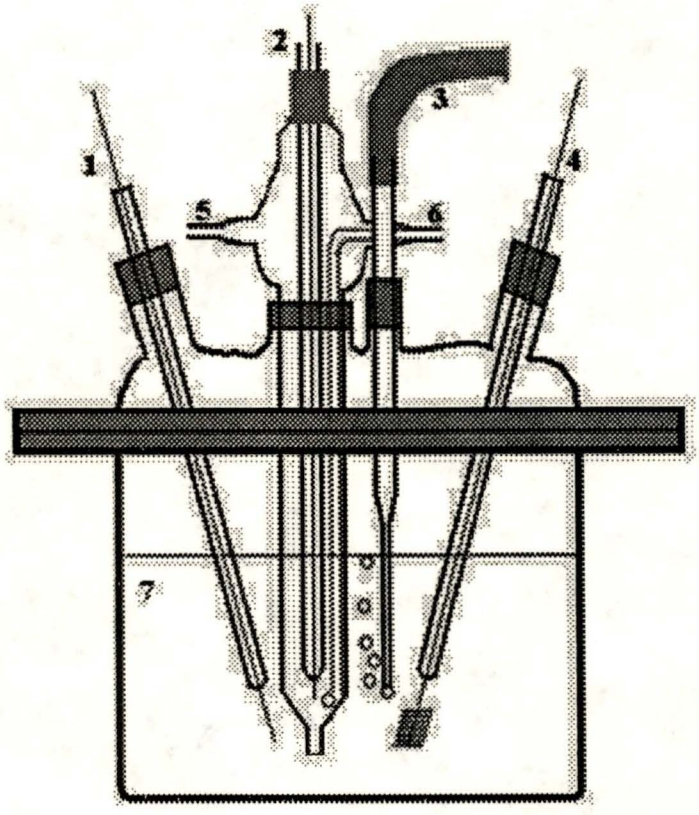

Fig. 2.1 Schematic representation of the cell used in all experiments. 1: working electrode, 2: reference hydrogen electrode, 3: argon gas inlet to keep a non-oxygen atmosphere, 4: counter electrode, 5: hydrogen outlet, 6: hydrogen inlet, 7: electrolyte solution.

2.3 Solution-Exchange Experimental Procedure:

The glassware apparatus used to inject the solution for mixing with the electrolyte solution in the cell is shown in Fig. 2. 2. Before mixing, both solutions were bubbled with argon for more than half an hour. In most cases, after a steady-state CV was achieved following repeated scans, the electrode potential was held at the required value and the injection solution was mixed into the original one by pressure in less than 5 seconds. Any transient current responses were recorded. Another variation to this solution change

experiments is while running the cyclic voltammograms, the solution is injected at the required potential. But it is obvious that the method of holding potentials while injection is much more sensitive than the one with scanning potentials [50].

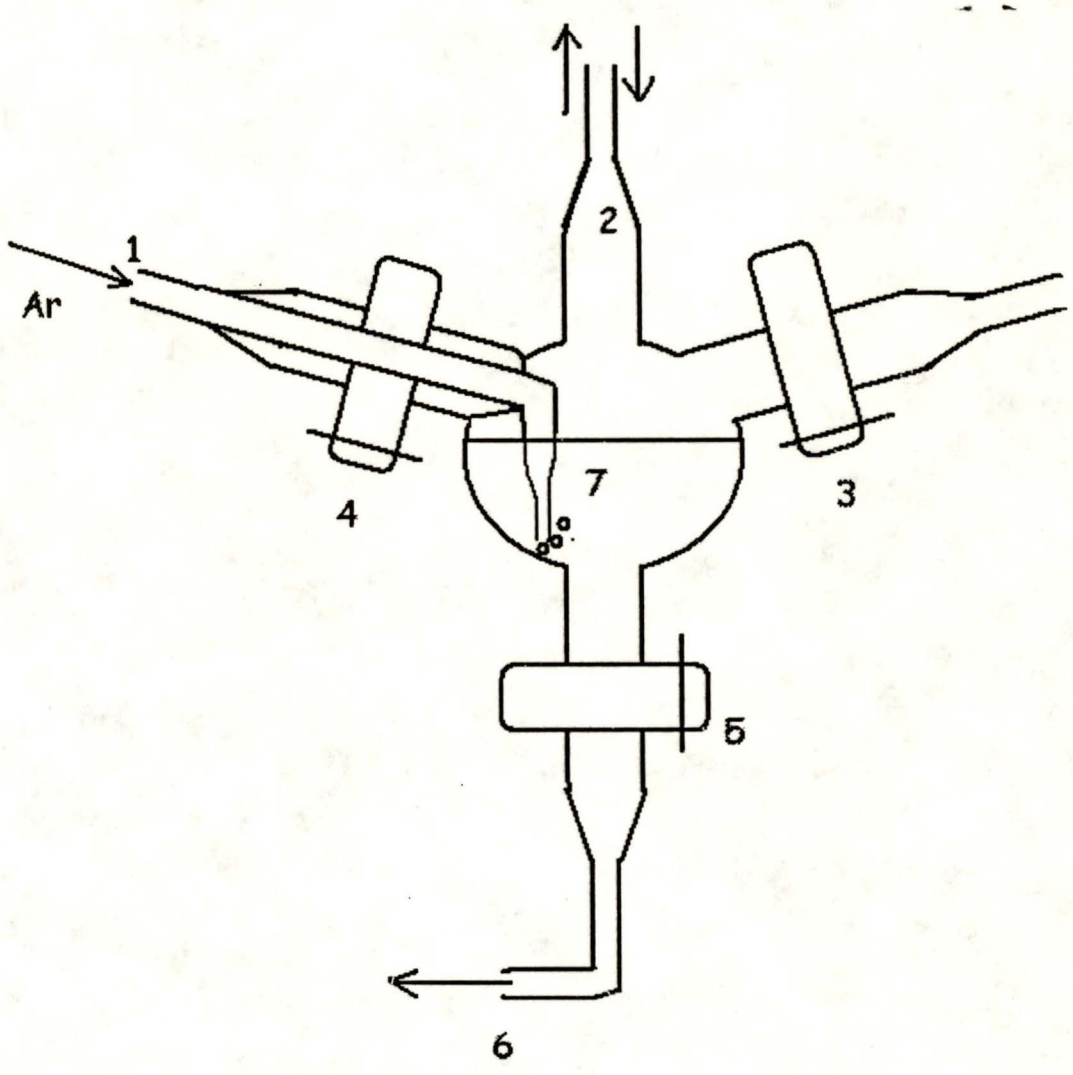

Fig. 2.2 Glassware to inject the mixing solution. The compartment 7 is used to hold the exchange solution. Before injection, Ar is bubbled through inlet 1 to deoxygenate the solution while tap 3 and 4 are off. After long enough time bubbling, i.e. 30 minutes, the outlet 6 is connected to the cell, and tap 3 and 4 are off, tap 5 open and then Ar is connected to inlet 2 to produce the pressure driving the solution to inject into the cell.

2.4 General Electrochemical Methods:

A diagram of the instruments used for electrochemical experiments is shown in Fig. 2.3.

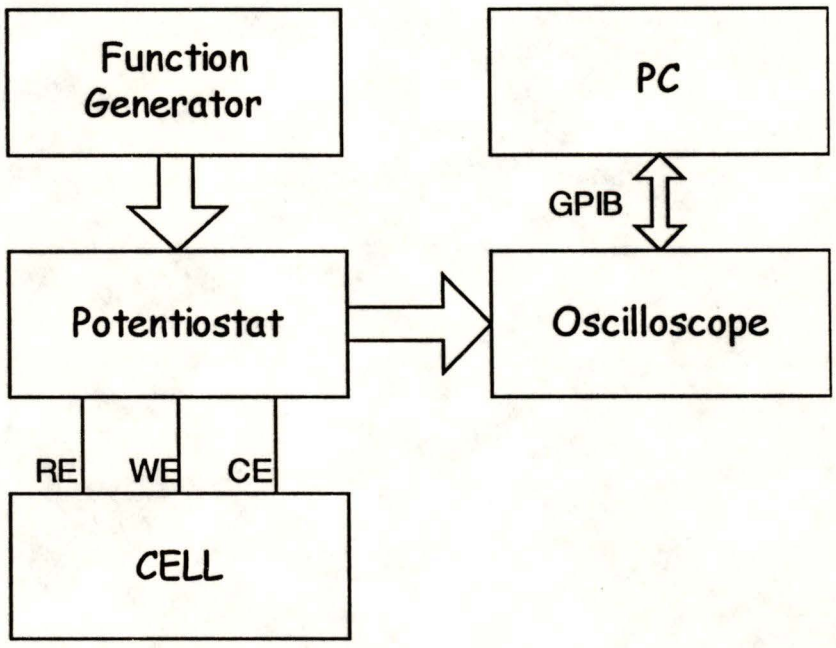

Fig. 2.3 Diagram of instrumentation used for common electrochemical experiment. RE: reference electrode; WE: working electrode; CE: counting electrode.

Cyclic voltammograms were measured by connecting a triangular wave potential from the function generator (EG&G PAR Model 175) to a potentiostat (Hokuto Denko HAB 51 model or a Thompson electrochemistry E401), which applies the signals to the cell. The potential responses of the electrochemical system were collected by the potentiostat and digitized by a Nicolet 530 oscilloscope, which had a GPIB interface with a PC. Current responses were sampled through an extra adjustable resistor paralleled with a capacitor as a filter (Fig. 2.4).

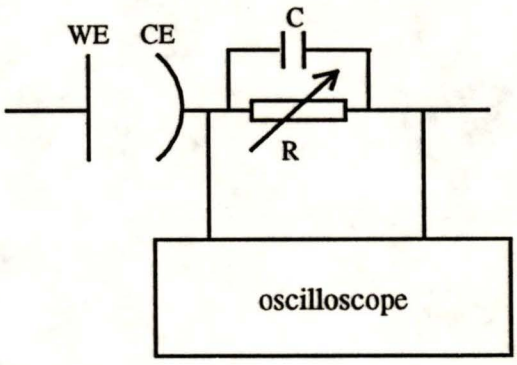

Fig. 2.4 Sampling and filtration circuit to collect current response from the cell.

2.5 Calibration of the Surface Area

For Pt (111) surface, the unit cell area can be calculated as unit cell area = $\frac{\sqrt{3}}{2}\times 2.78^2$ Å^2 (2.78 Å is the unit cell size). Thus we can calculate for a full coverage adsorption of hydrogen atoms on atop sites of platinum, the charge due to this adsorption would be 1.60×10^{-19}/unit cell area = 241 μC cm^{-2}. It is generally accepted that on polycrystalline platinum the hydrogen adsorption charge is 220 μC cm^{-2}. So in this work, the hydrogen adsorption charge density is integrated in CV (about 0.05 to 0.35 V vs. RHE), and divided by 220 μC cm^{-2} to calculate the surface area.

2.6 Data Fitting Methods

The direct logarithmic law between charge density, j, and time, t, for sweep-hold experiments is found for constant-potential conditions; the equivalent expression of current with time was used here instead to fit the data: $j = P_1 + \frac{P_2}{P_3 + t}$. The nonlinear least-squares fitting, which uses χ^2 to judge the fitting results, was implemented in Origin

Version 5, a scientific software from Microcal Software, Inc., and was used to fit the empirical data.. The fitting is an iterative procedure which was run long enough to guarantee all the parameters had converged and also that χ^2 had minimized (more details in the Part 3).

2.7 *Data Recovered from Filtration*

As we know, for a low-pass filter, as shown in Fig. 2.5, the high-frequency part of the signal ($f > \frac{1}{2\pi RC}$) will be removed by the capacitor. Because the experimental results are not just the DC signals, some of transient part needed will also be discarded by the filter and lost. Here we show that the lost signal can be recovered in some degree using a simple calculation.

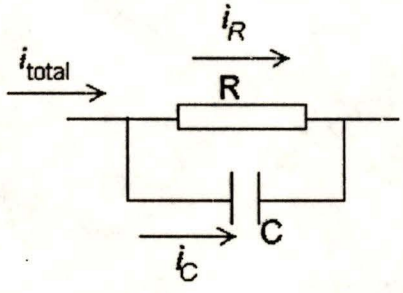

Fig. 2.5 Filtration circuit used to sample current and filter noise. R: sampling resistor, C: filtering capacitor. The current flowing through this circuit would lose some components due to the filtration though that is expected for the noise filtration.

The current from the cell is divided into two parts, one flowing through the resistor and another through the capacitor. Since the measured current is just the part through resistor, the part through the capacitor was lost. A simple calculation shows that:

$$i_{total} = i_R + i_C \qquad (2.1)$$

$$iC = C\frac{d(i_R R)}{dt} \tag{2.2}$$

where i_{total} is the current flowing from the cell, i_R is the current through the sampling resistor and i_C is the current through capacitor. Combining these two equations, we find that

$$i_{total} = iR + RC\frac{di_R}{dt} \tag{2.3}$$

Note i_R is the measured current shown on the oscilloscope. Thus the real current flowing through the cell can be recovered by using Equation 2.3. For numerical calculation of the differentiation of i_R, this formula was used:

$$i_n' = \frac{i_{n+1} - i_{n-1}}{2\Delta t} \tag{2.4}$$

because the current was sampled by oscilloscope in every Δt interval. Here i_n' is the current slope at the nth current data point. i_{n+1} and i_{n-1} are the currents of the (n+1)th and (n-1)th data points respectively. Using a small program the real current flowing through the cell is recovered. The capacitor used in this work was 8.2 μF and the resistor for sampling ranged from 500 Ω to 5 kΩ depending on the sweep rate and magnitude of the signal. For example, when the sweep rate was 50 mV s^{-1} or 100 mV s^{-1}, the resistor used for filtration was 5 kΩ and while the sweep rate was above 2 V s^{-1} a resistor of 500 Ω is used.[1] The Δt in this work is chosen as 10 ms for 100 mVs^{-1} sweeps, and 1 ms for 1 Vs^{-1} sweeps and so on.

---

[1] Please note the validity of using this method to recover the data. The essence is to use Equation (2.4) to calculate the differentiation or slope of the data points. Because these data points are not continuous, but discrete, the differentiation through this equation is just an approximation. Obviously the more steep the slope of the data points, the more error in using this equation. It was verified in this work that errors of fitting those fast scans were larger than those of slow scans. And the time interval the oscilloscope

3 Data & Results

3.1 CV Features of Pt in 0.5 M sulfuric Acid Aqueous Solution

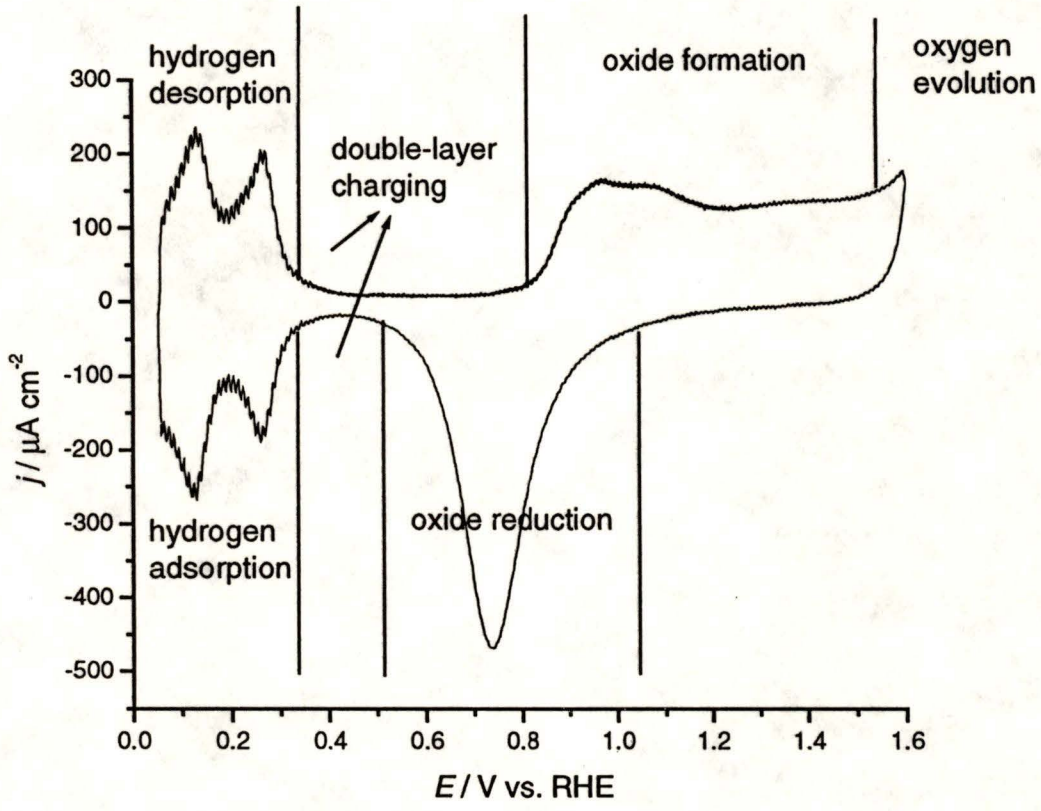

Fig. 3.1 A typical cyclic voltammogram of Pt in 0.5 M H_2SO_4 solution. Sweep rate: 200 mV s^{-1}. The CV in the forward direction is divided into four regions: from hydrogen desorption to double-layer charging and then oxide begins to form and then water dissociates into oxygen.

A typical cyclic voltammogram (CV) of Pt in strong acid solution, e.g., 0.5 M sulfuric acid, is shown in Fig. 3.1. In general the CV is divided into several parts in which different reactions or processes take place.

---

employed to sample the data is also relevant. The smaller the time interval (Δt) is, the more accurate are results using this method.

The reaction in the hydrogen adsorption/desorption region:

$$Pt + H^+ + e^- \rightarrow Pt\text{-}H\ (ads) \qquad (3.1)$$

The multi-peak character of the adsorption/desorption of hydrogen on Pt can be attributed to the many kinds of surface sites, for example, kink, step and ridge, which have different interaction energies with adsorbed hydrogen.

Double-layer charging occurs during the potential scan, the double-layer capacitor (assumed to be constant) is charged or discharged, with the current $i=C \bullet v$, where C is the double-layer capacitance and v is the potential sweep rate applied by a potentiostat. Since the potential is controlled to scan at a certain sweep rate, the double-layer region would be flat if the solution was clean and no other process happened.

The oxide formation and reduction is the topic of this work, though much can be obtained from the literature.

When the potential goes high enough, water can be oxidized into oxygen and evolve:

$$2H_2O \rightarrow 4H^+ + O_2 + 4e^- \qquad (3.2)$$

The terms used below and in other places in this thesis are defined here as follows.

- Hydrogen region: about 0.05 V to 0.35 V vs. RHE in the CV.
- Double-layer region: about 0.35 V to 0.80 V vs. RHE.
- Oxide formation region: from 0.85 V to 1.55 V vs. RHE. The earlier stage of oxide growth will refer to the potential region from 0.85 V to 1.15 V vs. RHE since in this range the oxide growth charge is less than one electron per platinum and, as mentioned in the introduction part, this stage of oxide growth is partly reversible.

3.2 Experiments on Anion Adsorption

Fig. 3.1 is the typical clean platinum CV. If anion adsorption[2] takes place, it would certainly influence the cyclic voltammogram shape. It can be expected that if adsorbed anions occupy the platinum surface sites even in the hydrogen region, then the hydrogen adsorption/desorption charge would decrease. Some anions have a strong interaction with Pt, e.g., chloride, and the adsorption process would even affect the oxidation state of Pt, as will be discussed from the experimental results below. The first study in this work is the adsorption process of sulfuric acid on platinum surfaces because most recent platinum studies were performed in this solution. The effect of bisulfate/sulfate ions adsorption is thus very important to investigate before other experiments.

3.2.1 Bisulfate/Sulfate Adsorption

Fig. 3.2 is a transient current record of injection of $HClO_4$ into H_2SO_4 solution when the potential was held in the double-layer region. A cathodic current response was found though it is very small. And Fig. 3.3 is the equivalent plot for H_2SO_4 injected into $HClO_4$ solution. Anodic current was found first and then a cathodic current.

For the perchloric acid injection into sulfuric acid case, we know, perchloric acid is a very strong acid that dissociates fully. The components of perchloric acid are only H^+ and ClO_4^-:

$$HClO_4 \rightarrow H^+ + ClO_4^- \qquad (3.3)$$

---

[2] Please note the adsorption discussed here is specific adsorption which means there is a chemical interaction between the anions and the platinum surface.

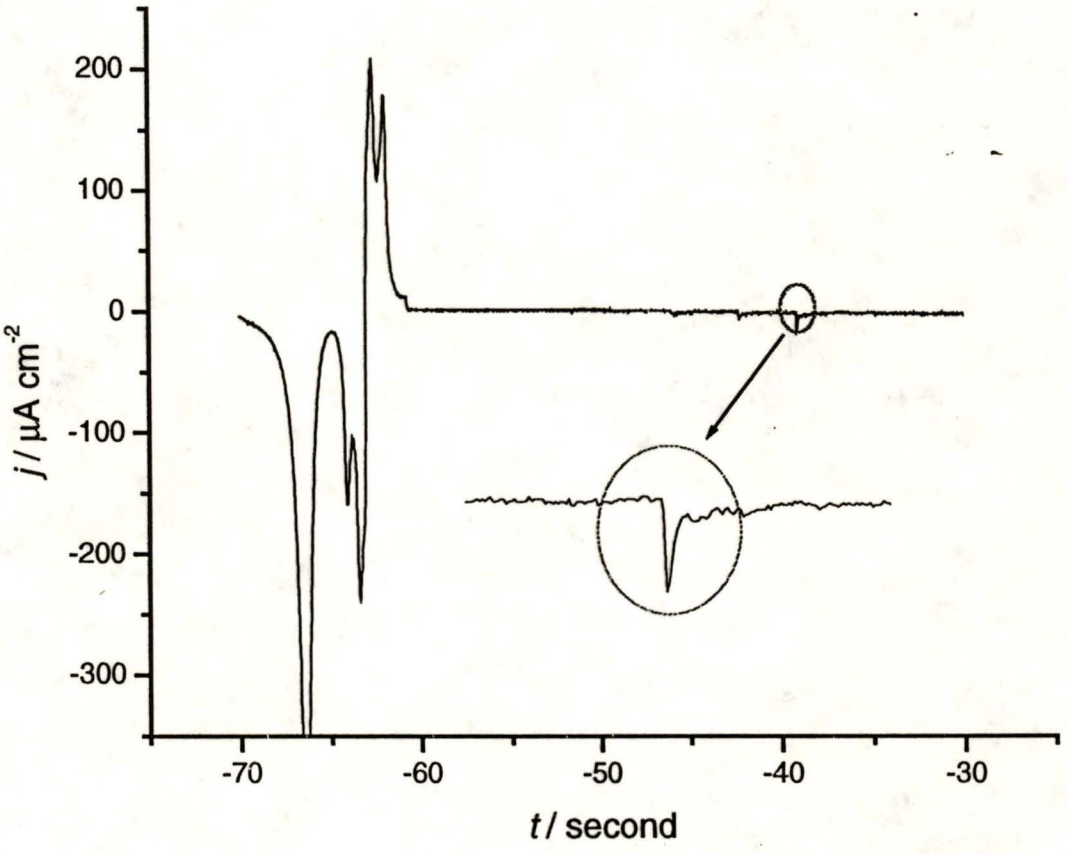

Fig. 3.2 Injection of 1 ml 0.92M $HClO_4$ into 50 ml 0.5M H_2SO_4 while the potential was held at 0.515 V vs. RHE. sweep rate: 200 mV s^{-1}.

Many previous adsorption experiments study the double-layer. For example, Frumkin's work showed that there is nearly no specific adsorption of ClO_4^- on platinum. It is believed that no or very weak chemical interaction occurs between ClO_4^- and platinum. Thus when $HClO_4$ was injected into the H_2SO_4 solution, because of the concentration gradients in the solution, ClO_4^- would diffuse into the double-layer, which behaves like a kind of electron flow toward the surface. That is, a cathodic current transient response results. We know before injection the charges distributed around the electrode are balanced, i.e., if there are 7 positive charges on the surface, there should be

7 negative charges on the solution side of the double-layer. Now there are more negative charges (ClO_4^-) moving from the bulk toward the surface and then into the double-layer region because of the concentration gradients, and then these extra negative charges should be consumed since the electrode potential is held constant and the double-layer charge should be kept balanced. So it is similar to the way that some electrons are consumed on a surface, which is a reduction process. But this kind of current is due to the double-layer charging process, and is not Faradaic.

But certainly it is not the same simple case for injection of H_2SO_4 into $HClO_4$. We observed an anodic current response followed by a cathodic response, which means there is a different injection effect of sulfuric acid from perchloric acid. There should be another process happening to explain this anodic transient. We can explain the difference of these two results from difference in the chemistry between the two acids. Although both of them are strong acids, for sulfuric acid, that it is strong only means that the first step of dissociation is carried out fully. The second proton is only partly dissociated.

$$H_2SO_4 \longrightarrow HSO_4^- + H^+ \qquad (3.4)$$

$$HSO_4^- \rightleftharpoons H^+ + SO_4^{2-} \qquad (3.5)$$

We argued above that there is no specific adsorption of ClO_4^- on platinum. But this does not guarantee there is no specific adsorption of bisulfate or sulfate onto platinum, especially because bisulfate is not as symmetrical as sulfate or perchlorate ions. The following reaction is possible when sulfuric acid is injected into perchloric acid.

$$Pt + HSO_4^- \longrightarrow Pt\text{-}HSO_4(ads) + e^- \qquad (3.6)$$

which gives an anodic transient current. And similar to the case of injection of $HClO_4$ into H_2SO_4, the diffusion of bisulfate and sulfate ions behaves like an electron flow

toward the electrode and the extra charge flow should be consumed on the electrode. So the combination of these two currents gives the plot of Fig. 3.3.

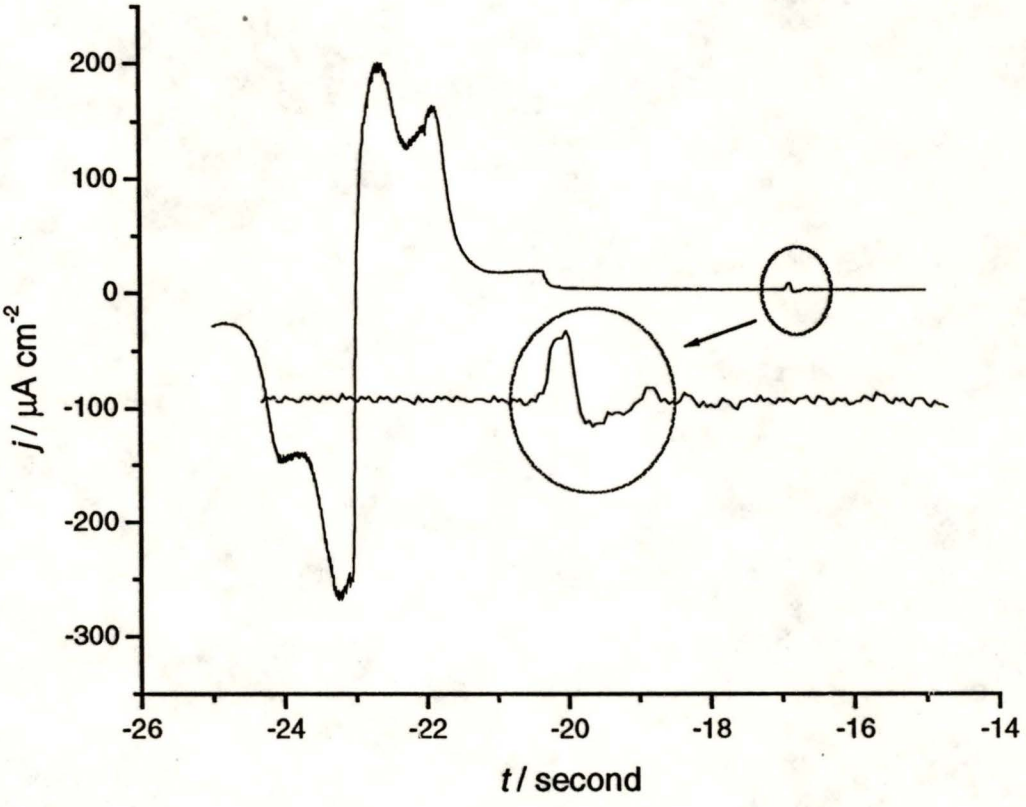

Fig. 3.3 Injection of 1 ml 0.5 M H_2SO_4 into 50 ml 0.92 M $HClO_4$ solution when the potential was held at 0.593 V vs. RHE. Sweep rate: 200 mV s^{-1}.

As stated above, ClO_4^- is considered to be a non-polarizable ion. There is no chemical interaction of the adsorbed ClO_4^- to the Pt electrode. The nature of adsorption is only the physical electrostatic attraction. Thus the CV of Pt in 1 M $HClO_4$ can be chosen as the baseline of Pt behavior in acid solution to investigate adsorption of other anions. Fig. 3.2 and Fig. 3.3 show some kind of specific adsorption of bisulfate/sulfate. We also

expect that there will be some differences in the CVs besides the solution exchange transients. Fig. 3.5 is a plot of CVs of Pt in $HClO_4$ before and after some H_2SO_4 solution was mixed in.

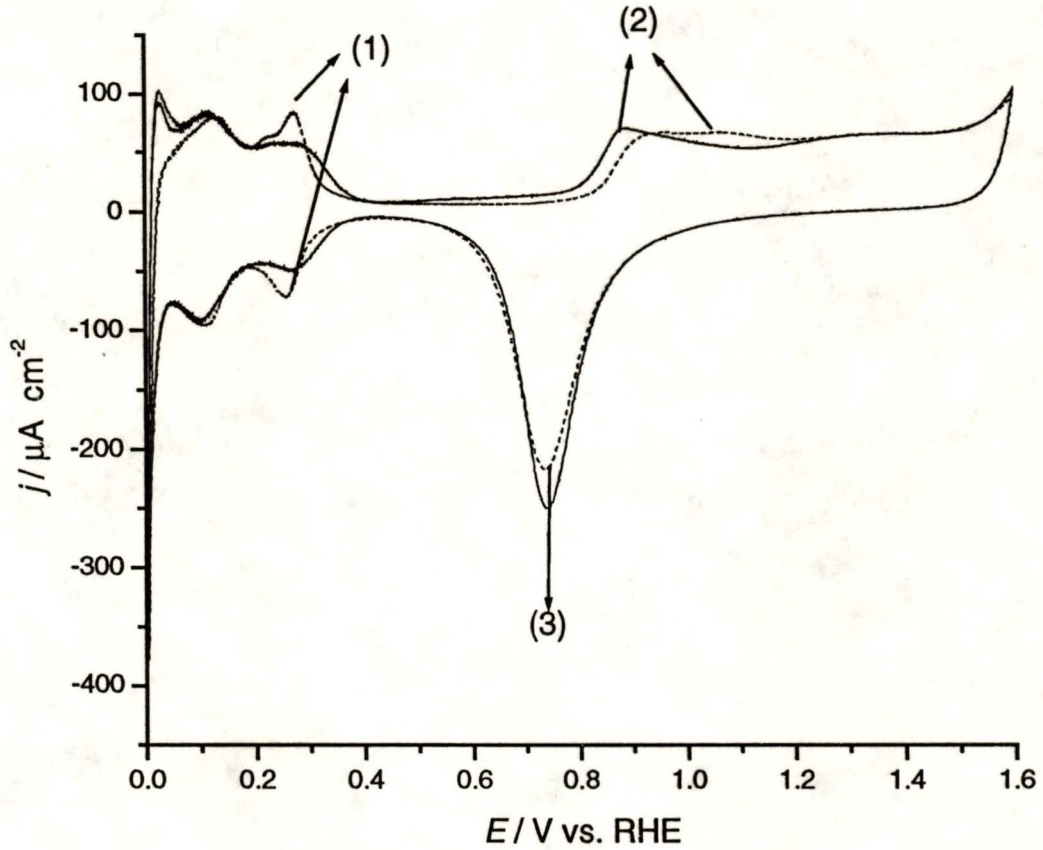

Fig. 3.4 CVs of Pt in 100 ml 0.92 M $HClO_4$ solution before and after the mixing of 20 ml 0.5 M sulfuric acid. Solid line: in pure $HClO_4$ solution. Dotted line: in mixture of the two acids. Sweep rate: 100 mV s^{-1}. Three main differences of these two CVs are marked as (1)-(3).

It is obvious that there are three differences between the two CVs:

(1) The shape of the second peak of hydrogen adsorption changes or shifts though the total charge does not change much.

(2) The double-layer region is flat when the solution contains sulfuric acid while in pure perchloric acid solution there is a small current.

(3) From the reduction peak of platinum oxide, it can be observed that in pure $HClO_4$ solution more oxide is formed than in the mixture of the two acids.

The only explanation for these differences is that bisulfates/sulfates adsorb on Pt and they block the surface sites and delay oxide growth. The start of the adsorption is at the second peak of hydrogen desorption/adsorption (0.25 to 0.3 V), where it changes the hydrogen adsorption/desorption peak shape. It is difficult to decide where they desorb to allow the oxide growth. Some of them seem to remain on the surface and then less oxide is formed compared to the same scan in pure perchloric acid solution. This agrees with the literature results especially the FTIR spectra and radiotracer experimental results. The main result of this work is that it is found the adsorption of bisulfate/sulfate ions occurs with charge transfer, which cannot be studied by infrared spectroscopy and radioactive element assay [35, 43, 45].

3.2.2 Halide Adsorption

Cl^- and SCN^- were tested in these experiments. Their adsorption gives anodic current responses whenever they were injected into the solution in the double-layer region or in the earlier stage of oxide growth. Fig. 3.5 is a plot of the current response for injection of Cl^- into H_2SO_4 solution in the double-layer region. The same plot for SCN^- injection into H_2SO_4 solution is in Fig. 3.6.

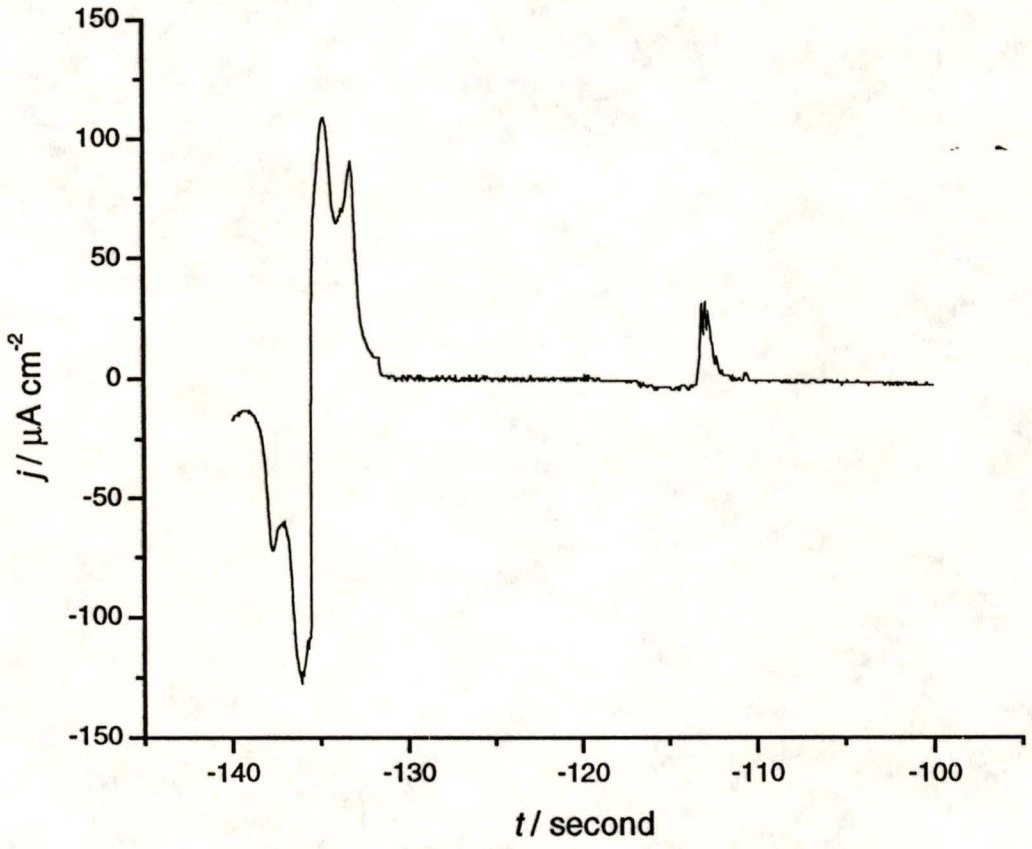

Fig. 3.5 Injection of 1ml 0.1 M KCl into 50 ml H_2SO_4 solution while potential was held at 0.445V vs. RHE. Sweep rate: 100 mV s^{-1}.

Because from the CV we know that both Cl^- and SCN^- are not active on the Pt surface in the double-layer potential window, the anodic current cannot be attributed to their oxidation. However, there can be a double-layer changing current, similar to the case of adsorption of HSO_4^-. They are able to adsorb on the surface as shown by the reduction of the H adsorption peaks after injection. Thus, the explanation of the anodic transient current response of these two ions is simple. The reactions can be written as:

$$Pt + Cl^- \rightarrow Pt\text{-}Cl + e^- \quad (3.7)$$

$$Pt + SCN^- \rightarrow Pt\text{-}SCN + e^- \quad (3.8)$$

The above two reactions are oxidation processes. And their adsorption must be very strong because a second injection did not give any further transient signals.

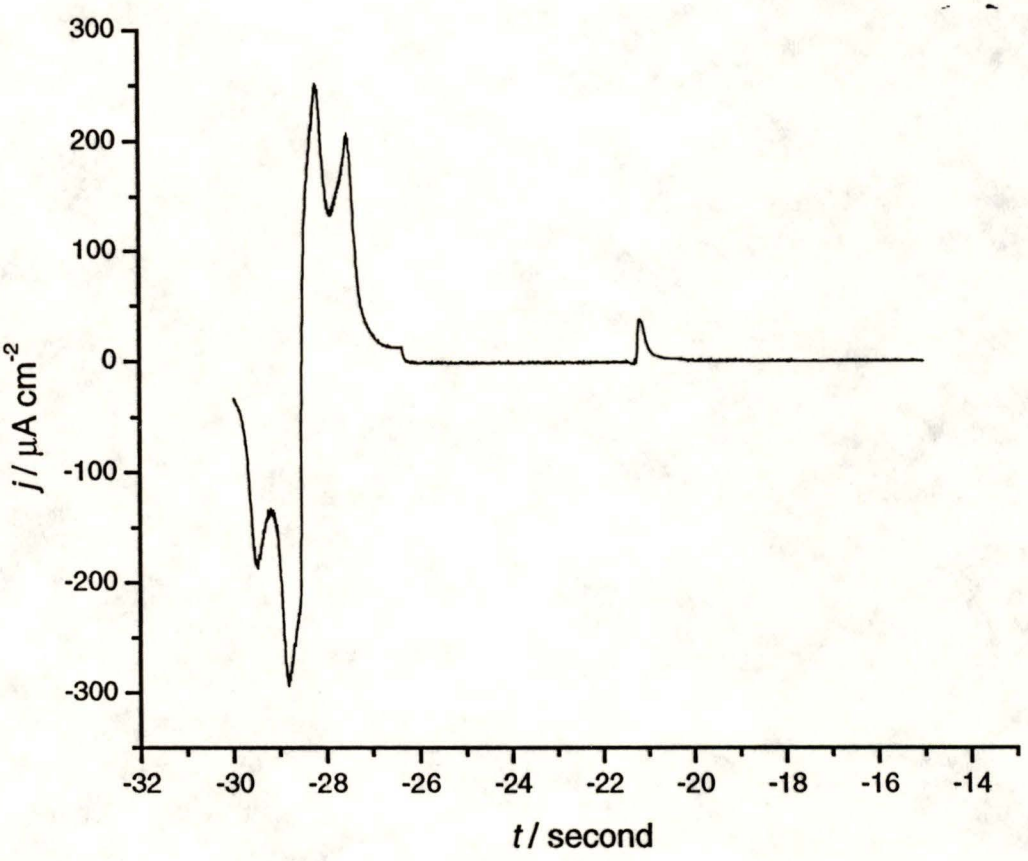

Fig. 3.6 Injection of 1 ml 0.1 M KSCN into 50 ml H_2SO_4 solution while potential was held at 0.485 V vs. RHE. Sweep rate: 200 mV s^{-1}.

To test for the influence of chloride on the oxide growth, the following experiment was performed: the CV was scanned to the early stage of oxide growth, the potential was held and then the chloride-containing solution was injected. Then the potential was reversed and scanned back. The CV is shown in Fig. 3.7.

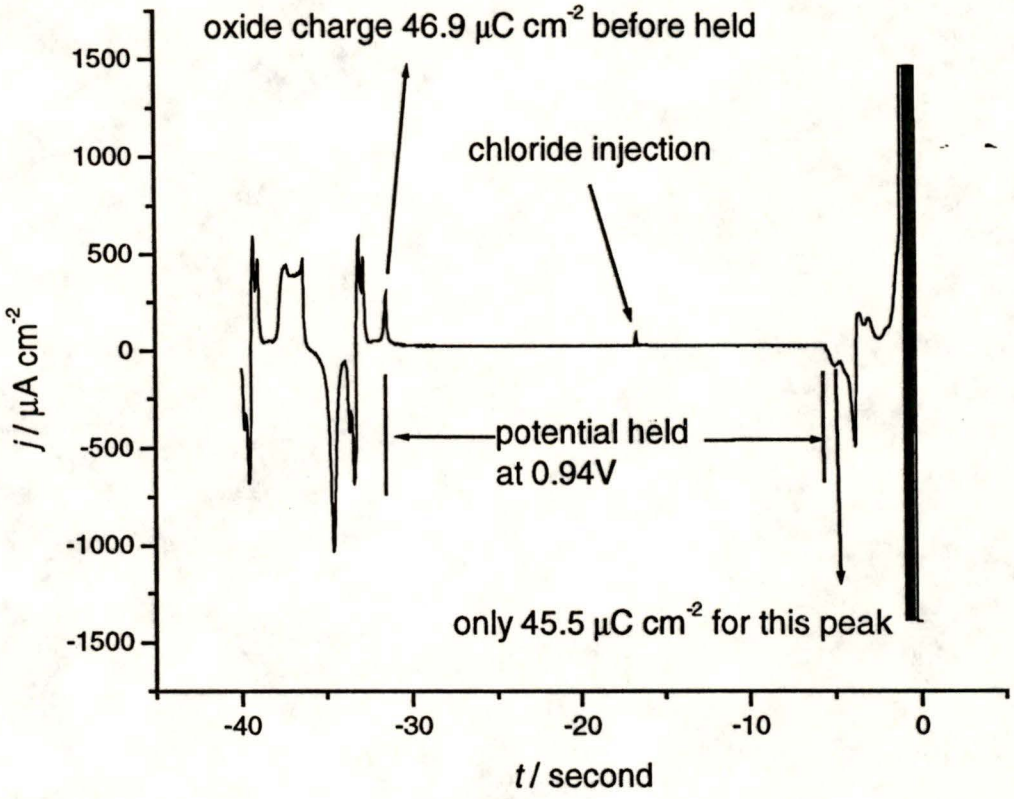

Fig. 3.7 Injection of chloride into 0.5 M sulfuric acid when the potential was held in the early stage of oxide growth and then swept back.

The charge due to oxide before injection of Cl^- is about 159+47=206 μC cm^{-2} where 159 μC cm^{-2} is the charge after the hold but before the injection. It is possible some oxide might be reduced in the hydrogen region. The difference between the hydrogen adsorption and desorption charges in this plot (after injection) is about 68 μC cm^{-2}. So the total reduction charge of oxide is 68+45=113 μC cm^{-2}, which is much less than the oxidation part. This suggests that the chloride in solution or adsorbed would dissolve the oxide already grown. The possible mechanism is similar to the dissolution of platinum or gold in a mixture acid of nitric acid and hydrochloric acid:

$$PtO_x + 4Cl^- + \frac{x}{2}H^+ + (\frac{x}{2} - 2)e^- \rightarrow PtCl_4^{2-} + xH_2O \qquad (3.9)$$

3.2.3 Acetonitrile (AN) and 1-Butanethiol

The adsorption of AN on a Pt surface is of a particular interest though it has been studied by Conway [39]. In the double-layer region and also in the earlier stage of Pt oxide growth, AN is chemisorbed with a cathodic transient current. Fig. 3.8 is a plot of the current transient for injection of AN into sulfuric acid at a potential in the earlier stage of Pt oxide growth. Conway compared the results of injection of AN and methanol which gave an anodic transient current response and concluded that there was no dissociative adsorption of the methyl-H atoms. Therefore the –CN group was adsorbed directly at the Pt surface with the –CN π-orbitals conjugated with the metal electron system.

It was also found by Conway that the adsorbed AN on the Pt surface undergoes a more or less reversible oxidation in the double-layer potential region. This suggests that AN would be oxidized when injected at potentials in the earlier stage of oxide growth. Thus, there must be some other processes happening to produce the cathodic transient current response. One possibility is that AN replaces the anions already adsorbed on the surface and the anions diffuse and leave the double-layer to give cathodic current response. The anion cannot be ClO_4^- because in the 0.92 M $HClO_4$ solution the diffusion of ClO_4^- keeps the charge balance and cannot be detected. Also, because there is no chemical interaction between Pt and ClO_4^-, the adsorption/desorption of ClO_4^- would not produce any current. So one probable anion is OH^-. If we neglect the oxidation of AN here, the chemical processes can be represented as:

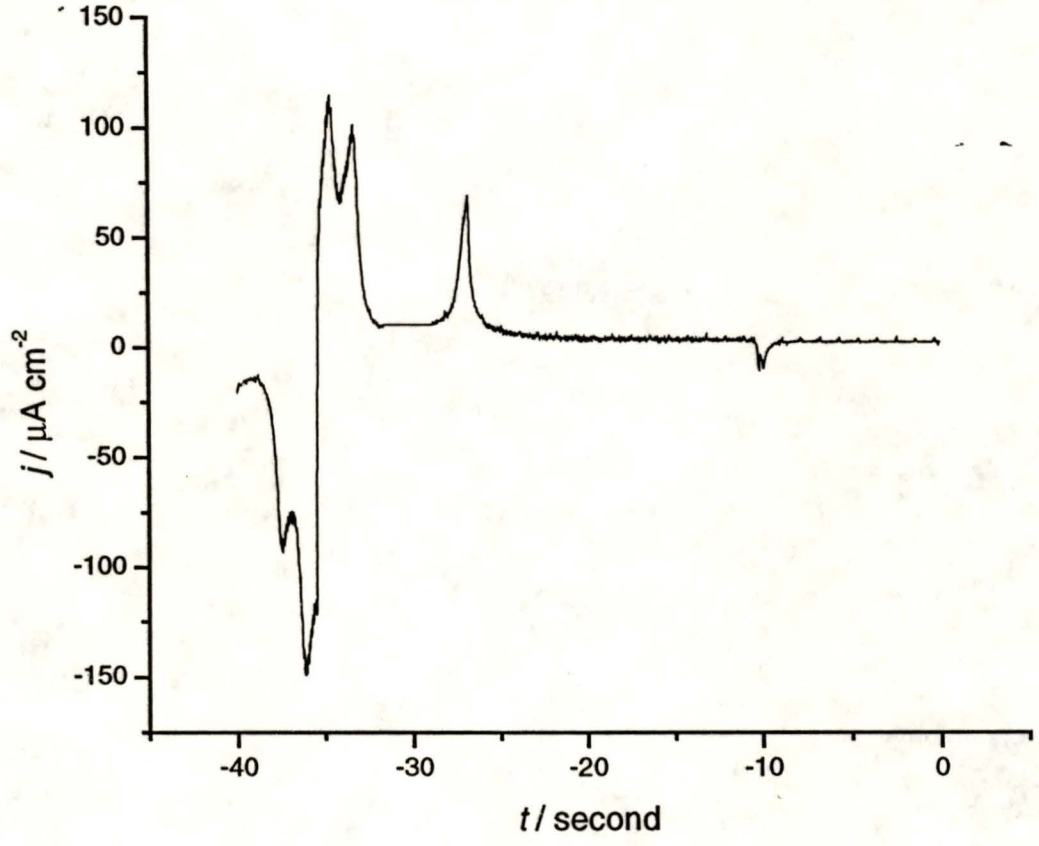

Fig. 3.8 Injection of 10 ml acetonitrile into 50 ml 0.5 M H_2SO_4 solution while potential was held at 0.922 V vs. RHE. Sweep rate: 50 mV s^{-1}.

$$Pt\text{-}OH + H^+ + e^- + CH_3CN \rightarrow Pt\text{-}NCCH_3 + H_2O \quad (3.10)$$

or

$$Pt\text{-}OH + CH_3CN + e^- \rightarrow Pt\text{-}NCCH3 + OH^- \quad (3.11)$$

Similar to the adsorption of SCN^-, the addition of 1-butanethiol into sulfuric acid in which a Pt electrode is held potentiostatically at a potential in the double-layer potential region invokes an anodic transient current, which is shown in Fig. 3.9. It was also found from the CV after injection that 1-butanethiol is stable on the Pt electrode in the double-layer region. Thus the anodic current response can only be attributed to the adsorption of

1-butanethiol. As suggested from the adsorption of halide ions, the anodic transient can be explained by this reaction:

$$Pt + HS(CH_2)_3CH_3 \rightarrow Pt\text{-}S(CH_2)_3CH_3 + H^+ + e^- \quad (3.12)$$

which is a dissociative adsorption process.

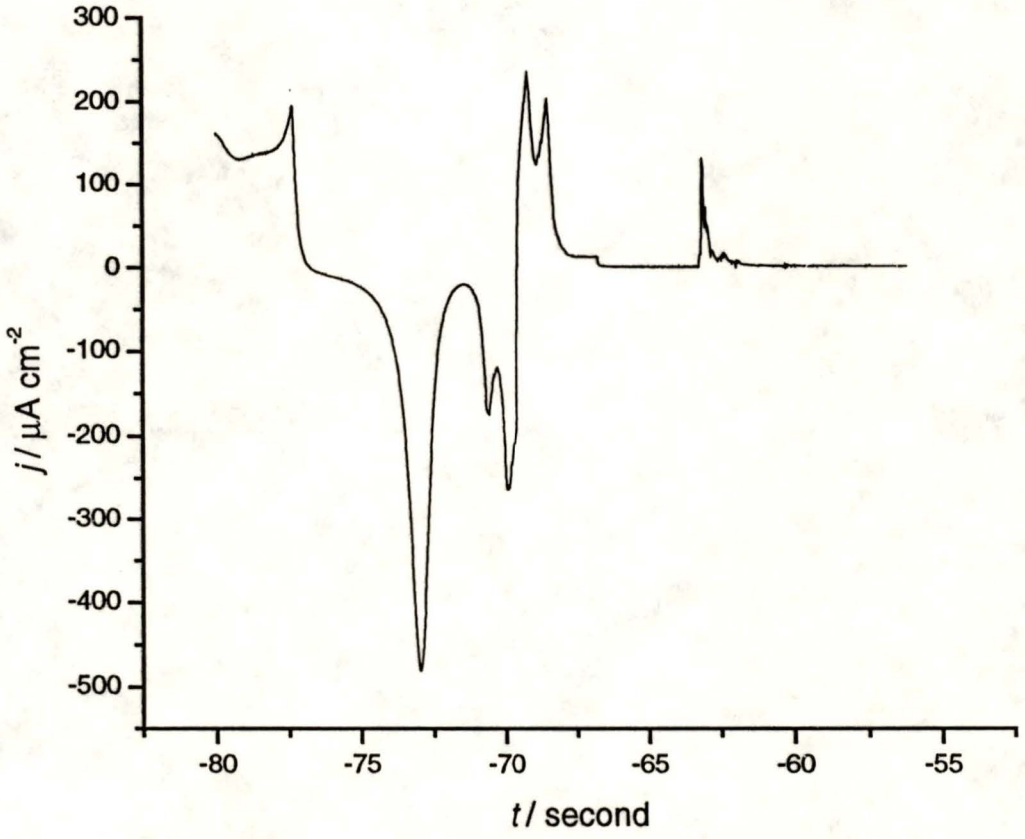

Fig. 3.9 Injection of 0.5 ml 1-butanethiol into 50 ml H_2SO_4 solution while the potential was held at 0.63 V vs. RHE. Sweep rate: 200 mV s^{-1}.

To check this mechanism by integrating the charge of adsorption was not feasible here because 1-butanethiol is not soluble in aqueous solution. Even bubbling the solution with argon hard for additional stirring, 1-butanethiol did not distribute evenly in the solution (the density of this thiol is less than water and it stayed on the top layer). Thus it

is difficult for the electrode to contact the thiol. This is seen from the CV after injection. The oxidation current of 1-butanethiol was found to increase and then become constant after some cycles.

3.2.4 Summary on the Anion Adsorption Effect:

The anion effects on platinum surface can be summarized as these three kinds:

(1) There is no chemical interaction between the anions and platinum. If this kind of anion is also inactive at the potential studied, then there are only small transients expected due to the charge transition because of the concentration gradients. This is the case for ClO_4^- studied above.

(2) There is no interaction between the anions and platinum, but the anions are active on the surface, that means it can be reduced or oxidized. It is expected that some transients (oxidation or reduction current) besides the charge transition driving by concentration gradients. No anions of this type are studied here.

(3) The anions are not active at the potential studied but have strong or weak interactions with the surface. The adsorption process would in some degree oxidize or reduce the surface. If there are already some adsorbates on surface and the injected anion has a stronger interaction with platinum then the latter will replace the old adsorbate and give a reduction or oxidation transient.

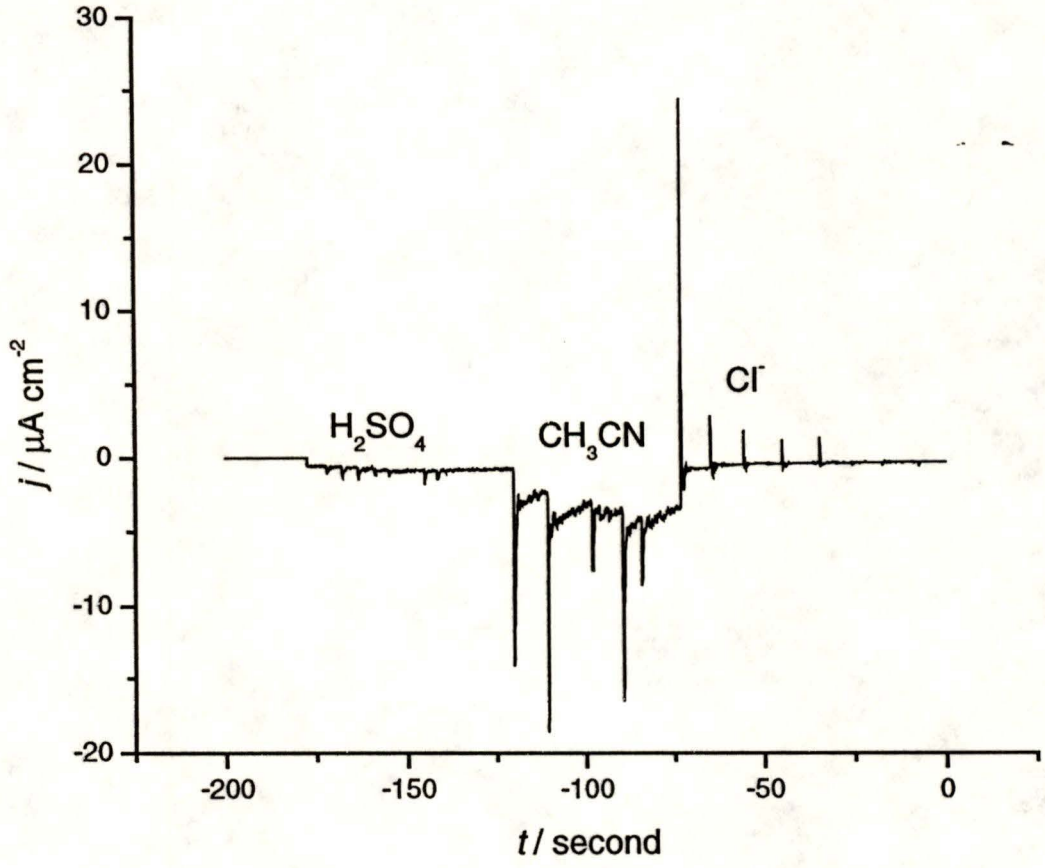

Fig. 3.10 Injection into $HClO_4$ which has already been injected by H_2SO_4 for three times by the following anions and molecules in order: 7 times of H_2SO_4 following by 5 times of AN and then 5 times of Cl^-, when potential was held at 0.505 V vs. RHE.

From the experimental results above, it is suggested that the adsorption of ClO_4^- and HSO_4^-/SO_4^{2-} is much weaker than halide ions and also acetonitrile and thiol. The order of these strong adsorbates was investigated from the experiments by changing the injection order. Fig. 3.10 is a plot of injection of seven times of 1ml H_2SO_4 followed by 5 times of acetonitrile and then 5 times of chloride into $HClO_4$ solution already injected by H_2SO_4 three times. Because there are already some bisulfate/sulfate ions in solution, the injection of sulfuric acid again did not produce any anodic transient but only the cathodic

part. It is clear in this plot that the adsorbed bisulfate or sulfate ions are easily replaced by the acetonitrile and then the acetonitrile can be replaced by chloride. Thus the order of the interactions of these adsorbates with Pt is as follows:

ClO4- < SO_4^{2-}/HSO_4^- < CH_3CN < Cl^-, SCN^-, 1-butanethiol.

3.3 *Hydrogen-Saturated Solution Experiments*

Easily-adsorbed small organic molecules and anions such as chloride, which can behave like an indicator for the platinum surface, but hydrogen or oxygen molecules can also probe the surface since hydrogen can be oxidized on Pt nearly in the whole CV potential region and oxygen in solution is also very sensitive because of its reduction. The idea of using hydrogen as indicator originated from the study of bisulfate/sulfate adsorption in this work by the scheme that hydrogen in the solution would compete with the bisulfate/sulfate ions to adsorb on the surface and then some features of bisulfate/sulfate adsorption would be found. Unfortunately such results were not detected. But it is found the hydrogen can be a nice indicator of the oxide growth, which was unexpected. The voltammograms of platinum in 0.5 M sulfuric acid with and without hydrogen saturation are shown in Fig. 3.11.

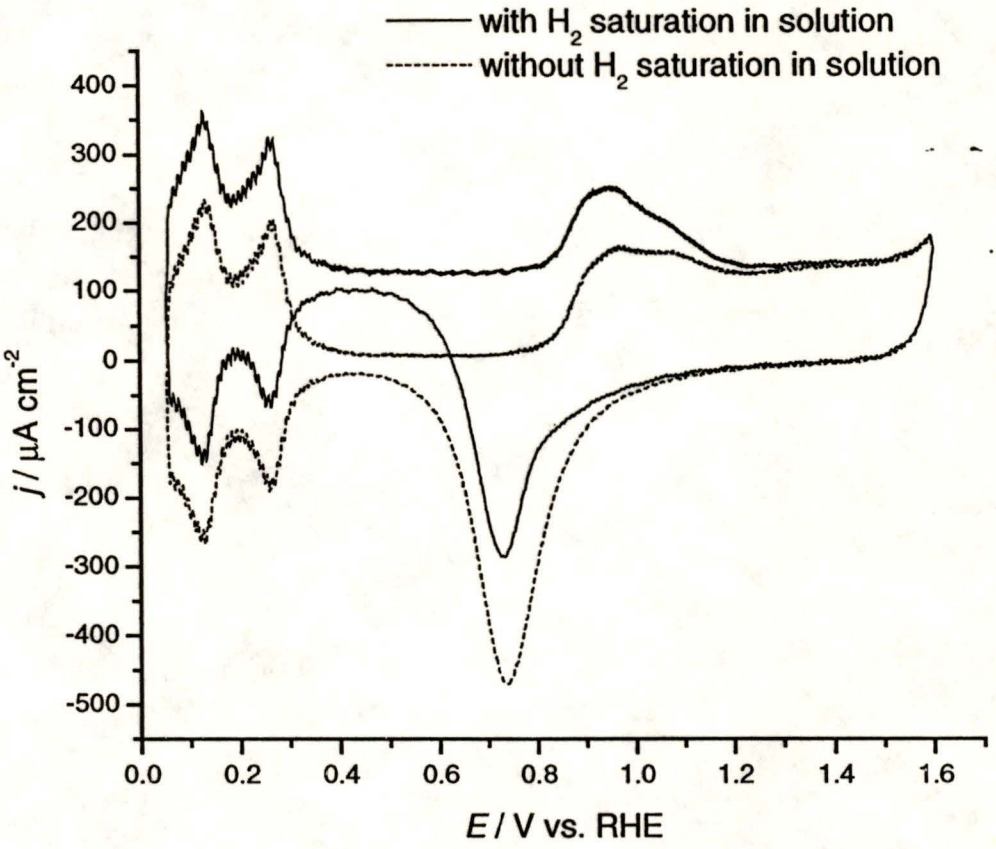

Fig. 3.11 Voltammograms of platinum in 0.5 M sulfuric acid with and without hydrogen saturation. With hydrogen bubbling in the solution, the CV shifts due to the hydrogen oxidation on the surface. Sweep rate: 200 mV s^{-1}.

Obviously, the current shift in this voltammogram is due to the hydrogen oxidation on the surface. Theoretically, hydrogen can serve as a kind of indicator for bare platinum sites since we know that hydrogen can only be oxidized on the platinum surface, not on the platinum oxide surface. This is also clear from the CV above: before the oxide growth, nearly all of the current shifts by the same value in the anodic direction. But when the oxide starts to grow, i.e., from potentials higher than 0.85V, the shift diminishes and when more oxide is on the surface, the two CVs converge, which means that no hydrogen can be oxidized at that potential. The two reactions: hydrogen oxidation and

oxide growth compete for the active surface sites. The current difference between the two curves is presented in Fig. 3.12.

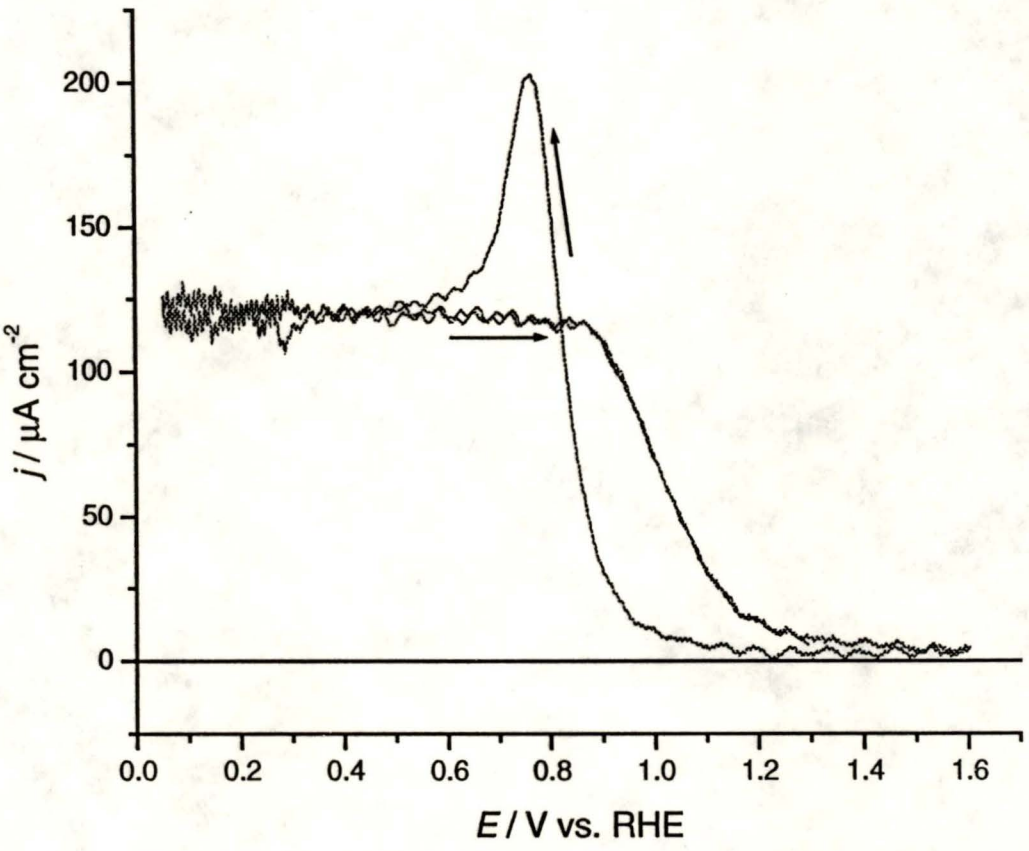

Fig. 3.12 Current difference of the two CVs presented in Fig. 3.9. The current shift due to hydrogen oxidation is nearly constant before oxide growth, i.e., 0.85 V vs. RHE and then it decays.

In the forward sweep, below 0.85 V, the current shift due to hydrogen oxidation is independent of the potential, which also implies that the hydrogen oxidation reaction is diffusion limited (electrochemical control would show an increasing current as the potential became more positive). That the solution was saturated by hydrogen was verified by using a platinum electrode in the same solution without a separate

compartment as the reference hydrogen electrode. Thus we can assume that in this potential region the electrode surface was fully active for hydrogen oxidation. When the oxide grows, the current difference begins to decrease and at potentials higher than ca. 1.15 V the current shift is nearly zero. A picture which explains these results is as follows:

1) Before oxide growth, only hydrogen oxidation takes place and the surface is fully clean. In the surface coverage (θ) concept, $\theta=0$ or $1-\theta=1$.
2) After 1.15V vs. RHE, the surface is fully covered by oxide and no naked platinum sites exist on the surface. At this time, $\theta=1$ or $1-\theta=0$.

Now, what is most interesting is the part where the current difference decays, i.e., for potentials between 0.85V and 1.15V. As we know, the oxide amount can be estimated from the charge of the CV by integration. This leads to a plot of free surface coverage inferred from the hydrogen oxidation current vs. oxide amount inferred from integration of charge, which is shown in Fig. 3.13. Here the horizontal axis uses the unitless value of $\sigma/220\ \mu C\ cm^{-2}$ which is the number of electrons per platinum.

The plot of this curve follows the line of the function $f(x)=1-x$, though not exactly. This indicates that after one electron oxidation per Pt takes place, there are nearly no free surface sites for hydrogen oxidation. This leads to two conclusions about oxide growth and hydrogen oxidation:

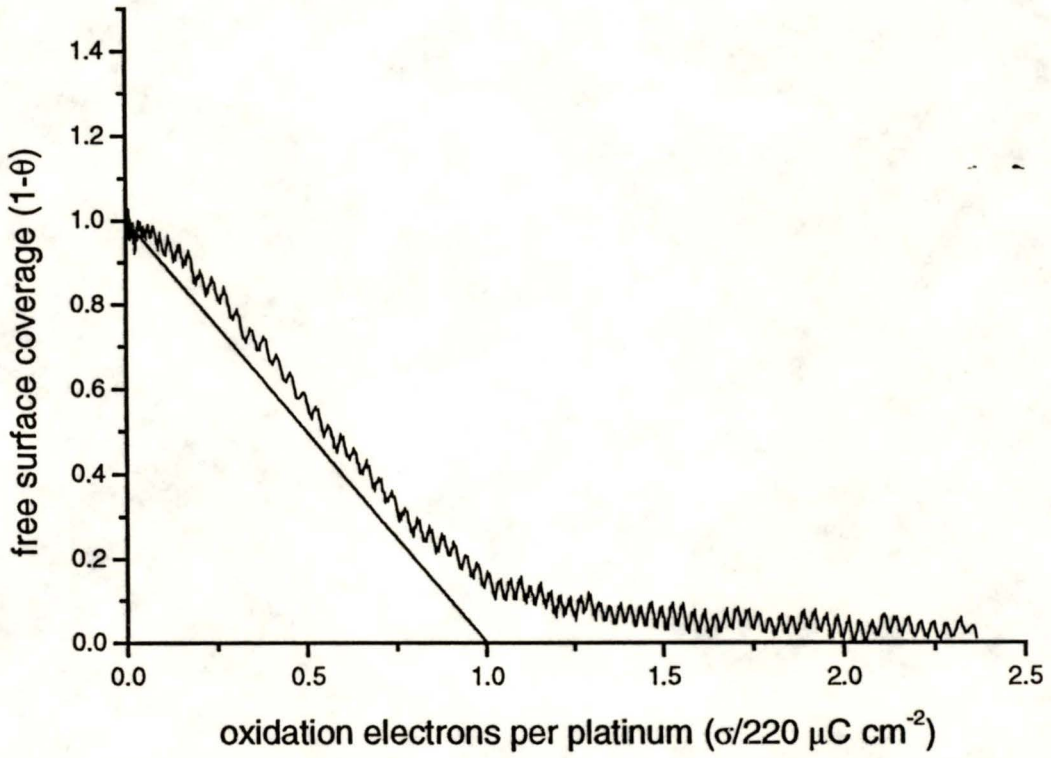

Fig. 3.13 Plot of free surface coverage inferred from the hydrogen oxidation current with the oxidation electrons per platinum calculated from the oxide charge integration.

1) The earlier stage of oxide growth give a Pt(I) species and one possible form is PtOH. If the oxidation state is higher than one, then the hydrogen oxidation current should not decrease to zero after one electron per platinum oxidation. At least there should be half of the surface sites not covered by oxide if the adsorption of other anions is neglected, as has already been assumed.
2) How does the oxide grow in the early stage? The curve in Fig. 3.13 shows a small deviation from the function $f(x)=1-x$. If there was exact agreement, then it means that the oxide on the surface is uniform because only uniform PtOH or some other Pt(I) oxide on the surface with one-electron oxidation could occupy all the surface

sites and prevent hydrogen oxidation. The upward trend shows that when one electron oxidation has been reached, the hydrogen oxidation current does drop to a small value, but not zero. This implies that oxide PtOH or some other Pt(I) oxides are not so uniform on the surface and there is some oxide growth on top of the oxidized platinum rather than the free surface sites, which is very possible. This will be discussed further below.

3.4 Sweep-Hold Experiments to Study Kinetics

To study the kinetics of oxide growth, sweep-hold experiments were performed. The basis for this kind of experiment is that by controlling the sweep period one can get the oxide charge to any desired value. The object in the kinetics of platinum oxide growth is to find a rate law or mechanism to get a reasonable explanation of the CV shape. As shown in Fig. 3.1, the oxide growth starts with some bumps and then is a nearly flat region. Conway *et al* did some CV in high purity sulfuric acid solutions and then separated those bumps into three peaks (OA1-3). He argued that those peaks were due to the formation of Pt_4OH, Pt_2OH, and PtOH, respectively. The group also did some potential step experiments and concluded a direct logarithmic rate law which has such an expression: [29]

$$j = \frac{d\sigma}{dt} = a\exp(-b\sigma) \tag{3.13}$$

Later Harrington [31] did some sweep-hold experiments and tried to find more information about a and b in the above equation. He deduced a to be exponential with the applied potential and b to be constant. But the experimental results seem not that simple

and need more investigation. That's the objective of these series of sweep-hold experiments.

3.4.1 Experiment Data and Fitting Results

In this work a series of sweep-hold experiments were performed similar to experiments of Conway and Harrington: sweep the potential at a certain sweep rate v and hold at some potential, E_h. Different sweep rates from 50 mV s^{-1} to 4 V s^{-1} were used for the sweep period and hold potentials from 1000 mV to 1600 mV. A typical plot of the voltammogram is shown in Fig. 3.14, which gives the general current response for a sweep-hold experiment. As shown in the figure, the potential was scanned at 100 mV s^{-1} to 1.20 V vs. RHE. The start of the hold period at 1.20 V defines t_0 (zero in this plot) and the current density then decays.

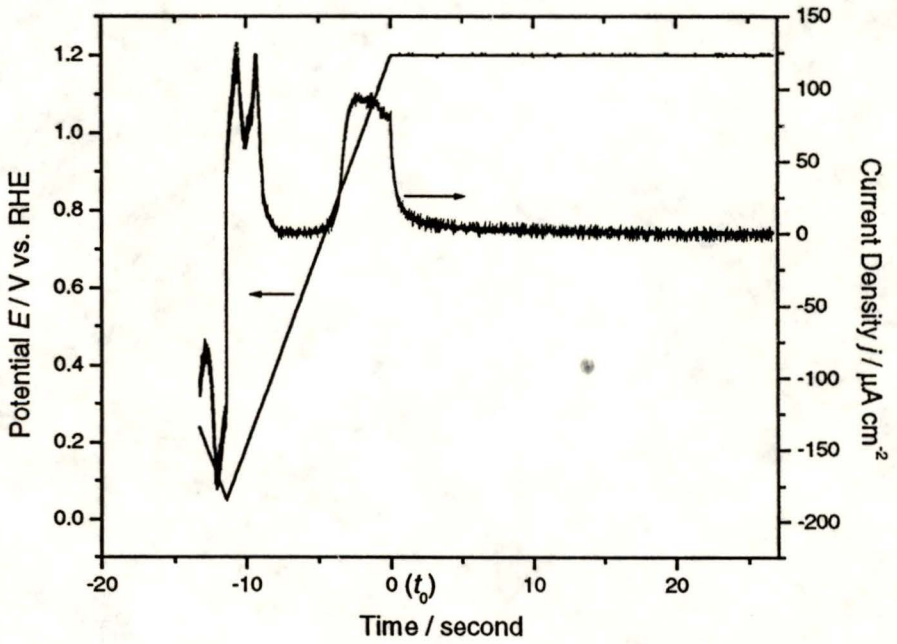

Fig. 3.14 A typical plot of sweep-hold experiments. The sweep rate for the triangular period of potential is 100 mV s^{-1}. Potential held: 1200 mV.

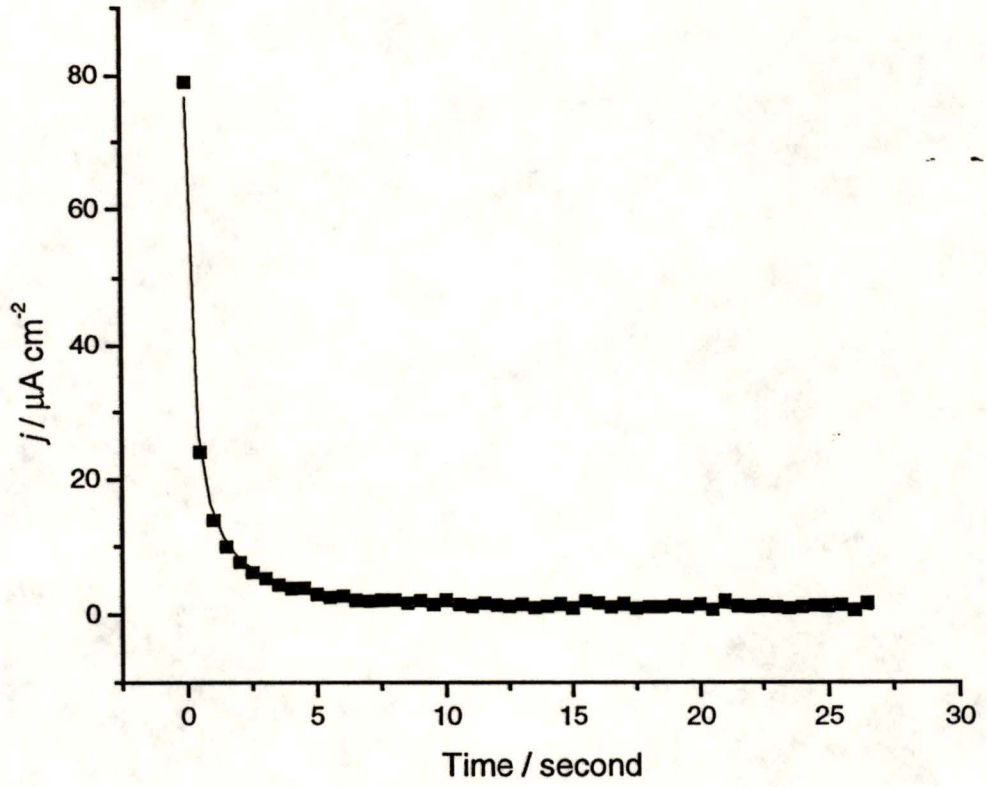

Fig. 3.15 A typical plot of the raw data and fitted curve. Sweep rate: 100 mV s^{-1}. Held potential: 1200 mV. Fitting Parameters: P_2=18.60 ± 0.07446, P_3=0.26 ± 0.00203. About 1 out of every 50 data points are shown here. Line is the fitted curve. The nonlinear least square error is expressed in χ^2. χ^2=0.256 (for about 2000 data points) **for this example.**

Fig. 3.15 shows a typical fit of the current density decay data points. The quality of fit is give by $\chi^2 = \frac{1}{N-3}\sum_{i=1}^{N}(j_{\text{fit},i} - j_{\text{experiment},i})^2$, where N is the number of data points, 3 represents three parameters used in fitting. This had a value of 0.256 for the 2000 data points used. The errors of P_2 and P_3 are shown in the caption of Fig. 3.15.The fit to the experimental data implies the consistency with the direct logarithmic law. Thus several data tables were collected which contain information about the sweep rate v, the held

potential E_h, held time t_0, the current density at t_0, the charge density σ_0 [3] at t_0, fitting parameters P_1, P_2, P_3. P_1 was then found to be an experimental artifact due to the scale alternation of oscilloscope used to record the data and thus it was treated as the baseline. (See attached data sheets in appendix A).

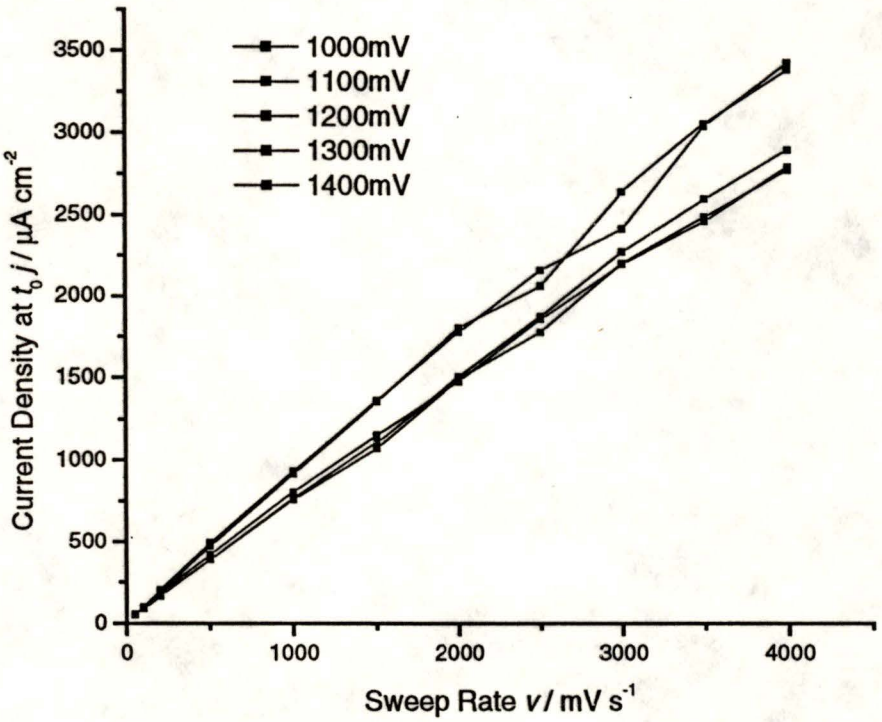

Fig. 3.16 Current density at held time t_0 vs. sweep rate at different held potentials. The nonlinear least square slopes of these plots fit through origin are from 0.68 ~ 0.83 mF cm^{-2}.

[3] Please notice that charge by integration from CV after double-layer charge deduction is σ_0, total charge density of the oxide for all forms of platinum oxide.

The scan rate dependence of the current density at held time t_0, j_0, was found to be nearly linear with the relationship $j_0 = (0.68 \sim 0.83 \text{ mF cm}^{-2})v$. (Fig.3.16) This number is close to Harrington's $j_{plat}=(0.62 \text{ mF cm}^{-2})v$ measured at 1.4V [31]. Conway instead had j_{plat} vs. $\log(v)$. The assumption of a plateau still seems reasonable here since the slope of the plot of j_0 with v at different potentials does not change much.

As stated above, the fitting expression used in this work is:

$$j = P_1 + \frac{P_2}{P_3 + t} \tag{3.14}$$

for the constant potential condition. Until now no assumption is made here, since the direct logarithmic law is an experimental empirical law, no matter what mechanism the oxide growth is. Discarding P_1 as the baseline and integrating Equation (3.14) with initial condition ($t=t_0$, $\sigma=\sigma_0$) yields

$$\sigma = \sigma_0 + P_2 \ln \frac{t + P_3}{t_0 + P_3} \tag{3.15}$$

Substitution of $t+P_3$ as a function of σ from Equation (3.15) into Equation (3.14), the relationship between j and σ can be reached:

$$j = \frac{P_2 \exp(\frac{\sigma_0}{P_2})}{t_0 + P_3} \exp(-\frac{\sigma}{P_2}) \tag{3.16}$$

We know that the empirical rate law can be written as:

$$j = \frac{d\sigma}{dt} = a \exp(-b\sigma) \tag{3.17}$$

By Comparing Equation (3.16) and (3.17), we can get the relationship between those parameters:

$$P_2 = 1/b \tag{3.18}$$

$$P_3 + t_0 = \frac{1}{ab}\exp(b\sigma_0) \tag{3.19}$$

or

$$a = \frac{P_2}{t_0 + P_3}\exp(\frac{\sigma_0}{P_2}) = j_0 \exp(\frac{\sigma_0}{P_2}) \tag{3.20}$$

The plot of $1/P_2$ or b as a function of E_h from the results of fitting is shown in Fig. 3.17. The value of $1/P_2$ ranges from 0.03 to 0.08 μC^{-1} cm^2 nearly identical to Harrington's result (see Fig. 4 in reference [31]). And as already pointed out by Harrington, b decreases with potential, while here P_2 increases with held potentials (from 12.5 to 32.5 $\mu C\ cm^{-2}$).

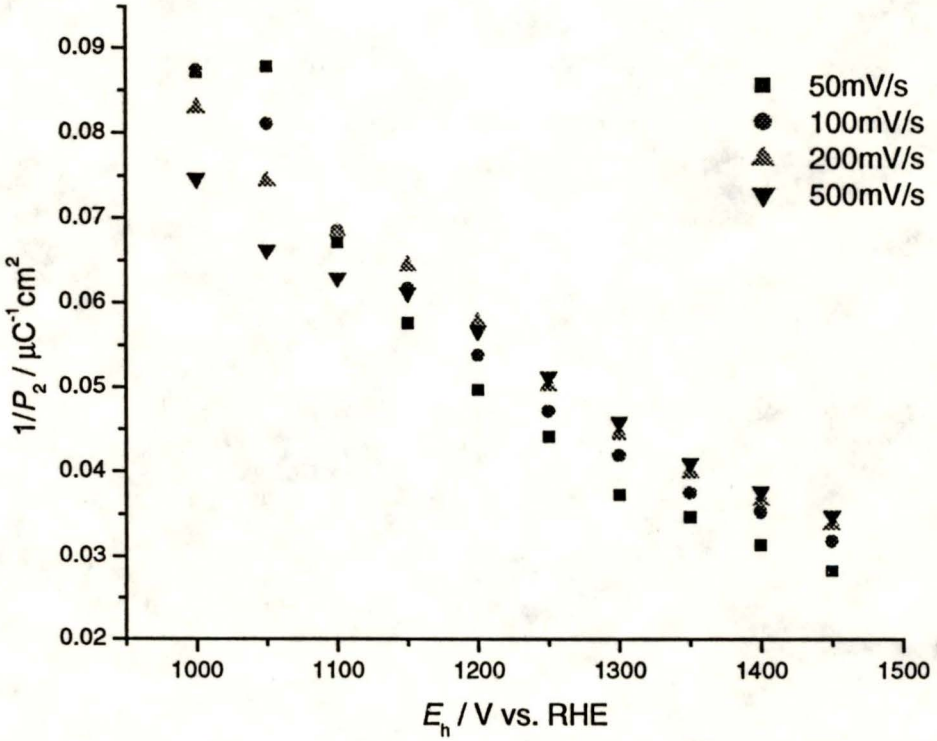

Fig. 3.17 $1/P_2$ dependence on held potentials from fitting results for different scan rates.

It is interesting that t_0+P_3 is linearly dependent on the hold potential (Fig. 3.18). Furthermore, the slopes and intercepts of the fitting curves are also linearly dependent on the reciprocal of sweep rate (Fig. 3.19). From Fig. 3.18 and 3.19, an empirical equation can be deduced:

$$t_0 + P_3 = \frac{5.35\times10^{-2} E - 4.10\times10^{-2}\,\mathrm{V}}{v} \tag{3.21}$$

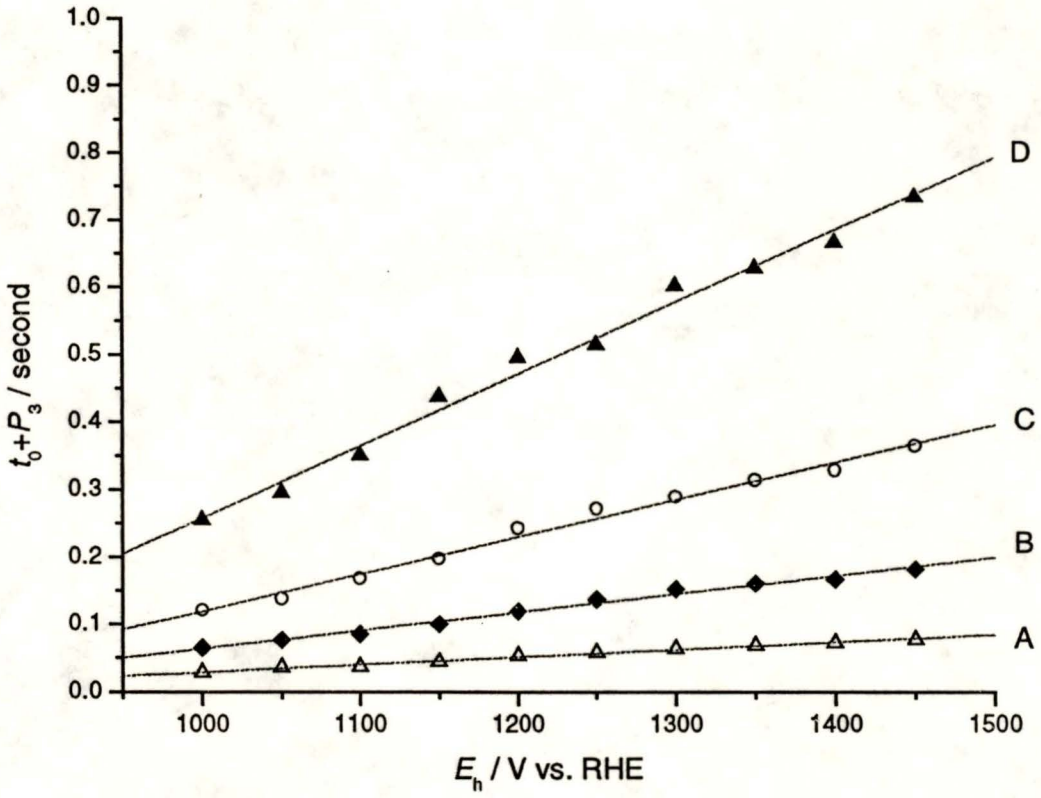

Fig. 3.18 t_0+P_3 from fitting results vs. hold potential for different sweep rates. A: 500 mV s^{-1}, B: 200 mV s^{-1}, C: 100 mV s^{-1}, D: 50 mV s^{-1}. Points are the experimental data, and lines are the fitted curves.

Thus,

$$P_2 = j_0(t_0 + P_3) = \frac{j_0(5.35\times10^{-2} E - 4.10\times10^{-2}\,\mathrm{V})}{v} \tag{3.22}$$

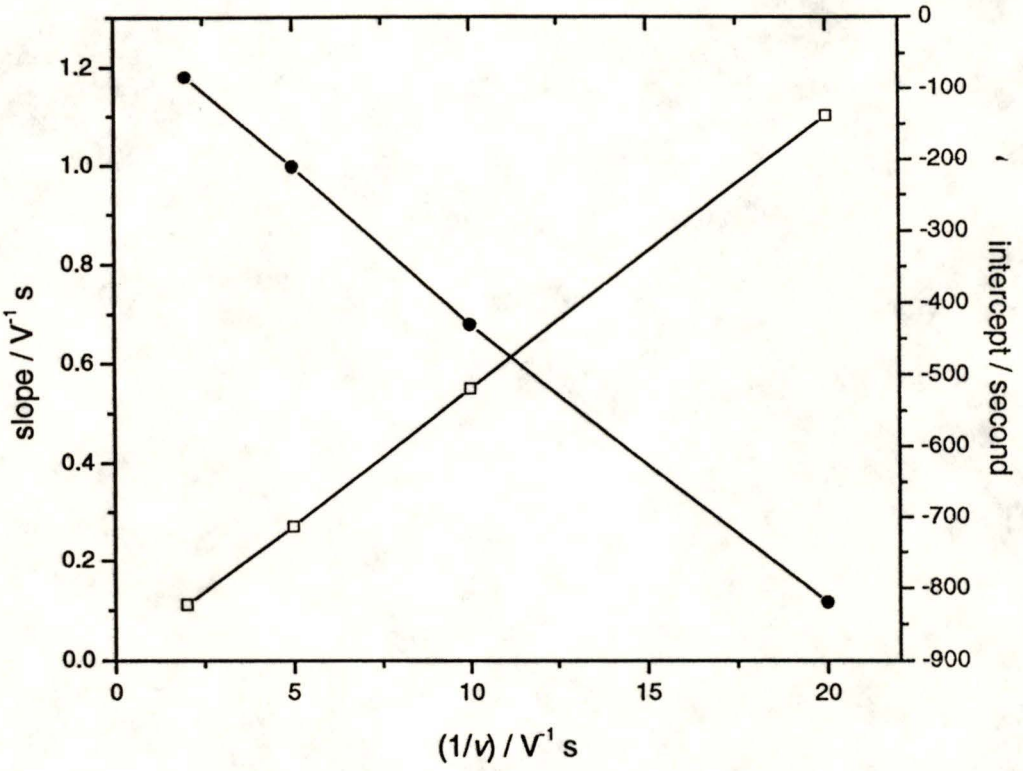

Fig. 3.19 Slope and intercept parameters extracted from Fig. 3.18 vs. (1/*v*) (sweep rate before hold).

From Fig.3.13, j_0=(0.68 ~ 0.83 mF cm^{-2})v,

P_2=(0.68~0.83 mF cm^{-2})(5.35×10^{-2}E – 4.10×10^{-2}V) (3.23)

If adopting the plateau concept, Equation (3.22) indicates the linear relationship of P_2 or $1/b$ with E implying that the trend in Fig. 3.17 is hyperbolic.

Now we come to a, slightly more complicated than b which can be obtained directly from P_2. Equation (3.20) gives a and Fig. 3.20 is a plot of a with potential E at 100 mV s^{-1} sweep rate before holding. It was found that a is increasing at less positive potentials but tends to a constant value at higher potentials (E > 1.15 V vs. RHE) and in this region a is also not dependent on the sweep rate. The plot of a averaged from different sweep

rates for the same hold potentials with potential is shown in Fig. 3.21. This may imply that there are at least two different processes of the mechanism taking place; one before 1.15V and one after that potential.

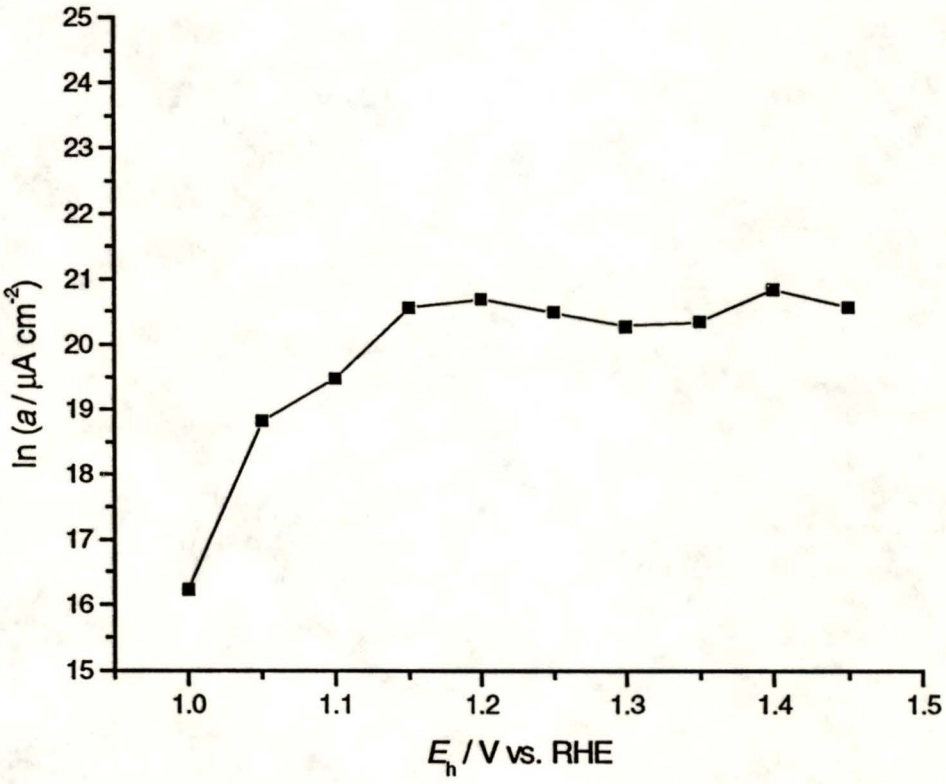

Fig. 3.20 ln (*a*) calculated from Equation (3.7) with potential (all data at the same sweep rate 100 mV s^{-1} before holding).

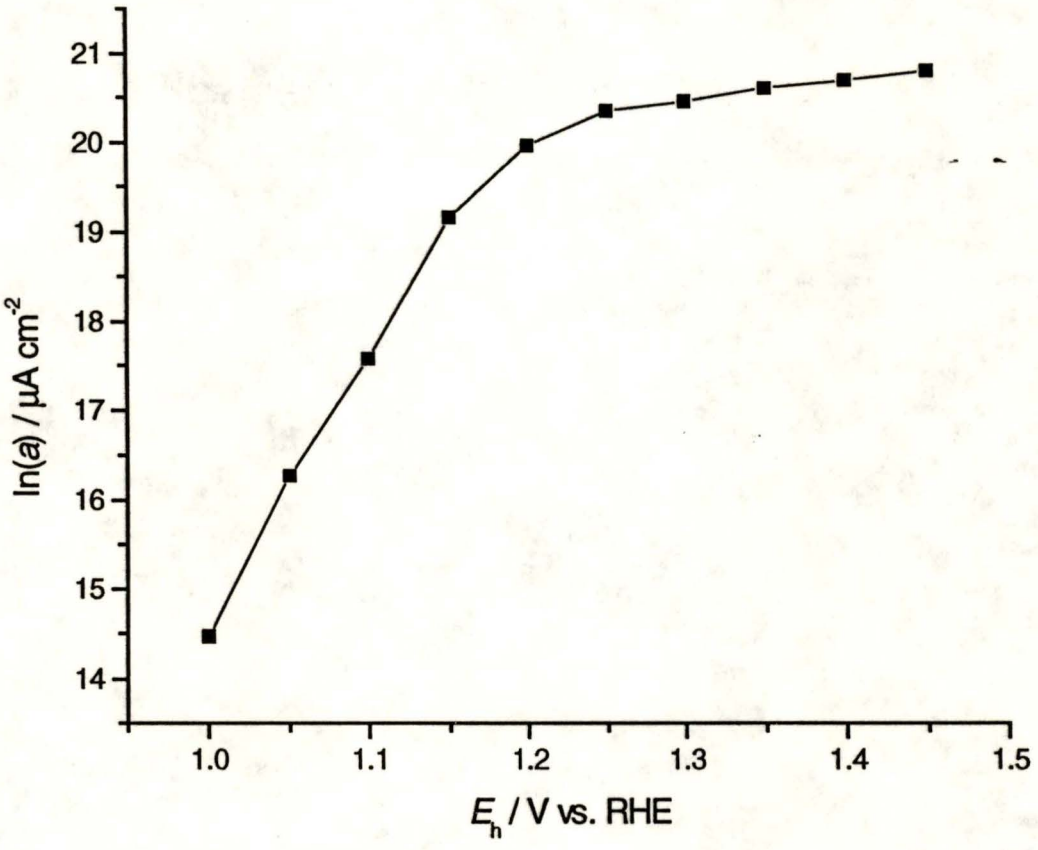

Fig. 3.21 Plot of average ln (a) value of different sweep rates at the same hold potentials with E_h.

From the above discussion and simulated results, a better empirical rate law can be derived:

$$j = a' \exp\left(-\frac{b'\sigma}{E - 0.766\text{V}}\right)$$
$$\ln(a'/\mu\text{A cm}^{-2}) \approx 20.5 \qquad (3.24)$$
$$b' \approx (2.25 \sim 2.75) \times 10^{-5}\ \text{cm}^2\ \mu\text{F}^{-1}$$

3.4.2 Discussion

3.4.2.1 One Fundamental Question: What Parameters does Current Density Depend on?

Before discussing the rate law, we should test whether the direct logarithmic law is correct and worthy to fit the experimental data to. In other words, the question is: is j a unique function of only the applied potential, and the charge density, which is indicated from the direct logarithmic law? Fortunately, the answer to this question is "yes", proved by the experimental results in this work. The sweep rate is neglected here because while both potential and charge density are functions of time, the sweep rate is just the differentiation of potential and it is not necessary to introduce it separately into the rate law.

If the current density only relies on the potential and charge density, we can have $j = f(E, \sigma)$. Otherwise additional parameter(s) need to be added. The test can be easily carried out from the sweep-hold experimental results. For those data with a same held potential E_h, it is convenient to check whether the same σ is produced if the current density decays to the same value for different sweep rates (Fig. 3. 20). Table. 3.1 gives one example of the test. The potential was held at 1200 mV vs. RHE. The charge densities achieved at 79.05 μA cm^{-2} were investigated.

Table 3.1 Charge density achieved at the decay current density 79.05 μA cm^{-2} for the same held potential of 1200 mV.

v (mV s^{-1})	100	200	500	1000	1500	2000	2500	3000	3500
σ μC cm^{-2}	303.6	294.9	303.3	325.9	309.3	312.1	313.5	314.5	314.8

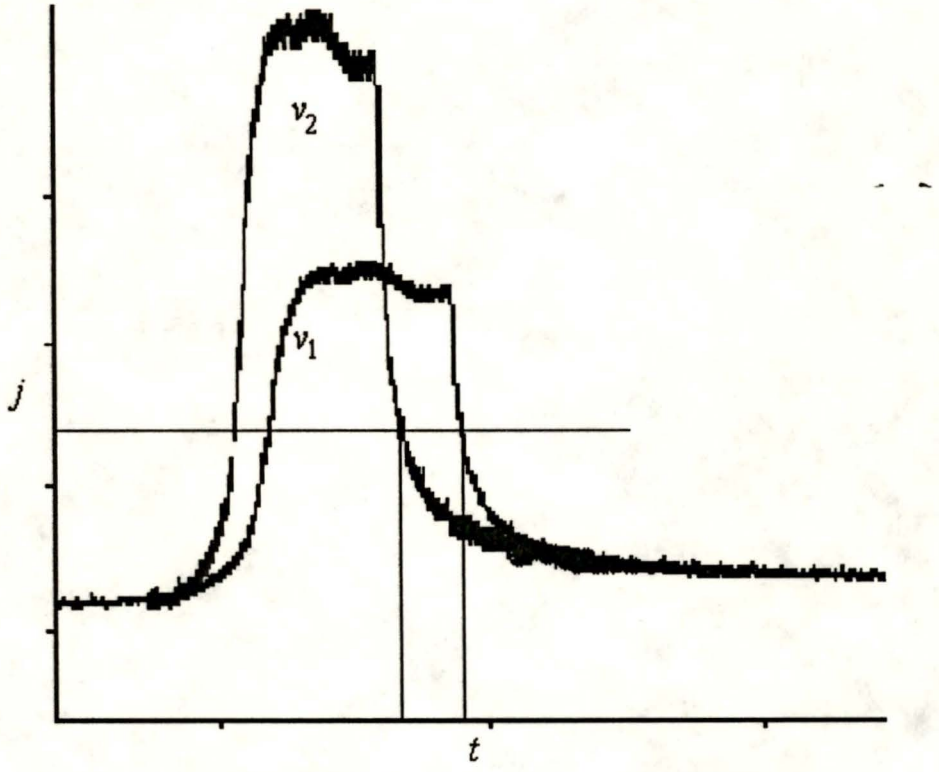

Fig. 3.22 Diagram to show the data extraction to test the dependence of current density with applied potential and charge density. The two curves in this plot are from two sets of data from sweep-hold experiments at the same hold potential but with different sweep rates before the hold. Charge densities were integrated at the same decay current as shown by the horizontal line. Before the hold the double-layer charging was used for the baseline. For the post-hold period it was assumed that the double-layer does not get any more charge since the potential is held and so in theory, the baseline should be j=0. But due to some of the experimental errors, the parameter P_1 (different for these two curves) is accepted as baseline to calculate the charge.

The data in Table 3.1 may not be accurate, due to the uncertainty on the correction for double-layer charging. The assumption was made that the double-layer charging current is the same as in the "double-layer" region of the voltammogram for the sweep part, and negligible for the hold part. Nonetheless, the variation is less than 5%. Therefore, it is reasonable to say that the current density only depends on the applied potential and the charge density. Once potential and charge density are given, there is a unique value of the current density.

3.4.2.2 Is the Plateau Concept Approximation Reasonable?

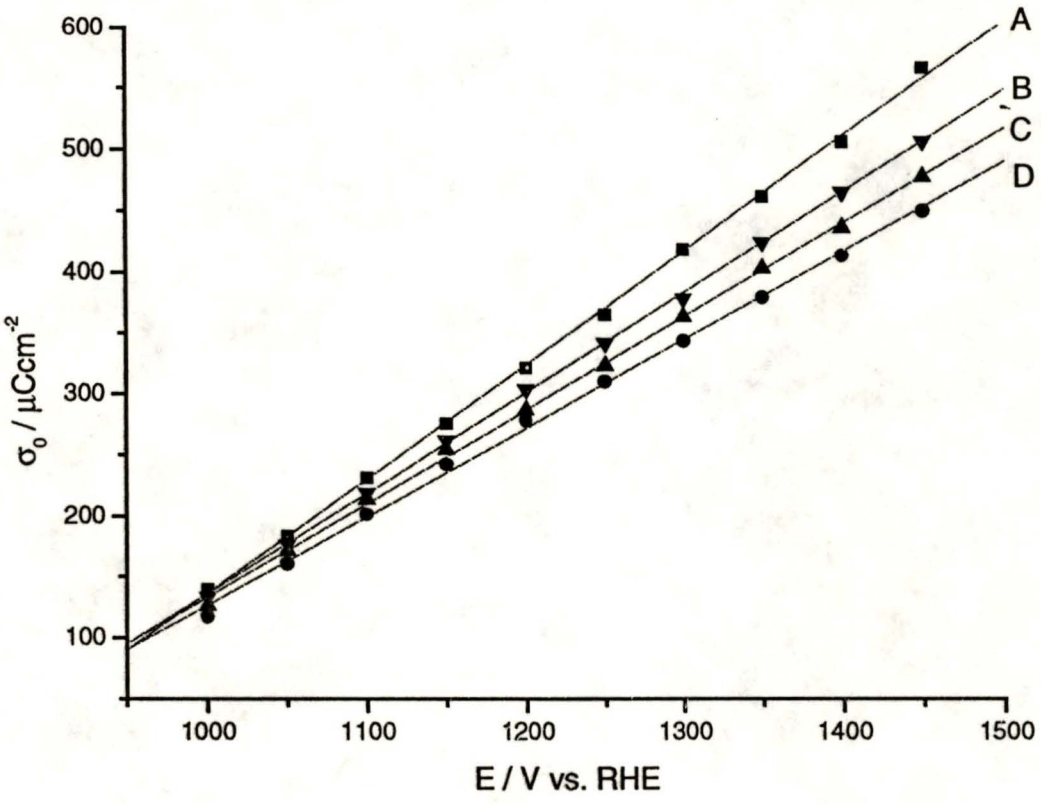

Fig. 3.23 Plot of charge density increase with potential from cyclic voltammograms at different sweep rates. Sweep rates: A: 50 mV s^{-1}, 100 mV s^{-1}, 200 mV s^{-1}, 500 mV s^{-1}. Experimental data are shown as symbols, while the line is the fitted results.

The assumption of a plateau means that current density does not change significantly in cyclic voltammograms when the applied potential is more positive than 1.1 V vs. RHE. One piece of evidence for the plateau is the approximately linear increase of charge density integrated from CV with the scanning potential (Fig. 3.23). That is also the approximation obtained above: $j_0 = (0.68 \sim 0.83\ \text{mF cm}^{-2})v$ for $\frac{j}{v} = \frac{d\sigma / dt}{dE / dt} = \frac{d\sigma}{dE}$.

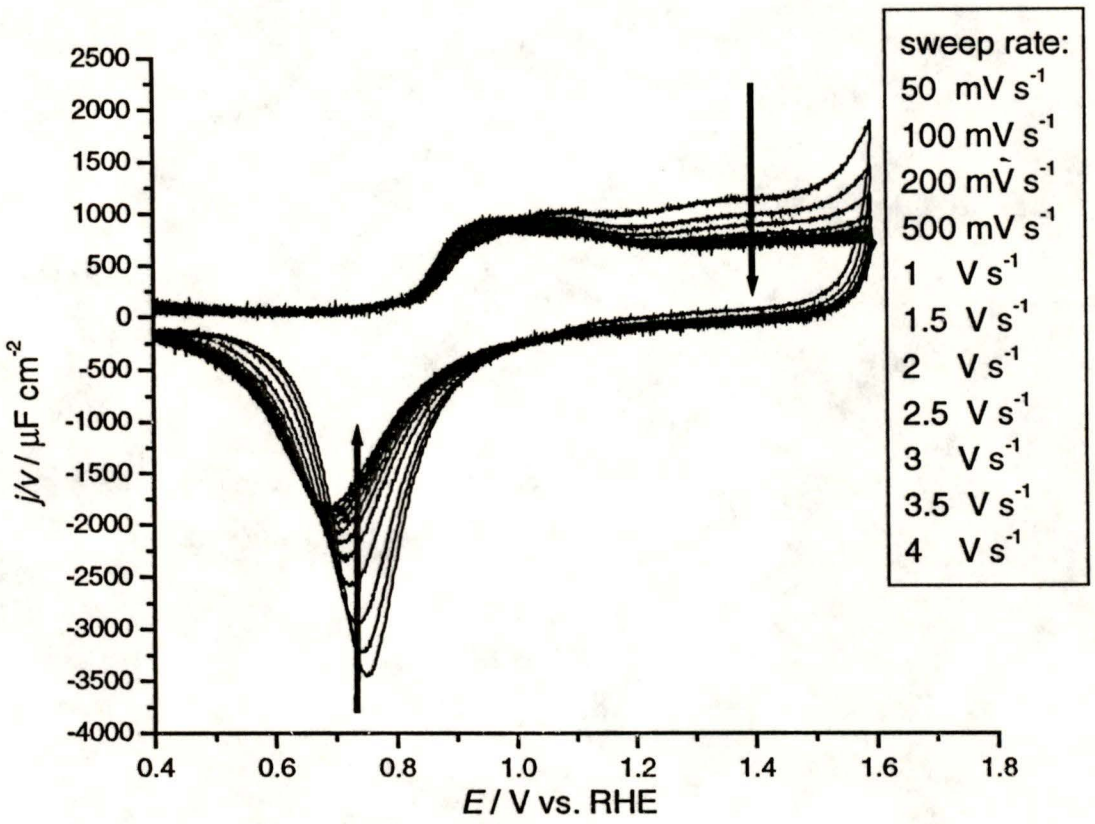

Fig. 3.24 Plot of *j/v* vs. *v*. Arrows show the increase of sweep rate *v* from 50 mV s^{-1} to 4 V s^{-1}. Data were collected from common cyclic voltammograms, which is the plateau current density.

To check this, the plot of *j/v* vs. *E* (a scaled version of the CV) is shown in Fig. 3.24. It is very clear in this plot that the "plateau" concept is valid only for fast scans, i.e., v>500 mV s^{-1}. And for fast scans the value of *j/v* is not dependent of the sweep rate, which means that the oxide growth process behaves like a capacitor charging. Fig. 3.24 also shows that the oxide growth before about 1.15 V is not dependent on the sweep rate. This may also imply that there are two different processes before and after this potential.

3.3.3.3 Kinetics and Mechanisms:

Here we mainly discuss Conway's mechanism on platinum oxide growth since some evidences for two-process were also found in this work. Conway's model has an OH adsorption step followed by place-exchange and then further oxidative growth [1], while Harrington insists on a one species PtO process and the key role of fast surface diffusion [32]. Evidence of Conway's mechanism is a fast and reversible component in the earlier stage of oxide growth (not necessarily OH adsorption) also mentioned in the literature survey. And AC impedance results from Harrington showed that if there is a fast OH adsorption step, it should be super-fast (above the frequency used in the AC signal applied: 50 kHz) because in the AC impedance experiment no fast process was found [14]. The scheme for Conway's mechanism is as follows:

$$Pt + H_2O \rightleftharpoons PtOH + H^+ + e^- \quad (3.24)$$

$$PtOH \rightleftharpoons OHPt \quad (3.25)$$

$$OHPt \rightleftharpoons PtO + H^+ + e^- \quad (3.26)$$

- Because of Harrington's AC voltammetry experiment, step (3.24) cannot be slow; otherwise, it would be distinguished in the impedance results. So it can be assumed that step (3.24) is very fast which means that the coverage of OH remains constant, step (3.25) can be considered to be the rate-determining step. Though from the equations step (3.25) will use PtOH generated from step (3.24) for continuing oxidation, step (3.24) is fast enough to keep the coverage of PtOH constant. Using the steady-state approximation with step (3.25) as the rate-determining step,

  $$v_1=v_2=v_3 \quad (3.27)$$

  and

  $$j = F(v_1 + v_3) = 2Fv_2 \quad (3.28)$$

In Conway's paper [1, 2], v_2 can be deduced to be proportional to exp(-$L\sigma$) (L is one parameter) and thus the direct logarithmic law can be deduced.

- If step (3.24) is also reversible, such that step (3.24) would be kept at equilibrium at all potentials, then we may derive this equation:

$$\frac{f(\sigma_{OH,equ})}{1-\theta_{OH,equ}} = \exp(\frac{F\eta}{RT}) \tag{3.29}$$

$f(\sigma_{OH,equ})$ is the equilibrium value of a function of σ_{OH}. The reason we use $f(\sigma_{OH,equ})$ instead of $\theta_{OH,equ}$ is because we do not know the structure of the adsorbed OH. It can be a 2-D structure in which coverage θ would be proportional to the charge density σ of oxide or 3-D in which there would not be a direct clear relationship between θ and σ (Fig. 3. 25). For example, if it is a 2-D structure and the Langmuir isotherm applies, then the above equation can be written as:

$$\frac{\theta_{OH,equ}}{1-\theta_{OH,equ}} = \exp(\frac{F\eta}{RT}) \tag{3.30}$$

Whatever the expression is, we know that the coverage or some function related to coverage is in equilibrium and only related to the applied potential.

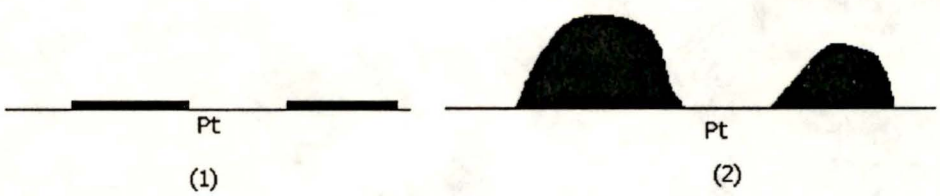

Fig. 3.25 Diagram to illustrate the relationship of θ and σ. Line is the substrate of Pt and filled regions are OH adsorbed. In (1), only submonolayer or monolayer OH is adsorbed, then $\sigma = F\Gamma_m\theta$. In (2), $\sigma > F\Gamma_m\theta$. Γ_m is the surface concentration for full monolayer coverage and $\Gamma = \Gamma_m\theta$.

- Now σ_0 instead of $\sigma_{ox,0}$ is available from experiment results. At any time they should keep this relationship for the mechanism above:

$$\sigma_0 = \sigma_{ox,0} + \sigma_{OH,0} \tag{3.31}$$

$$a = j_0 \exp(\frac{\sigma_{ox,0}}{P_2}) = j_0 \exp(\frac{\sigma_0}{P_2}) \exp(-\frac{\sigma_{OH,0}}{P_2}) \tag{3.22}$$

$$\ln j_0 + \frac{\sigma_0}{P_2} = \ln a + \frac{\sigma_{OH,0}}{P_2} \tag{3.33}$$

The charge will always include two parts: one is for the place-exchange behavior, the other for the OH adsorption. $\sigma_{OH,0}$ (charge density due to OH adsorption at t_0) cannot be treated as a constant due to the place-exchange and also the adsorption of OH continues in the potential region studied. Equation (3.33) indicates that the plot of ($\ln j_0 + \sigma_0/P_2$) with $1/P_2$ would be linear with slope σ_{OH} and intercept $\ln(a)$. (Fig. 3.26) Table 3.2 gives the σ_{OH} extracted from a series of plots similar to Fig. 3. 26.

Table 3.2 σ_{OH} extracted from a series of plots similar to Fig. 3. 26.

E_h(V) vs. RHE	1.15	1.20	1.25	1.30	1.35	1.40	1.45
$\ln(a)$	7.688	7.665	8.112	7.869	8.825	7.434	6.515
$\sigma_{OH,0}$ ($\mu C\ cm^{-2}$)	211.8	244.1	263.9	299.1	336.5	375.9	435.2

From Table 3.2 $\sigma_{OH,0}$ increases from nearly one monolayer (220 $\mu C\ cm^{-2}$) at 1.15V vs. RHE to two monolayers at 1.45V vs. RHE. Referring to the attached table of the values of σ_0, $\sigma_{OH,0}$ is less than σ_0 for slow scans i.e. $v < 2\ V\ s^{-1}$ and nearly equal to σ_0 for less positive potentials held ($E < 1.2$ V). At fast scans and at more positive potentials, σ_0 is less than $\sigma_{OH,0}$. The linear shape of Fig. 3.26 somewhat conforms to the assumption of super-fast OH adsorption. But the results also show inconsistency because no mechanism

can allow $\sigma < \sigma_{OH}$. The indication of more than one full monolayer can be explained as shown in Fig. 3.27. This is also supported from the data of the hydrogen saturation experiments in which the decay of hydrogen current does not reach zero exactly when there is one electron per platinum oxidation.

The conclusion is that the OH adsorption model correctly predicts the constancy of $\sigma_{OH,0}$ but somehow is inconsistent with $\sigma_{OH} < \sigma$. This may be due to the adsorption of anions i.e., bisulfate or sulfate ions.

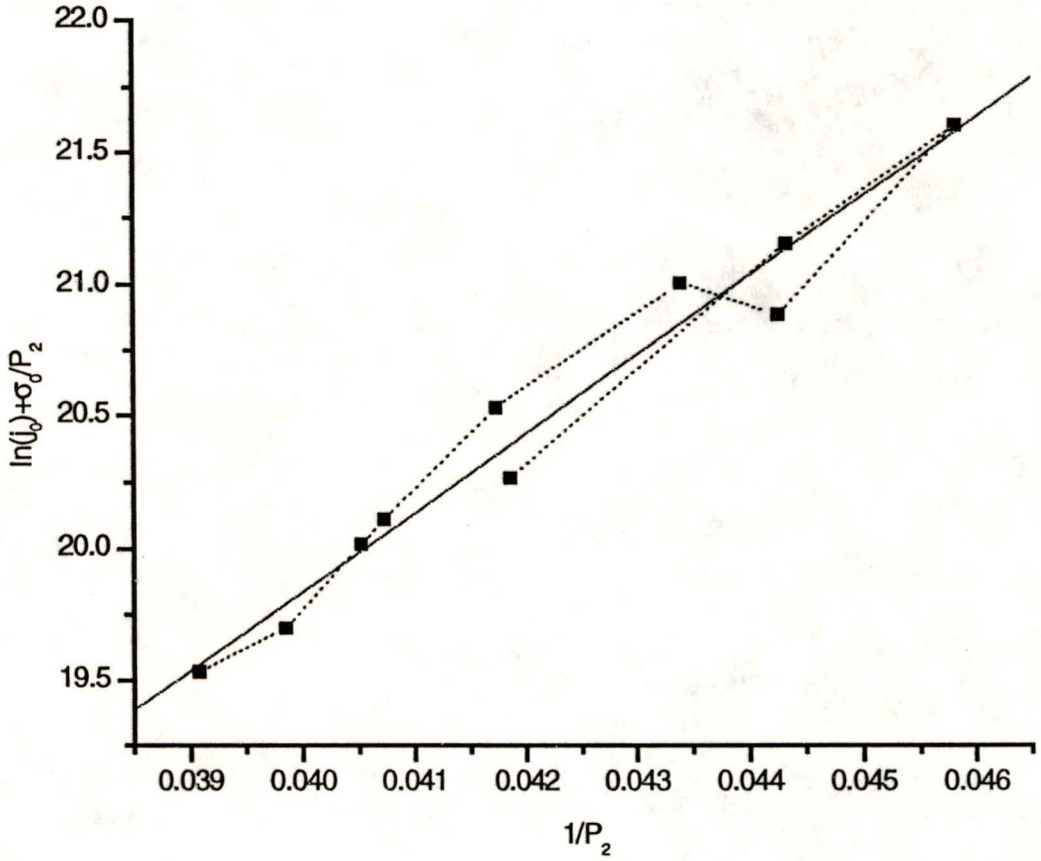

Fig. 3.26 Plot of $\ln j_0 + \sigma_0/P_2$ vs. $1/P_2$ at different sweep rates gives a slope of σ_{OH} and intercept of $\ln(a)$. Held potential: 1.3 V vs. RHE. Fitting results: $\ln(a/\mu A\ cm^{-2})=7.87$, $\sigma_{OH}=299\ \mu C\ cm^{-2}$.

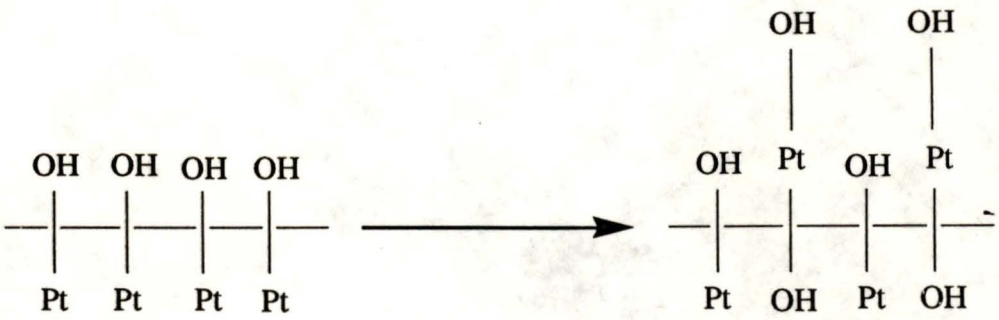

Fig. 3.27 Diagram to show that OH adsorption coverage can be more than one monolayer (one per platinum). Because of the fast adsorption of OH, after place-exchange takes place, there would be OH adsorbed on the Pt already oxidized. At most two monolayers of oxide are assumed here. Though it is clear that the OH adsorbed on oxidized Pt is different from OH on Pt(0), for qualitative result the analysis still applies.

4 Discussion

In this part, a number of topics on the platinum oxide growth are further discussed. Essential to the oxide growth is the mechanism: how many processes are involved and what is the intermediate. Is it possible to deduce the direct logarithmic rate law from the mechanism? A bunch of anions are ready to adsorb on the platinum surface. Whether they influence the mechanism of oxide growth is also an important question to answer.

4.1 Mechanisms of Oxide Growth

As was mentioned above, explanations of the mechanisms of oxide growth have been developed into two main directions. One is the one proposed by Conway to explain the reversible and irreversible components of the fast scan in cyclic voltammograms. Another is just the single-step two-electron oxidation proposed by Harrington. The differences between these two mechanisms lead to two key questions:

1) Is there one process or two processes involved in the oxide growth?

2) Is OH species adsorption in the early stage of growth the reversible component?

4.1.1 One Process or Two Processes?

Evidence for the reversible component comes from three sources:

1. In rapid cyclic voltammetry in the early stage of oxide growth the reverse scan shows a reduction peak with a shoulder on the more positive side than the

general oxide reduction peak potential (0.8V). This shoulder disappears when the scans are reversed at higher potentials [1, 2, 8, 51].

2. In AC voltammetry at 32.5 Hz, there is no hysteresis for sweep reversal in early stage of growth, but substantial hysteresis for the later reversals [13, 14].
3. In reflectance experiments no hysteresis was observed for sweep reversals in early stage of growth, but hysteresis was seen for later reversals [1].

That the reversible component could only be found in rapid sweep reversals in the early stage of oxide growth indicates that if this reversible component is due to one process, it should be fast, compared to the further oxidation. As pointed out by Harrington, the fast process for the reversible component would necessarily lead to high-frequency features in the ac impedance spectra, which were not found in his experiments. He therefore concluded that the reversible component could not be attributed to another new process, i.e., fast adsorption. Other qualitative explanations for the reversible and irreversible components were suggested, e.g., surface reconstruction which would reduce the facility of surface diffusion of oxides and change the reversible component to irreversible one.

It seems that there is not a significant conflict between the previous experiments from which the two processes were deduced and Harrington's AC voltammograms because we know the equivalent circuit for this case can be represented as the double-layer capacitor in parallel with the Faradaic processes and then the combination in series with the solution resistor.

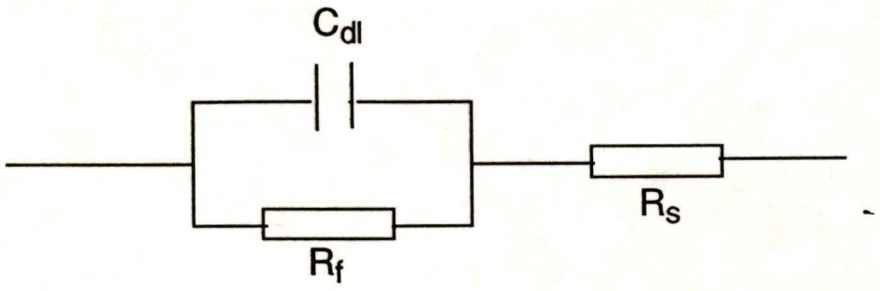

Fig. 4.1 Equivalent circuit of a common electrochemical process. C_{dl}: double-layer capacitor, R_f: Faradaic process resistor, R_s: solution resistor.

The Faradaic process can be much more complicated than just one resistor, e.g., adsorption capacitor, Warburg impedance or constant phase element (CPE) etc. But as analyzed above, the Faradaic process if it exists in this situation should be fast, which means the R_f should be smaller which would make this paradox: to catch up with this process high frequencies should be used to probe this element, but at high frequency the double-layer capacitor would short-circuit the resistor or other components and only the solution resistance can be found, which is the result of Harrington's ac impedance results. Thus it is difficult to find the subtle experimental conditions to study this process if it is there. The conclusion to the above analysis is that the absence of a high-frequency impedance feature in ac impedance spectra does not necessarily mean there is not a fast process, which could correspond to the reversible component in rapid cyclic voltammograms.

Supported evidence of a two-process mechanism in this work comes mainly from the hydrogen saturation experiments (see section 3.2). The plot of Fig. 3.13, which is the relationship between the free sites implied from the hydrogen oxidation current with the number of electrons oxidized implied from the oxide charge, shows that there are no bare platinum sites for hydrogen oxidation after one electron per platinum oxidation. The

direct conclusion of this experiment is that there is a Pt(I) oxide in the early stage of growth to count the one electron per platinum oxidation. And after growth of this Pt(I) oxide saturates, further oxidation can occur.

4.1.2 What's the Pt(I) Oxide? Is It OH Adsorption?

A Pt(I) oxide could possibly be formed by the following reactions:

$$Pt + H_2O \rightarrow PtOH + H^+ + e^- \quad (4.1)$$

$$2Pt + H_2O \rightarrow Pt_2O + 2H^+ + 2e^- \quad (4.2)$$

or more complicated reactions e.g.,

$$2Pt + 3H_2O \rightarrow PtOPt(OH)_3 + 5H^+ + 2e^- \quad (4.3)$$

All these reactions produce Pt in the +1 oxidation state. If we do the electrochemical quartz crystal microbalance mass experiments, the mass change expected for these reactions would be 17, 8 and 33.5 g per mol of electrons respectively. As mentioned in the introduction, the previous mass experiments indicated the mass change per electron for the oxide is about 8 ± 0.5 g per mol of electrons [25]. So the accepted Pt(I) state oxide can only be Pt_2O and reaction (4.2) is the right one happening in the early stage of oxide growth. The conclusion of Pt_2O product does not have any conflict with the present experimental results. The cathodic current transient response of the solution exchange experiments by acetonitrile can be explained as this reaction:

$$Pt_2O + NCCH_3 + 2H^+ + 2e^- \rightarrow Pt\text{-}NCCH_3 + H_2O \quad (4.4)$$

The explanation of the kinetics using Pt_2O will be discussed in the following section.

4.1.3 Is Surface Diffusion Important in the Oxide Growth?

Surface diffusion now is generally accepted in gas-phase catalysis. To study the surface diffusion a small part of the surface is cleaned and then spectroscopies are used to detect the molecules which diffuse from other parts of the surface. The surface diffusion coefficients can then be estimated.

But this method cannot be extended to solution electrochemical studies. Until now, there seems no method to detect surface diffusion directly. That's why surface diffusion is not widely accepted and discussed in electrochemistry.

The evidence for surface diffusion happening in platinum oxide growth is the topography change observed with scanning tunneling microscopy. Surface reconstruction was found in just a few cycles of cyclic voltammetry scans. Conway explained this in terms of "place-exchange", and Harrington by surface diffusion of oxidized platinum species formed after breaking Pt-Pt bonds. It is difficult to decide which is likely and which is not. But we can discuss some cases of surface diffusion below:

1. Fast surface diffusion:

If a fast surface diffusion process occurs on an electrode surface, then what would happen? Assume species A is adsorbed on the surface and can move freely due to the fast surface diffusion. The first implication is that the interaction of A and the substrate could not be very strong. The second one is that it would not influence any process we study since the surface diffusion could not be the rate-determining process. And also in this case, surface diffusion is nearly impossible to detect.

2. Slow surface diffusion:

If surface diffusion is slow compared to the process of interest then it would be the rate-determining step in some cases. The visual picture is that if the coverage of adsorbed species is high, the surface diffusion would not influence the reaction process much. But if the coverage is low, surface diffusion might influence the observed rate. This means to detect the surface diffusion, experiments should be performed at low coverage.

We can check the platinum oxide in the early stage of growth where the oxide charge density is less than 220 $\mu C\ cm^{-2}$. Table 4.1 is the data from sweep-hold experiments at held potential E_h=1000 mV with all the data collected at 80 $\mu A\ cm^{-2}$.

Table 4.1 Oxide amount comparison when electrode potential was held at the same 1000 mV and decay current measured at the same current of 80 $\mu A\ cm^{-2}$.

Sweep rate ($mV\ s^{-1}$)	100	200	500	1000	1500	2000	2500	3000	3500
Charge density σ ($\mu C\ cm^{-2}$)	136.3	137.4	141.6	144.6	144.9	149.2	149.7	150.7	149.3

It should be noted that the measurement error of the experiment is small: for data fitting, less than 1% (1/177); for baseline compensation, also small, about 1%. The trend in Table 4.2 may inply that there is surface diffusion which is not fast and which gives different charge densities even at the same potential and same current. But further experiments are required for a definitive proof. And there are many other effects involved e.g., anion adsorption, especially the adsorption of bisulfate/sulfate since the sweep-hold experiments were performed in sulfuric acid, which will be discussed further below. But one conclusion that can be made here is that whether the trend in Table 4.2 is due to surface diffusion or not, there will only be a small effect in the results of sweep-hold experiments.

4.2 Effects of Anions on the Early Stage of Oxide Growth

Anions are present in any electrolyte solution used in electrochemical studies. Unfortunately, platinum oxide growth, especially in the early stages, is very sensitive to the anions in the bulk solution. Sulfuric acid was used in most of this work because it is available in high purity. Although perchloric acid is known to have negligible anion adsorption, the high purity reagent is difficult to make. The main contaminant ion in perchloric acid is chloride which has a major influence on the oxide. But as shown in the experimental results and previous work by other groups, there is adsorption on platinum by bisulfate or sulfate ions although the effect is much smaller than chloride, iodine, etc.

The most obvious effect of anions on platinum is that they block the early stage of oxide growth, as seen in cyclic voltammograms. For the pure perchloric acid electrolyte solution, the double-layer region is not so flat as the one in sulfuric acid solution which may indicate some early stage oxide growth charge.

It is believed that the adsorbed anions affect the oxide growth mechanism. But exactly how they are involved has not been determined. Except for ClO_4^-, which has no chemical interaction with Pt, all other anions' adsorption is believed to be oxidative.

For the case of bisulfate/sulfate, bisulfate is the dominant adsorbed species because the adsorption occurs with charge transfer, as inferred from the solution exchange experiments between perchloric acid and sulfuric acid (section 3.2.1). In the CV of platinum in sulfuric acid, the charge due to its adsorption is considered to be in the hydrogen adsorption region, similar to the case of single-crystal platinum on which the

adsorption of hydrogen and bisulfate can be separated. It should be mentioned here that the part of the charge in the hydrogen adsorption region on polycrystalline platinum electrode due to anion adsorption does not influence the method used in this work to estimate the surface area. Adsorption and desorption of bisulfate can be represented as:

$$Pt\text{-}HSO_4^- + H^+ + e^- \rightleftharpoons Pt + HSO_4^- \qquad (4.5)$$

where adsorption and desorption are oxidation and reduction processes respectively. From the mass experiments and IR data, these adsorbed anions stick on the surface. Otherwise large mass changes due to the heavy bisulfate/sulfate should be observed. Therefore it is reasonable to assume that the bisulfate/sulfate ions adsorbed are already on surface and just move around in a way similar to surface diffusion, which would not influence the oxide growth much.

Other anions including halides and sulfides have a much bigger effect on oxide growth than bisulfate/sulfate. In most cases tested in this work it was found that these anions' existence in solution would dissolve the oxide formed in the early stage. This may increase the surface roughness as shown in Fig. 4.2.

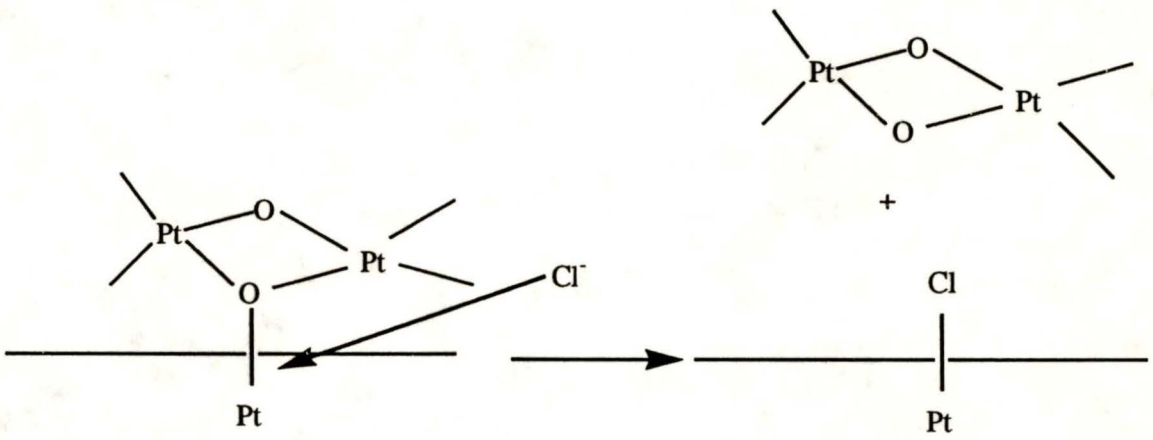

Fig. 4.2 A simple picture to show that the adsorption of chloride would break the bonds of platinum oxide outside the bulk surface and then the oxide would leave the surface, resulting in dissolution.

These anions desorb at higher potentials, i.e., >1.5V. Most of them are oxidized, e.g., chloride is oxidized to chlorine. Because the oxygen evolution will be dominant at this potential and higher, to investigate the process here in mass experiments or by spectroscopic techniques would be difficult.

4.3 Nature of the Oxide

From the above discussion, it is concluded that the oxide state in the early stage of growth is Pt_2O, instead of Conway's suggestion of PtOH. Also from the hydrogen saturation solution experiment it seems that there are two processes instead of just the single two-electron oxidation step proposed by Harrington. From the previous microbalance experiments, the oxide should be anhydrous; otherwise the mass change would be 17 g per mol of electrons. The solution exchange experiments presented here show that this early stage of oxide involves some kind of adsorption since the oxide can be easily replaced by other anions. The oxide should therefore be written as Pt_2-O(ads). Surface diffusion is likely possible for this kind of O-species. From the hydrogen saturation experiment, we also know that this early stage process is not fast, and until this adsorption occurs to the extent of nearly one full monolayer, the further oxidation does not take place.

From the work in this group by Frode Seland [52] on methanol oxidation, it was found that there is an initial oxygen-containing species on surfaces before the oxide growth in sulfuric acid. This species, which is supposed to be Pt-OH_2(ads), adsorbed water, oxidizes the adsorbed carbon monoxide on surface to carbon dioxide, in a

nucleation-growth-collision mechanism. Thus the whole process of the oxide formation can be depicted as shown in Fig. 4.3.

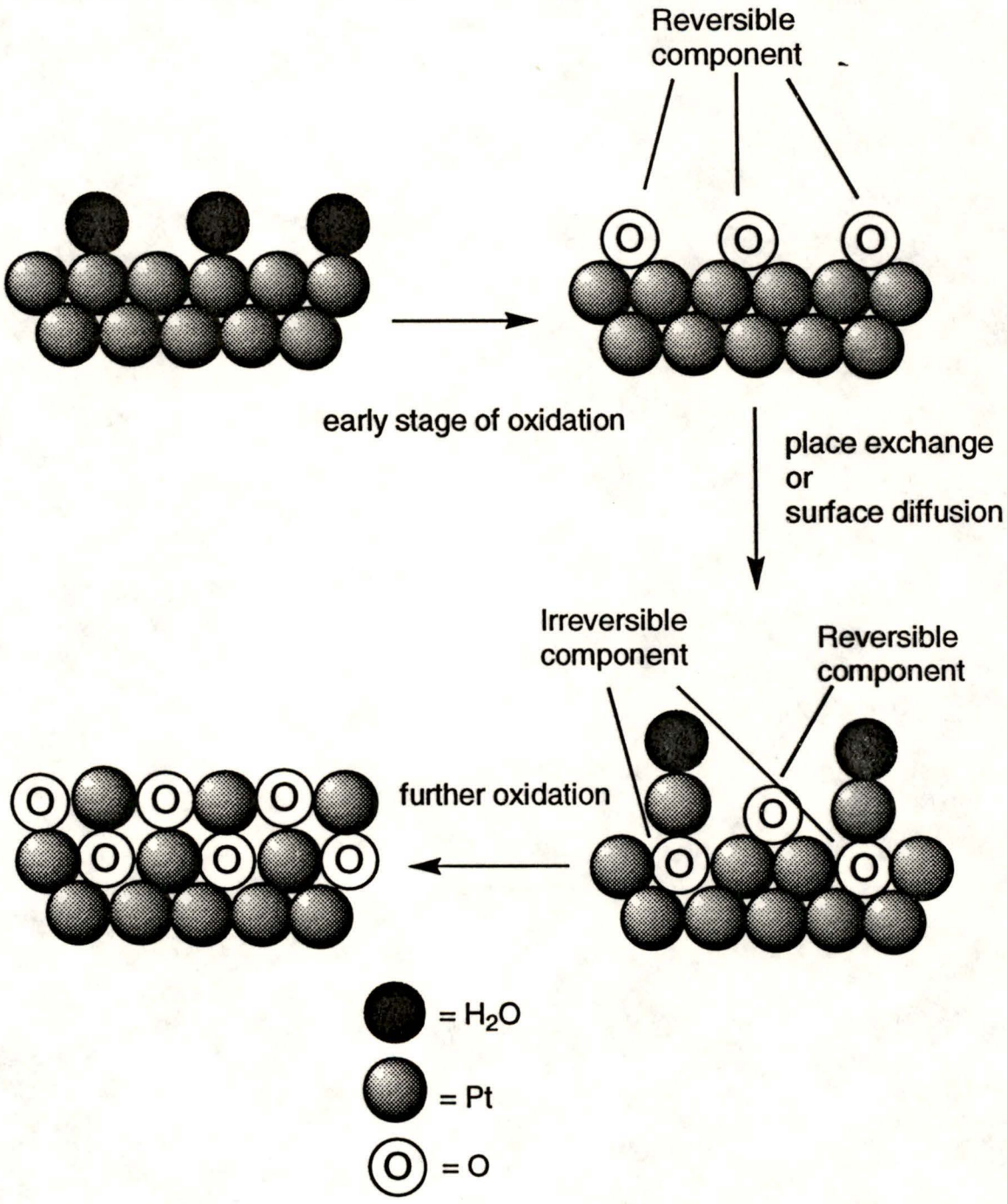

Fig. 4.3 Model for stages of oxide growth from adsorption of water to early stage and then further oxidation.

4.4 Rate Law Discussion

From the oxide growth process illustrated by Fig. 4.3, the reactions are assumed here to be:

$$Pt + H_2O \rightarrow Pt\text{-}OH_2(ads) \qquad \text{(fast)} \qquad (4.6)$$

$$Pt + Pt\text{-}OH_2(ads) \rightarrow Pt_2O + 2H^+ + 2e^- \qquad \text{(slow)} \qquad (4.7)$$

$$Pt_2O + H_2O \rightarrow 2PtO + 2H^+ + 2e^- \qquad \text{(fast)} \qquad (4.8)$$

with step (4.7) as the rate-determining step. The surface diffusion or place-exchange is assumed to be fast. Thus, in the early stage of oxide growth before reaction (4.8) becomes significant, using Frumkin isotherms,

$$\begin{aligned} j &= 2Fv_2 \\ &= 2F\{k_{ox}^0(1-\theta_{Pt_2O}-\theta_{H_2O})\theta_{H_2O}\exp(-\frac{g\theta_{Pt_2O}}{2})\exp[\frac{\alpha F(E-E^0)}{RT}] \\ &\quad -k_{red}^0\theta_{Pt_2O}\exp(\frac{g\theta_{Pt_2O}}{2})\exp[\frac{(1-\alpha)F(E-E^0)}{RT}]\} \end{aligned} \qquad (4.9)$$

Now since step (4.6) is fast, it can be assumed to be in equilibrium, with $\frac{\theta_{H_2O}}{1-\theta_{H_2O}-\theta_{Pt_2O}} = K$, the equilibrium constant for step (4.6). If we also assume high coverage of water (near unity as an approximation), then since its adsorption is fast and coverage of oxide is low, we can find:

$$\begin{aligned} j &= 2Fv_2 \\ &= 2F\{k_{ox}^0 K\theta_{H_2O}^2\exp(-\frac{g\theta_{Pt_2O}}{2})\exp[\frac{\alpha F(E-E^0)}{RT}]\} \\ &= 2F\{k_{ox}^0 K\exp(-\frac{g\theta_{Pt_2O}}{2})\exp[\frac{\alpha F(E-E^0)}{RT}]\} \end{aligned} \qquad (4.10)$$

Since we know that the coverage of Pt_2O is the equivalent to the charge density and then Equation (4.10) becomes:

$$j = \frac{d\sigma}{dt} = a\exp(-b\sigma)\exp(\frac{\alpha FE}{RT}) \tag{4.11}$$

which is the empirical rate law.

A similar equation can be reached using Harrington's mechanism. His fitting of this law to the sweep-hold experiments gave that α is from 0.5 to 0.9. Considering that the rate-determining step proposed here is a two-electron step, the electrochemical parameter β is half of α and would be from 0.25 to 0.45, which are quite reasonable values.

The discrepancy between the rate law deduced here with the sweep-hold experimental result can be attributed to many reasons. One is the simplified model used; in reality it could be much more complicated and the real equation might not be easily deduced. Then it is possible that only numerical results can be acquired. Another reason that the model may not be a perfect fit is that other effects happen in the earlier stage of oxide growth, such as anion adsorption.

5 Conclusions

1. Mechanism of the electrochemical oxide growth:

   a. From the results of hydrogen saturation solution experiments, it is found that the plot of bare platinum sites (inferred from the hydrogen oxidation current) with the number of electrons calculated from the oxide charge in CV has a slope near minus one. It is also found that after one electron per platinum oxidation, the current due to hydrogen oxidation diminishes nearly to zero, which indicates the film formed is in the +1 oxidation state.

   b. Solution exchange experiments in the early stage of growth imply the existence of oxide species with negative charges, which can be replaced by acetonitrile.

   c. From literature results of electrochemical quartz-crystal microbalance experiments, both the early and later stages of growth show a mass change of 8 ± 0.5 g per mol electrons. This indicates that the oxide is anhydrous. Combined with the results of this work, the Pt(I) oxide cannot be PtOH, but is probably Pt_2O. The mechanism can be written as:

   $Pt + H_2O \rightarrow Pt\text{-}OH_2(ads)$ (fast)

   $Pt + Pt\text{-}OH_2(ads) \rightarrow Pt_2O + 2H^+ + 2e^-$ (slow)

   $Pt_2O + H_2O \rightarrow 2PtO + 2H^+ + 2e^-$ (fast)

2. Kinetics of the oxide growth:

   a. Sweep-hold experiments were performed for a variety of sweep rates and hold potential. The direct logarithmic rate law predicts a hyperbolic

relationship between the current density and decay time. The relationship was used to fit all the data and acceptable fits were found. The fitting for relatively slow scans, i.e. <1.5 V s^{-1}, is nearly perfect since the double-layer charging current is negligible. The error for the fitting was less than one percent. At faster scans the error increased to 5 percent.

b. The simulated results show that the rate law is not the simple equation discussed by Harrington: $j = a\exp(-b\sigma) = a_0\exp(cE)\exp(-b\sigma)$. The parameter a was found not to be related to electrode potential in a simple exponential relationship. An improved empirical rate law was deduced:

$$j = a'\exp(-\frac{b'\sigma}{E-0.766\text{V}})$$

$$\ln(a'/\mu\text{A cm}^{-2}) \approx 20.5,$$

$$b' \approx (2.25 \sim 2.75)\times 10^{-5}\ \text{cm}^2\ \mu\text{F}^{-1}$$

although the physical significance of this equation is not understood.

c. Using the mechanism in the 1c above, it is easy to deduce the direct logarithmic rate law if the following assumptions are made:

(1) the adsorption of water molecules is fast and the coverage of adsorbed water molecules is high.

(2) The oxidation of adsorbed water molecules to Pt_2O is slow and treated as the rate-determining step;

(3) The adsorption Pt_2O is assumed for follow the Frumkin isotherm.

d. The presence of surface diffusion was tested in the sweep-hold experiments by checking that current density is a unique function of the charge density and the applied potential. A unique function was found.

Nonetheless, the possibility of surface diffusion cannot be ruled out since very fast surface diffusion cannot be detected in the experiments and very slow surface diffusion would not have a significant effect on the experimental results.

e. The assumption that the formation of adsorbed Pt_2O occurs in a concerted two-electron step was consistent with the fitting results, where the α in $j = \frac{d\sigma}{dt} = a\exp(-b\sigma)\exp(\frac{\alpha FE}{RT})$ was from 0.5 to 0.9 and so the symmetry factor $\beta=\alpha/2$ is from 0.25 to 0.45, which are quite reasonable values.

f. The remaining discrepancy between the new empirical rate law and the above mechanism can arise from many effects, e.g., the adsorption of bisulfate or sulfate ions, or the difficulty of double-layer charging baseline correction.

3. Bisulfate and sulfate adsorption

a. The adsorption of bisulfate/sulfate was proved from the difference between the CV of platinum in pure perchloric acid and the CV with some sulfuric acid mixed with the perchloric acid. The sulfate/bisulfate adsorption delayed the oxide growth. For the same potential range sweep, less oxide was produced compared with pure perchloric acid solution.

b. Sulfate/bisulfate adsorption was also verified from the solution exchange experiments. Injection of perchloric acid into sulfuric acid only invokes a cathodic current transient response, while injection of sulfuric acid into perchloric acid produces an anodic current transient first and then a cathodic current transient. This indicates the adsorption of bisulfate/sulfate

occurs with charge transfer. The CV comparison results also indicate that bisulfate/sulfate adsorb even in the hydrogen adsorption region, and adsorb in the whole potential range investigated.

4. Future work: The work in this thesis raises some issues that require future work for their resolution:

   a. More specially designed experiments should be carried out to reveal the components of the thin film oxide, e.g., fluorescence experiments, which have very high sensitivity to the *d* orbitals of platinum.

   b. The suitability of the place-exchange mechanism remains unclear: the flipping of the dipoles by the electric field could be replaced by a more convincing model.

   c. More experiments should be performed to check where bisulfate/sulfate begins to adsorb and where it desorbs and how it affects the mechanism.

   d. The effect of surface diffusion on oxide growth on platinum is expected to be detectable under some special conditions, and should be sought in other experiments.

Appendix A

Sweep-Hold Experimental Data and Fitting Results

E_h (mV)	j_0 ($\mu A\ cm^{-2}$)	$\left.\frac{dj}{dt}\right\|_{t_0}$ ($\mu A\ cm^{-2}\ s^{-1}$)	σ_0 ($\mu C\ cm^{-2}$)	Fitting parameters		
1600						
v ($V\ s^{-1}$)				P_1 ($\mu A\ cm^{-2}$)	P_2 ($\mu C\ cm^{-2}$)	P_3 (s)
0.05	94.7034	-87.3941	755.7908	14.8406	5210.038	67.4298
0.1	142.1610	-243.6441	660.2208	14.8779	7680.0772	62.4949
0.2	232.6271	-720.3390	605.2300	18.1291	11946.7655	55.3960
0.5	478.8136	-3177.9661	561.5723	24.5498	24812.8185	50.6705
1.0	855.9322	-8474.5763	531.1561	28.7084	49073.2289	52.5654
1.5	1203.3893	-16949.1532	512.3799	8.3271	109388.9666	79.5475
2.0	1546.6102	-23304.8729	494.7694	4.9073	114755.6789	63.2078
2.5	1885.5932	-33898.0932	484.2258	5.1329	118191.1780	53.0245
3.0	2224.5763	-38135.5932	471.6342	0.0005 (not good)	127472.4382	47.03119
3.5	2550.8475	-42372.8814	458.7546	5E-8 (not good)	132191.4136	42.5192
4.0	2877.1186	-46610.1695	443.1568	1.7E-6 (not good)	138646.9630	38.8289

E_h (mV) 1500 v ($V\ s^{-1}$)	j_0 ($\mu A\ cm^{-2}$)	$\left.\frac{dj}{dt}\right\|_{t_0}$ ($\mu A\ cm^{-2}\ s^{-1}$)	σ_0 ($\mu C\ cm^{-2}$)	Fitting parameters		
				P_1 ($\mu A\ cm^{-2}$)	P_2 ($\mu C\ cm^{-2}$)	P_3 (s)
0.05	61.9703	-71.5042	617.0788	9.2924	2139.7506	40.7175
0.1	106.1441	-243.6441	560.2024	11.8998	3701.5329	36.8529
0.2	190.6780	-762.7119	518.2511	16.7880	6816.4147	35.83
0.5	432.2034	-2442.7966	485.7112	30.9700	16743.0469	37.60
1.0	819.9153	-8474.5763	460.6840	50.5000	37206.9257	42.0552
1.5	1171.6101	-15889.8305	441.2550	47.1062	41377.2209	30.4009
2.0	1514.8305	-23304.8729	427.7339	31.3458	93832.2367	53.2795
2.5	1894.0680	-33898.3051	412.6878	76.6403	98922.9849	45.0060
3.0	2216.1017	-42372.6695	399.8030	58.7963	106941.6575	40.5210
3.5	2546.6101	-50847.4576	390.3871	55.1164	113652.8137	36.7991
4.0	2877.1186	-59322.0339	381.4858	50.8927	119954.2712	33.9719

E_h (mV) 1550 ν ($V\ s^{-1}$)	j_0 ($\mu A\ cm^{-2}$)	$\left.\frac{dj}{dt}\right\|_{t_0}$ ($\mu A\ cm^{-2}\ s^{-1}$)	σ_0 ($\mu C\ cm^{-2}$)	Fitting parameters		
				P_1 ($\mu A\ cm^{-2}$)	P_2 ($\mu C\ cm^{-2}$)	P_3 (s)
0.05	70.8686	-74.4525	681.4750	10.8689	2974.1426	49.7192
0.1	118.2203	-233.0508	606.9224	14.0568	4743.2574	45.7199
0.2	204.6610	-805.0847	565.5360	19.6849	8197.3759	42.9740
0.5	452.1277	-3191.4894	528.4383	34.9836	19300.7816	42.6041
1.0	843.2203	-9533.8983	496.7311	55.9752	41129.5334	45.8267
1.5	1190.6780	-15889.8305	473.5742	52.3789	44427.6398	32.9102
2.0	1531.7797	-23304.8729	463.7920	38.0229	100993.8225	56.9525
2.5	1927.9661	-29661.0169	449.7794	80.424	107250.3744	48.4080
3.0	2258.4746	-38135.3814	437.7672	75.2547	11500.8538	43.1838
3.5	2584.7458	-50847.4576	425.3384	70.2659	121085.3579	39.2022
4.0	2915.2542	-63559.322	414.0896	7.5E-8	393383.1735	113.9426

E_h (mV)	j_0 ($\mu A\ cm^{-2}$)	$\left.\frac{dj}{dt}\right\|_{t_0}$ ($\mu A\ cm^{-2}\ s^{-1}$)	σ_0 ($\mu C\ cm^{-2}$)	Fitting parameters		
1450						
v ($V\ s^{-1}$)				P_1 ($\mu A\ cm^{-2}$)	P_2 ($\mu C\ cm^{-2}$)	P_3 (s)
0.05	58.1568	-79.4492	565.7379	8.3973	1772.1140	34.7324
0.1	101.2712	-286.0169	511.5957	10.6256	3146.9132	33.7730
0.2	183.0508	-847.4576	439.3000	14.2121	5567.0470	30.3578
0.5	423.7288	-3442.7966	450.3531	26.5976	15288.5832	34.8456
1.0	805.0847	-9533.8983	426.0808	43.3528	34538.2280	39.2246
1.5	1150.4237	-16949.1525	406.7395	41.2980	37684.6421	28.3570
2.0	1489.4068	-25423.7288	396.6263	24.9702	87837.3947	50.2608
2.5	1872.8816	-33898.3051	381.3997	61.0900	95197.5234	43.1409
3.0	2199.1525	-42372.8814	376.7575	51.4418	103255.1530	39.2085
3.5	2538.1356	-50847.4576	362.8176	52.9566	108957.3084	34.8906
4.0	2860.1695	-59322.0339	351.8505	48.9828	114444.0511	32.4805

E_h (mV)	j_0 ($\mu A\ cm^{-2}$)	$\left.\frac{dj}{dt}\right\|_{t_0}$ ($\mu A\ cm^{-2}\ s^{-1}$)	σ_0 ($\mu C\ cm^{-2}$)	Fitting parameters		
1400						
v ($V\ s^{-1}$)				P_1 ($\mu A\ cm^{-2}$)	P_2 ($\mu C\ cm^{-2}$)	P_3 (s)
0.05	56.9915	-82.0975	505.8234	8.0837	1600.8983	30.6861
0.1	100.4237	-264.8305	464.9694	10.3430	2849.0694	30.3249
0.2	181.3559	-847.4576	437.7884	14.2612	5516.8072	31.7029
0.5	416.3136	-3707.4271	413.6041	26.0333	14186.4108	32.7309
1.0	796.6102	-11652.5424	390.5130	42.9662	32115.4317	36.8792
1.5	1137.7119	-18008.4746	376.8714	39.6735	35761.6400	26.9126
2.0	1476.6949	-27542.3729	364.3519	25.0383	83037.6839	47.7120
2.5	1851.6949	-33898.3051	353.2100	61.0857	89632.8722	41.0981
3.0	2190.3780	-42373.0932	340.2751	56.8362	96903.5607	36.4766
3.5	2538.1356	-50847.4576	360.5413	52.9268	108991.0702	34.9121
4.0	2855.9322	-63559.3220	317.0327	47.7692	109554.0300	30.9813

E_h (mV)	j_0 ($\mu A\ cm^{-2}$)	$\left.\frac{dj}{dt}\right\|_{t_0}$ ($\mu A\ cm^{-2}\ s^{-1}$)	σ_0 ($\mu C\ cm^{-2}$)	Fitting parameters		
1350						
ν ($V\ s^{-1}$)				P_1 ($\mu A\ cm^{-2}$)	P_2 ($\mu C\ cm^{-2}$)	P_3 (s)
0.05	56.3559	-92.6907	456.5010	7.7522	1484.9428	27.3810
0.1	97.6695	-338.9830	426.4274	9.8877	3673.6135	29.7340
0.2	179.2373	-932.2034	398.0221	13.9303	5074.5711	29.4354
0.5	408.8983	-3707.6271	375.6186	25.3947	13398.7191	30.2251
1.0	775.4237	-10593.2203	343.2565	41.7931	30095.5835	34.6490
1.5	1340.1356	-21574.2515	409.9547	47.5233	40037.7523	25.4565
2.0	1457.6271	-25423.7288	332.1462	24.1096	78935.0914	45.6514
2.5	4838.9830	-38135.5932	319.2798	60.8495	85250.2318	38.9895
3.0	3177.9661	-46610.4695	307.8807	57.0025	92012.2241	35.0778
3.5	2521.1864	-55084.5339	301.3794	52.2369	98206.4408	31.7150
4.0	2860.1695	-63559.3220	290.4448	46.0465	105060.6702	29.73602

E_h (mV) 1300 v ($V\ s^{-1}$)	j_0 ($\mu A\ cm^{-2}$)	$\left.\frac{dj}{dt}\right\|_{t_0}$ ($\mu A\ cm^{-2}\ s^{-1}$)	σ_0 ($\mu C\ cm^{-2}$)	Fitting parameters		
				P_1 ($\mu A\ cm^{-2}$)	P_2 ($\mu C\ cm^{-2}$)	P_3 (s)
0.05	56.1441	-100.6356	405.7969	9.4429	1339.6468	28.0839
0.1	94.7034	-317.7966	375.8016	9.6400	2401.1015	26.5920
0.2	173.7288	-974.5762	360.6779	13.8597	4567.9725	26.8535
0.5	399.3644	-3707.6271	341.1191	25.9185	12008.1079	27.8008
1.0	758.4749	-10593.2203	319.9142	44.6262	28568.6638	35.2225
1.5	1108.0508	-18008.4746	311.6897	40.7646	31059.2243	23.6704
2.0	1461.8646	-19661.0169	297.9276	25.4235	73541.1199	42.4537
2.5	1843.2206	-33898.0932	288.5117	60.7224	80141.9059	36.5598
3.0	2199.2515	-46610.4695	274.8497	54.4967	88945.6270	33.1895
3.5	2550.8475	-55084.7458	267.3400	51.2380	93860.3632	29.7271
4.0	2860.1695	-63559.3220	290.4417	46.4922	104591.4563	29.5162

E_h (mV)	j_0 ($\mu A\ cm^{-2}$)	$\left.\frac{dj}{dt}\right\|_{t_0}$ ($\mu A\ cm^{-2}\ s^{-1}$)	σ_0 ($\mu C\ cm^{-2}$)	Fitting parameters		
1250						
v ($V\ s^{-1}$)				P_1 ($\mu A\ cm^{-2}$)	P_2 ($\mu C\ cm^{-2}$)	P_3 (s)
0.05	51.5890	-108.5805	364.7192	7.1195	1135.9699	24.0087
0.1	90.8898	-349.5762	339.2876	9.1400	2125.3673	24.6417
0.2	165.6780	-1228.8157	286.2348	12.8804	3533.7018	21.5283
0.5	349.9491	-3972.4576	305.0525	25.4318	10608.6448	25.6588
1.0	756.3559	-11652.5424	285.1272	41.2696	25472.8593	29.7980
1.5	1120.7627	-19067.7966	274.6513	38.8943	29066.0735	21.7371
2.0	1474.5762	-31779.4492	265.8226	22.6740	69802.6901	39.4702
2.5	1885.5932	-38135.5932	256.4587	58.8164	77294.7247	34.4924
3.0	2258.4746	-50847.4576	244.4417	52.7751	83432.4391	30.4797
3.5	2639.8305	-63559.3220	235.8455	46.9050	92829.0101	27.9836
4.0	3000.0000	-72033.8983	224.6028	43.9437	97367.6278	25.8285

E_h (mV)	j_0 ($\mu A\ cm^{-2}$)	$\left.\frac{dj}{dt}\right\|_{t_0}$ ($\mu A\ cm^{-2}\ s^{-1}$)	σ_0 ($\mu C\ cm^{-2}$)	Fitting parameters		
1100						
v ($V\ s^{-1}$)				P_1 ($\mu A\ cm^{-2}$)	P_2 ($\mu C\ cm^{-2}$)	P_3 (s)
0.05	52.6483	-156.2500	231.3225	5.9411	740.0708	15.4395
0.1	99.1525	-508.4745	220.0956	7.8828	1474.7010	14.7238
0.2	193.2203	-1525.4237	211.4918	11.6144	3091.2888	14.7855
0.5	470.3390	-6091.1017	199.7809	22.1114	9425.5305	17.4062
1.0	934.3220	-14830.5085	180.5711	35.7066	25082.9115	22.2483
1.5	1355.9322	-27542.3729	165.4682	19.0879	61928.3713	37.7650
2.0	1764.8307	-38135.5932	159.2449	12.8819	70685.8100	32.0081
2.5	2203.3898	-50847.4576	147.5562	46.2695	80640.7231	29.3137
3.0	2572.0339	-63559.3220	135.6391	43.1211	86213.2371	26.6897
3.5	2915.2542	-76271.1864	124.6971	38.8660	92931.6435	25.0061
4.0	3237.2881	-84745.7627	120.6945	53.2523	75024.8156	5.6818

References

1. Conway, B.E., Progr. Surf. Sci., 1995. **49**(4): p. 331-452.
2. Conway, B.E., Progr. Surf. Sci., 1984. **16**: p. 1-138.
3. Bockris, J.O.M. and U.M.K. Shahed, Surface Electrochemistry: a molecular level approach. 1993, New York: Plenum Press.
4. Bard, A.J. and L.R. Faulkner, Electrochemical Methods: Fundamentals and Applications. 1980: John Wiley & Sons Press.
5. Gilman, B.S., Electroanal. Chem., 1967. **9**: p. 112.
6. Vetter, K.J. and J.W. Schultze, J. Electroanal. Chem., 1972. **34**: p. 141-158.
7. Vetter, K.J. and J.W. Schultze, J. Electroanal. Chem., 1972. **34**: p. 131-139.
8. Angerstein-Kozlowska, H., B.E. Conway, and W.B.A. Sharp, J. Electroanal. Chem., 1973. **43**: p. 9-36.
9. Jerkiewicz, G., G. Tremiliosi-Filho, and B.E. Conway, J. Electroanal. Chem., 1992. **332**: p. 359-370.
10. Parsons, R. and W.H.M. Visscher, J. Electroanal. Chem., 1973. **47**: p. 363.
11. Breiter, M.W., J. Electroanal. Chem., 1964. **7**: p. 38-49.
12. Conway, B.E. and S. Gottesfeld, J. Chem. Soc., Faraday Trans. I, 1973. **69**: p. 1090.
13. Geest, M.E.v.d., N.J. Dangerfield, and D.A. Harrington, J. Electroanal. Chem., 1997. **420**: p. 89-100.
14. Harrington, D.A., J. Electroanal. Chem., 1993. **355**: p. 21-35.
15. Allen, G.C., et al., J. Electroanal. Chem., 1974. **50**: p. 335.

16. Dickinson, T., A.F. Povey, and P.M.A. Sherwood, J. Chem. Soc., Faraday Trans. I, 1975. **71**: p. 298-311.

17. Hammond, J.S. and N. Winograd, J. Electroanal. Chem., 1977. **78**: p. 55-69.

18. Peuckert, M. and H.P. Bonzel, Surf. Sci., 1984. **145**: p. 239.

19. Rach, E. and J. Heitbaum, Electrochim. Acta, 1986. **31**(4): p. 477-479.

20. Aberdam, D., et al., Surf. Sci., 1986. **171**: p. 303-330.

21. Wagner, F.T. and P.N. Ross, Surf. Sci., 1985. **160**: p. 305.

22. Conway, B.E., Symposium of the Faraday Soc., 1970. **4**: p. 89.

23. Gottesfeld, S., et al., J. de Phys. Colloque C5, Suppl. 11, 1977. **38**(Nov.): p. C5-C145.

24. Benziger, J.B., et al., J. Electroanal. Chem., 1986. **198**: p. 65-80.

25. Birss, V.I., M. Chang, and J. Segal, J. Electroanal. Chem., 1993. **355**: p. 181-191.

26. Itaya, K., et al., J. Vac. Sci. Technol. A, 1990. **8**(1): p. 515-519.

27. Sashikata, K., N. Furuya, and K. Itaya, J. Vac. Sci. Technol. A, 1991. **9**(2): p. 457-464.

28. Rudge, A.J., et al., J. Electroanal. Chem., 1994. **366**: p. 253-263.

29. Conway, B.E., et al., J. Chem. Phys., 1990. **93**(11): p. 8361-8373.

30. Gilroy, D., J. Electroanal. Chem., 1977. **83**: p. 329.

31. Heyd, D.V. and D.A. Harrington, J. Electroanal. Chem., 1992. **335**: p. 19-31.

32. Harrington, D.A., J. Electroanal. Chem., 1997. **420**: p. 101-109.

33. Allen, G.C. and P.M. Tucker, J. Electroanal. Chem., 1974. **50**: p. 335-343.

34. Kim, K.S., N. Winograd, and R.E. Davis, J Am. Chem. Soc., 1971. **93**(23): p. 6296-6297.

35. Nart, F.C., T. Iwasita, and M. Weber, Electrochim. Acta, 1994. **39**(7): p. 961-968.

36. Peuckert, M. and H. Ibach, Surf. Sci., 1984. **136**: p. 319-326.

37. Peuckert, M., J. Electroanal. Chem., 1985. **185**: p. 379-391.

38. Angerstein-Kozlowska, H., et al., J. Electroanal. Chem., 1979. **100**: p. 417.

39. Angerstein-Kozlowska, H., et al., J. Electroanal. Chem., 1979. **100**: p. 417-446.

40. Balashova, N.A. and V.N. Kazarinov, in Electroanalytical Chemistry, ed. A.J. Bard. Vol. 3. 1969, New York: Marcel Dekker. 135.

41. Hoyanyi, G., Electrochim. Acta, 1980. **25**: p. 43.

42. Kranskopf, E.K., K. Chan, and A. Wieckowski, J. Phys. Chem., 1987. **91**: p. 2327.

43. Zelenay, P. and A. Wieckowski, J. Electrochem. Soc., 1992. **139**(9): p. 2552-2558.

44. Kunimatsu, K., M.G. Samant, and H. Seki, J. Electroanal. Chem., 1989. **258**: p. 163-177.

45. Nart, F.C. and T. Iwasita, J. Electroanal. Chem., 1991. **308**: p. 277-293.

46. Thomas, S., et al., J. Phys. Chem., 1996. **100**: p. 11726-11735.

47. Clavilier, J. and R. Albalat, J. Electroanal. Chem., 1992. **330**: p. 489-497.

48. Lane, R.F. and A.T. Hubbard, J. Phys. Chem., 1975. **79**(8): p. 808-815.

49. Macdougall, B., B.E. Conway, and H.A. Kozlowska, J. Electroanal. Chem., 1971. **32**: p. 15-30.

50. Orts, J.M., et al., Electrochim. Acta, 1994. **39**(11/12): p. 1519-1524.

51. Conway, B.E. and S. Gottesfeld, J. Chem. Soc., Faraday Trans. I, 1973. **69**: p. 1090-1107.

52. Seland, F., master thesis, *Kinetic Studies of Electrochemical Reactions with Adsorption: An ac impedance study of methanol oxidation on polycrystalline platinum in acid solution*. 1999, Norges Teknisk-Naturvitenskapelige Universitet: Norway.

Curriculum Vitae

Surname: Huang Given Name: Yin

Place of Birth: Fujian, People Republic of China

Educational Institutions Attended:

University of Victoria	1998 to 2000
Xiamen University	1990 to 1997

Degrees Awarded:

B. Sc.	Xiamen University	1994

PARTIAL COPYRIGHT LICENSE

I hereby grant the right to lend my thesis to users of the University of Victoria Library, and to make single copies only for such users or in response to a request from the Library of any other university, or similar institution, on its behalf or for one of its users. I further agree that permission for extensive copying of this thesis for scholarly purposes may be granted by me or a member of the University designated by me. It is understood that copying or publication of this thesis for financial gain shall not be allowed without my written permission.

Title of Thesis:

Electrochemical Oxide Growth on Polycrystalline Platinum

Author [redacted]

Yin Huang

August 30, 2000